

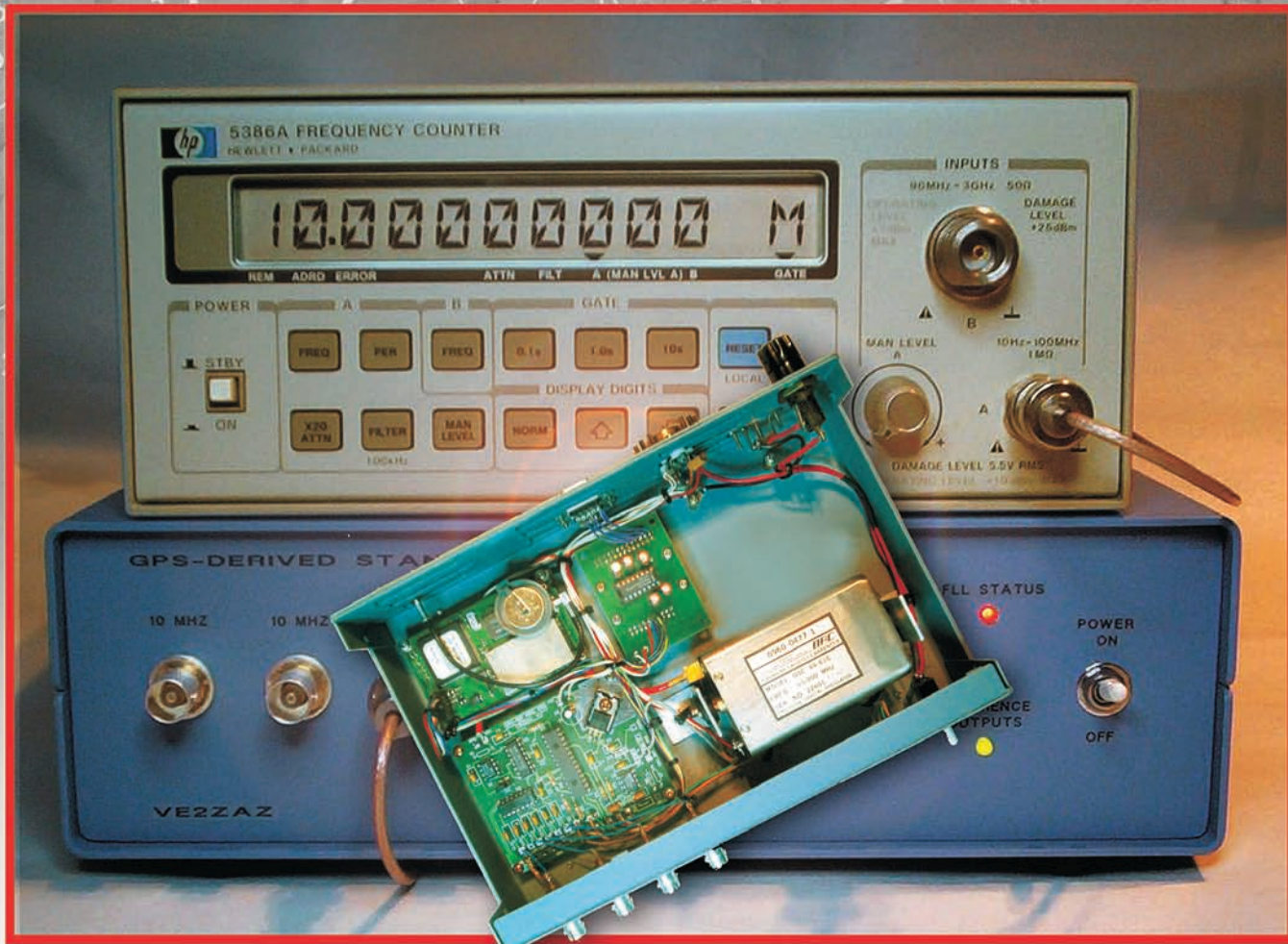


QEX

September/October 2006

A Forum for Communications Experimenters

Issue No. 238

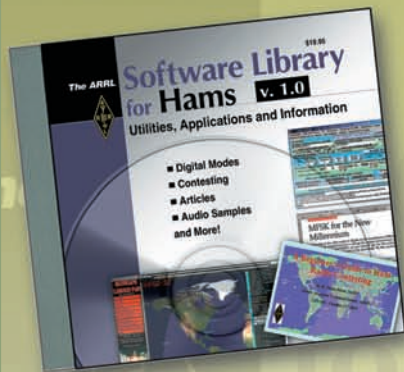


VE2ZAZ used the 1 pulse-per-second signal from a GPS receiver board to lock the output frequency of a 10-MHz oscillator.

ARRL The national association for
AMATEUR RADIO

225 Main Street
Newington, CT USA 06111-1494

NEW!



The ARRL Software Library for Hams

Quick access to utilities, applications and information:

- **Book excerpts** and a selection of articles from the pages of QST magazine
- **Contesting software**, including N1MM Logger
- **CW Decoder**
- **WinDRM** digital voice software
- **HF digital software** for PSK31, MFSK16, MT63, RTTY and more
- **WSJT** software for meteor scatter and moonbounce *and more!*

You'll also find programs for **APRS**, **Winlink 2000**, **packet radio** and **satellite tracking**. Plus, handy software tools for calculating transmission line loss, creating custom DSP audio filters, and more. Bonus files include ARRL screensavers, audio samples, video files, and PowerPoint presentations.

Minimum System Requirements: A 400 MHz Pentium PC with 256 MBytes of RAM and Microsoft® Windows® XP or Windows 2000. A sound card is required to listen to sound samples or use the sound-card-based digital communication software. Includes the free Adobe® Reader® and Microsoft® PowerPoint® viewer.

The ARRL Software Library for Hams

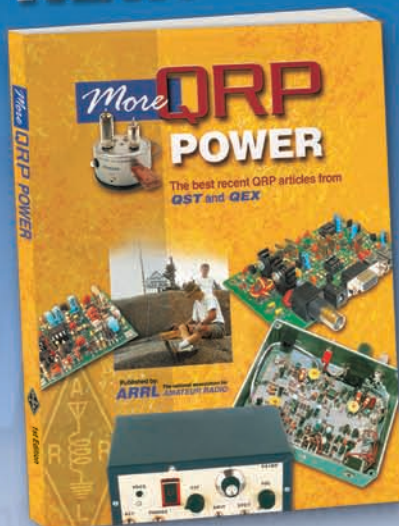
CD-ROM, version 1.0

ARRL Order No. 9620

Only \$19.95*

*shipping: \$6 US (ground)/\$11.00 International

NEW!



MORE EQUIPMENT, ACCESSORIES AND ANTENNAS FOR LOW POWER RADIO OPERATING!

Build a tiny station that you can take anywhere, or get on the air with a radio the size of a paperback book and an antenna that folds up into a briefcase or knapsack. In the spirit of the popular *QRP Classics* and *QRP Power* published in the 1990s, *More QRP Power* is an anthology of articles from recent issues of QST and QEX magazines. Here are *more projects and articles for low power radio operating*:

- Construction practices
- Transceivers
- Transmitters
- Receivers
- Accessories
- Antennas

More QRP Power

ARRL Order No. 9655

Only \$19.95*

*shipping: \$7 US (ground)/\$12.00 International

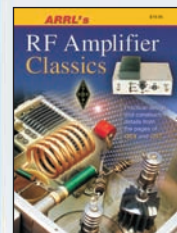
Also available from ARRL...

- **ARRL's Low Power Communication** #9175
- **Low Power Scrapbook** #LPSB
- **W1FB's QRP Notebook** #3657

Turn dreams of constructing your first amp or next brick into reality!

ARRL's RF Amplifier Classics

includes two-dozen projects and articles from the pages of QST and QEX, published between 1980 and 2003. There are amps for HF, MF, VHF and microwave.



These are high quality works from respected authors such as Gary Breed, K9AY; Jerry Pittenger, K8RA; Bill Sabin, WØIYH; Al Ward, W5LUA; Dave Meacham, W6EMD and others.

Use this book and...

- Shorten your discovery work
- Find practical designs and construction details for classic tube and solid-state amplifiers at power levels from 5 W to 1.5 kW
- Build safe and reliable amplifiers
- Produce loud and clean signals

Order Today!

ARRL's RF Amplifier Classics

ARRL Order No. 9310

— Only \$19.95*

*shipping: \$7 US (ground) / \$12.00 International



ARRL The national association for **AMATEUR RADIO**

SHOP DIRECT or call for a dealer near you.
ONLINE WWW.ARRL.ORG/SHOP
ORDER TOLL-FREE 888/277-5289 (US)

QEX 9/2006

QEX

QEX (ISSN: 0886-8093) is published bimonthly in January, March, May, July, September, and November by the American Radio Relay League, 225 Main Street, Newington, CT 06111-1494. Periodicals postage paid at Hartford, CT and at additional mailing offices.

POSTMASTER: Send address changes to: QEX, 225 Main St, Newington, CT 06111-1494 Issue No 238

Harold Kramer, WJ1B
Publisher

Doug Smith, KF6DX
Editor

Larry Wolfgang, WR1B
Managing Editor

Lori Weinberg, KB1EIB
Assistant Editor

L. B. Cebik, W4RNL
Zack Lau, W1VT
Ray Mack, WD5IFS
Contributing Editors

Production Department

Steve Ford, WB8IMY
Publications Manager

Michelle Bloom, WB1ENT
Production Supervisor

Sue Fagan
Graphic Design Supervisor

Devon Neal
Technical Illustrator

Joe Shea
Production Assistant

Advertising Information Contact:

Janet L. Rocco, W1JLR
Business Services
860-594-0203 direct
860-594-0200 ARRL
860-594-0303 fax

Circulation Department

Cathy Stepina, QEX Circulation

Offices

225 Main St, Newington, CT 06111-1494 USA
Telephone: 860-594-0200
Fax: 860-594-0259 (24 hour direct line)
e-mail: qex@arrl.org

Subscription rate for 6 issues:

In the US: ARRL Member \$24,
nonmember \$36;

US by First Class Mail:
ARRL member \$37, nonmember \$49;

Elsewhere by Surface Mail (4-8 week delivery):
ARRL member \$31, nonmember \$43;

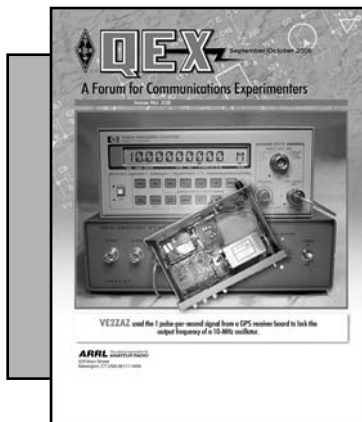
Canada by Airmail: ARRL member \$40,
nonmember \$52;

Elsewhere by Airmail: ARRL member \$59,
nonmember \$71.

Members are asked to include their membership control number or a label from their QST when applying.

In order to ensure prompt delivery, we ask that you periodically check the address information on your mailing label. If you find any inaccuracies, please contact the Circulation Department immediately. Thank you for your assistance.

Copyright ©2006 by the American Radio Relay League Inc. For permission to quote or reprint material from QEX or any ARRL publication, send a written request including the issue date (or book title), article, page numbers and a description of where you intend to use the reprinted material. Send the request to the office of the Publications Manager (permission@arrl.org).



About the Cover

Bertram Zauhar, VE2ZAZ, describes the construction and operation of a high-accuracy frequency standard based on a GPS receiver board. The cover photos show his project connected to an HP frequency counter, along with a view inside the project box.



Features

- 3 Get 1.5 kW from a New RF MOSFET: A Legal Limit HF Linear, Tokyo Style**
By Toshiaki Ohsawa, JE1BLI, and Nobuki Wakabayashi, JA1DJW
- 14 A Simplified GPS-Derived Frequency Standard**
By Bertrand Zauhar, VE2ZAZ
- 22 Installing Vertically Polarized Yagis in the T-Mount Configuration**
By Rick Littlefield, K1BQT
- 25 An IF Signal Generator**
By John Pivnichny, N2DCH
- 28 Magnetic Coupling in Transmission Lines and Transformers**
By Gerrit Barrere, KJ7KV
- 37 Easy Microwave Filters Using Waveguides and Cavities**
By Paolo Antoniazzi, IW2ACD, and Marco Arecco, IK2WAQ
- 43 Q Calculations of L-C Circuits and Transmission Lines: A Unified Approach**
By Jacques Audet, VE2AZX
- 52 Some Thoughts About the Quality Factor of a Coil**
By Pierre Desjardins, VE2PID
- 54 What's Your CQ? (Curiosity Quotient)**
By Eric P. Nichols, KL7AJ

Columns

- 54 Upcoming Conferences**
- 62 Letters**
- 55 Antenna Options**
- 63 Next Issue in QEX**
By L. B. Cebik, W4RNL

Sep/Oct 2006 QEX Advertising Index

American Radio Relay League: Cov II,
63, Cov III, Cov IV
ARA West: 64
Atomic Time: 13
Down East Microwave, Inc.: 64
Elkins Marine Training International: 64
National RF: 64

Nemal Electronics International, Inc.: 24
RF Parts: 27
Teri Software: 24
Timewave Technology, Inc: 51
Tucson Amateur Packet Radio Corp.: 21,
53



The American Radio Relay League, Inc. is a noncommercial association of radio amateurs, organized for the promotion of interest in Amateur Radio communication and experimentation, for the establishment of networks to provide communications in the event of disasters or other emergencies, for the advancement of the radio art and of the public welfare, for the representation of the radio amateur in legislative matters, and for the maintenance of fraternalism and a high standard of conduct.

ARRL is an incorporated association without capital stock chartered under the laws of the state of Connecticut, and is an exempt organization under Section 501(c)(3) of the Internal Revenue Code of 1986. Its affairs are governed by a Board of Directors, whose voting members are elected every three years by the general membership. The officers are elected or appointed by the Directors. The League is noncommercial, and no one who could gain financially from the shaping of its affairs is eligible for membership on its Board.

"Of, by, and for the radio amateur," ARRL numbers within its ranks the vast majority of active amateurs in the nation and has a proud history of achievement as the standard-bearer in amateur affairs.

A *bona fide* interest in Amateur Radio is the only essential qualification of membership; an Amateur Radio license is not a prerequisite, although full voting membership is granted only to licensed amateurs in the US.

Membership inquiries and general correspondence should be addressed to the administrative headquarters:

ARRL, 225 Main Street, Newington, CT 06111 USA.

Telephone: 860-594-0200

FAX: 860-594-0259 (24-hour direct line)

Officers

President: JOEL HARRISON, W5ZN

528 Miller Rd, Judsonia, AR 72081

Chief Executive Officer: DAVID SUMNER, K1ZZ

The purpose of QEX is to:

1) provide a medium for the exchange of ideas and information among Amateur Radio experimenters,

2) document advanced technical work in the Amateur Radio field, and

3) support efforts to advance the state of the Amateur Radio art.

All correspondence concerning QEX should be addressed to the American Radio Relay League, 225 Main Street, Newington, CT 06111 USA. Envelopes containing manuscripts and letters for publication in QEX should be marked Editor, QEX.

Both theoretical and practical technical articles are welcomed. Manuscripts should be submitted in word-processor format, if possible. We can redraw any figures as long as their content is clear. Photos should be glossy, color or black-and-white prints of at least the size they are to appear in QEX or high-resolution digital images (300 dots per inch or higher at the printed size). Further information for authors can be found on the Web at www.arrl.org/qex/ or by e-mail to qex@arrl.org.

Any opinions expressed in QEX are those of the authors, not necessarily those of the Editor or the League. While we strive to ensure all material is technically correct, authors are expected to defend their own assertions. Products mentioned are included for your information only; no endorsement is implied. Readers are cautioned to verify the availability of products before sending money to vendors.

Empirical Outlook

Doug Smith, KF6DX
kf6dx@arrl.org

A Brief Look Back

Over the span of QEX's existence, several design revolutions have devolved upon the communications world. Looking back, it's difficult to see how we survived without them.

In 1981, the IBM PC had just been introduced. Almost nobody knew who Bill Gates was. Highly integrated synthesizer chips were just coming onto the market. Printed circuit boards were manufactured in much the same way as they are now but we created artwork by manually laying crepe tape on Mylar sheets. Capable microprocessors were available for embedded designs but their widespread use in transceivers would wait several years. Digital signal processing (DSP) was impractical except in high-end applications, although the theory of it was quite advanced.

The 1980s saw vast improvements in all those areas. NEC introduced one of the first complete DSPs: the μ PD7720. AT&T was right there, too, with their DSP1. Both were presented at the IEEE International Solid-State Circuits Conference in 1980. Texas Instruments introduced the TMS32010 in 1983, which proved to be a huge success. Motorola entered the market with their MC56000 at around that time, as well. Analog-to-digital converter (ADC) technology was still in its infancy, though, by today's standards.

A landmark article appeared in QST in 1984 describing DSP and what was coming.¹ It's an excellent tutorial on the basics and it even makes some predictions that turned out to be quite accurate.

Complementary metal-oxide semiconductors (CMOS) were devised by Frank Wanlass at Fairchild in 1963; however, it wasn't until the early 1980s that the 4000 series of logic chips and CMOS microprocessors became popular. Low power drain — hence low digital circuit noise — made them practical in radio designs. CMOS phase-locked loop (PLL) chips, including the 4046, multiplied frequency synthesis applications. Led by Signetics and Motorola, advancement of PLLs on a chip proceeded rapidly.

Although hams had documented their experimentation with frequency synthesis since the 1960s, articles that included PLLs and microprocessor control didn't appear in amateur publications until the 1980s. In 1988, a noted article appeared in *ham radio* about direct digital synthesis (DDS).² It sent designers scurrying to explore the technique, although DDS and PLL had already been combined at Rockwell

Collins by the late 1970s. Qualcomm, Harris and others introduced integrated DDS chips that made the technique practical if not economical at first.

AMTOR, and then PACTOR, arrived in the 1980s, forcing manufacturers to pay attention to turn-around times between transmit and receive. Those developments also gave designers impetus to revisit their automatic gain control (AGC) and automatic level control (ALC) circuits for transient response.

The 1990s brought steady improvements in synthesizer phase noise, receiver dynamic ranges and frequency stability. DDS-driven PLLs began to win most synthesizer design decisions. Computer control became a standard feature on most transceivers. Units that exclusively used computer control, without manual front-panel controls, appeared. Some thought that would be the model for all future designs but it turned out not to be the case.

Near the turn of the millenium, we saw a split in design philosophies, with the advent of inexpensive, high-dynamic-range ADCs, the development of which was initially driven by digital audio and video applications. On the one hand, low-IF DSP rigs became the norm in high-performance designs. On the other hand, increasing ADC speeds, resolutions and dynamic ranges eventually made practical today's direct-conversion software radios.

In virtually every case, design improvements were spurred by demands for either better performance or lower cost, or both. Both goals have been achieved in both branches but there are still major gaps between them. Transmitter intermodulation distortion stands out as one area in which not much progress has been made.

All told, it's been an amazing journey. Some have asked, "What's the next big breakthrough?" To answer that question is to first look at the definition of breakthrough: "An act of breaking through an obstacle or barrier..."³ So what's the next big obstacle? Is it band crowding or interference? Cost of equipment? The survival of our Service? What do *you* think?

Notes

¹R. Olsen, N6NR, "Digital Signal Processing For The Experimenter," QST, Nov 1984, pp 22-27; available on the Web at www.arrl.org/tis/info/pdf/79135.pdf

²R. Zavrel, Jr, W7SX, "A Direct Digital Synthesis VFO," HAM RADIO, Sep 1988, pp 10-17.

³L. Brown, ed-in-chief, *The Shorter Oxford English Dictionary*, 5th ed, Oxford University Press, 2002.



Get 1.5 kW from a New RF MOSFET: A Legal Limit HF Linear, Tokyo Style

Legal limit output power on all amateur MF and HF bands from a pair of RF power MOSFETs in push-pull configuration.

Toshiaki Ohsawa, JE1BLI, and Nobuki Wakabayashi, JA1DJW

More than two decades have passed since Motorola introduced their T-MOS RF power FETs. Helge Granberg, K7ES, described a 1.5 kW amplifier using those transistors for *QEX* readers.¹ Since then, devices equivalent to the Motorola MRF150 as well as other new devices have been developed by several semiconductor manufacturers. Among them there is one interesting device called the ARF1500 developed by Advanced Power Technology, Inc of Bend, Oregon, USA (www.advancedpower.com). This device has a 500 V drain-to-source breakdown voltage rating and 1500 W of power dissipation capability. After looking at this specification, we thought a full-legal-limit HF power amplifier would be possible without any power combining. After many experiments, we have succeeded in designing a compact push-pull broadband amplifier with 1.5 kW output over 1.8 to 30 MHz.

The ARF1500 package has a unique construction, very different from conventional high power RF power

transistors. Instead of the conventional ceramic package and copper-tungsten flange, a large rectangular plastic molded cover and a special base material are used. The base material is beryllia (beryllium oxide — BeO) ceramic. It is a very good electrical insulator with very low thermal resistance, between that of copper and aluminum. It conducts the dissipated heat away from the transistor into the heat sink on which it is mounted. BeO is lethal if inhaled so you must never scratch the bottom surface.

Some excellent features of the ARF1500 are as follows:

- *High power:* It has a high enough power-handling capability that a single push-pull amplifier can build a practical amplifier with one kilowatt minimum output.

- *High voltage:* With a breakdown voltage rating of 500 V, the operating voltage can be at least two times higher than conventional RF devices. At the higher voltage, the drain impedance is much higher and the performance is less subject to dc power supply regulation, greatly simplifying the design of the power supply.

- *High current:* The maximum drain current specification is 60 A, a wide SOA

(safe operating area) can be expected. This, along with the high V_{dd} rating, makes it much more rugged than conventional power devices.

In addition, the internal structure is optimized for stable RF and dc performance. The mounting surface area is much larger than conventional transistors and this greatly facilitates heat sinking.

On the other hand, some tough points in the application are:

- *Low input impedance:* With 5000 pF of input capacitance, the gate input impedance becomes so low that matching it over a wide frequency bandwidth is much more difficult than with lower power devices.

- *Peripheral components selection:* The higher RF current will cause more heat generation due to the I²R losses in the passive components used around the ARF1500. Capacitor dielectric loss, magnetic saturation and heat dissipation of ferrite cores, etcetera must all be carefully considered.

- *Heat-sink design:* Due to the high dissipated power in the devices, the heat sink and cooling system must be very efficient to keep the junction temperature of the ARF1500 below a reasonable limit.

We set a design goal for a single stage push-pull pair of ARF1500s as follows:

Output power: 1.5 kW.

Frequency range: 1.8 ~ 30 MHz (amateur

¹Notes appear on page 13.

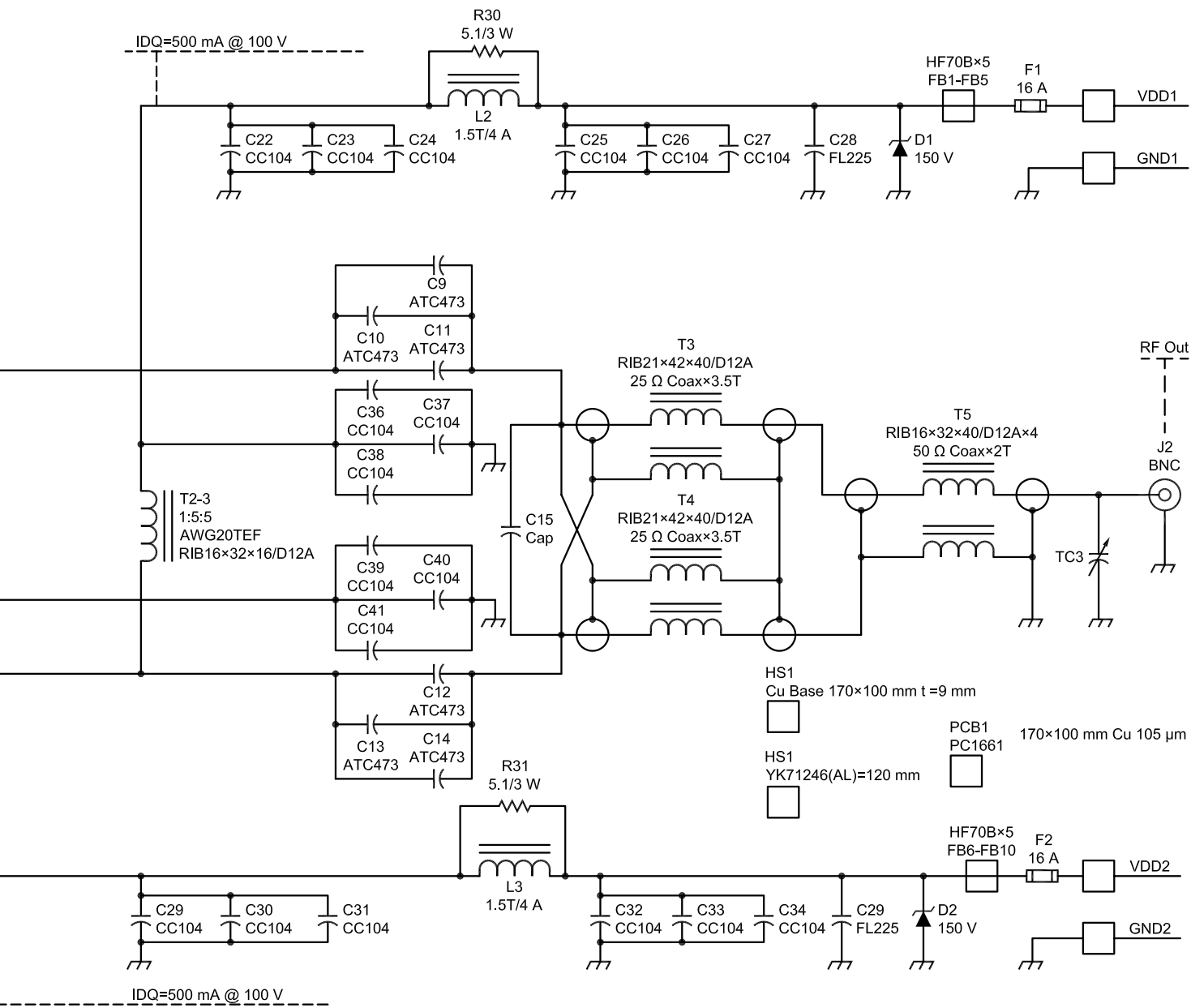


Figure 1 — Schematic diagram of the ARF1500 amplifier.

bands 160 m-10 m)
 Power gain: 13 dB minimum.
 DC supply voltage (V_{dd}): 100 V dc.
 Efficiency: 40% minimum.

The Input Circuit Design

Refer to Figure 1, a schematic diagram of the amplifier. The input circuit of this amplifier has a distinctive feature and has been designed with some calculations and estimations as stated below. See Table 1 for

Table 1
Input Impedance versus Output Impedance

F (MHz)	Z_{in} Ω	Z_{out} Ω
2.0	$6.7 - j12$	$7.5 - j0.8$
13.5	$0.45 - j2.5$	$7.1 - j1.7$
27	$0.22 - j0.67$	$6.1 - j3.0$
40	$0.2 + j0.19$	$5.0 - j3.6$

the ARF1500 input/output impedances, as given on the data sheet.²

From that data, we made an approximate calculation to obtain an estimated equivalent series input circuit with the following parameters:

- $C_{in} = 4,800$ pF
- $R_{in} = 30$ Ω
- $R_s = 0.2$ Ω
- $L_s = 3.5$ nH

That is a rough approximation and it is

advised that readers should not directly apply the above data parameters for SPICE simulation.

With those impedance characteristics it is almost impossible to design an input network that is entirely flat over the desired frequency range. After various experimental tries, and taking R_s and L_s into account, we have incorporated the following features in the design:

1) Input transformer T1 has a 5:1 winding ratio for low impedance drive.

2) At the high-frequency band edge, on 10 m, a tuned matching network is inserted to compensate for the device input capacitance and the inductance of printed circuit board patterns.

3) At the low-frequency end, gain and input impedance are lowered using negative feedback.

4) At midband, impedance matching and gain are improved by resonating the transformer leakage inductances with the coupling capacitors to form a broad series resonance.

5) Drain-to-gate RC feedback is applied directly on each ARF1500 to suppress low-frequency gain and further control the gate impedance.

Using these techniques, the input SWR is $< 2:1$ and the amplifier is stable and flat over 2 to 28 MHz. It still had plenty of gain, so a 3-dB attenuator was added on the input. This lowers the input SWR below 1.5:1, sets the maximum gain at 13 dB, within regulatory limits, and also protects the amplifier from overdrive.

Circuit Description

Under the conditions of $V_{dd} = 100$ V and $P_{out} = 1500$ W, the 12.5- Ω drain-drain load requires a 1:4 impedance ratio on the output transformer. This easily obtained ratio also provides, from our experience, the best broadband performance and efficiency. We have employed a transmission line type transformer, followed by a floating balun to enhance the symmetrical characteristics of the push-pull circuit. A conventionally wound "bead and tube" type transformer may be used in place of this output transformer chain at lower cost and lower performance.

The T2 secondary has a four-turn bifilar winding of AWG 20 wire. This transformer has a minimum inductance requirement for feeding the drains and the winding ratio provides most of the feedback as mentioned above. The mutual coupling between the primary and secondary windings is particularly important. To maximize the coupling, brass tubing was used for the negative feedback (NFB) winding. High permeability (μ_r) ferrite core material was selected to achieve high inductance per turn. The ferrite used for this

application has a μ_r of 250 and a high Curie temperature. The core size should be relatively small but with a large cross-sectional area. Note that the primary winding center tap is isolated.

The RF voltage at the drains is divided by eight by the dc feed transformer (T2) turns ratio and is fed back to the gates through the feedback resistors. This feedback controls both the gain and input impedance. This method also minimizes the heat dissipated in the feedback resistors.

Feeding DC Power

Special care has been taken on following points:

1) High current. Drain current reaches 30 A at peak. The printed circuit board pattern and windings in series with the dc supply circuit must all carry this current. To reduce current loading on the pc board pattern, the dc power feed is split between two channels. This also improves RF stability.

2) High voltage: 100 V dc is fairly high for a transistor circuit. The rated working voltage of most surface mount capacitors is usually 50 V or 100 V, not enough for this application. We also have to be careful with pattern spacings on the pc board and with the insulation (bulk resistivity) of the ferrite materials.

3) RF current: Most RF bypass capacitors, Z5U or X5V types, have a relatively high dielectric loss. Capacitors will overheat from the high RF current and burn up. For this reason, several capacitors are placed in parallel to split the bypass and coupling currents. These capacitors should be placed and grounded close to the FET source leads. The ideal decoupling choke will have small internal loss and no in-band resonance points. A Q-damping resistor may improve the total stability in some cases. Improperly designed decoupling circuits can often induce a parasitic oscillation. Electrolytic capacitors may explode with RF current applied. Low-loss film capacitors are recommended for large bypass capacitance values.

4) Surge protection: Transient high voltage spikes may be generated when switching the amplifier supply on and off. Surge absorbing Zener diodes have been inserted at the dc input terminal area.

5) Fuse: For safety, fast-acting, self-extinguishing fuses are suggested — high voltage types, not slow-blow.

Gate Bias Supply Circuit

The dc bias supply is constructed separately from the main dc power supply. A simple circuit is often seen where only a potentiometer is used to provide the necessary gate voltage. For this amplifier, a regulated and thermally compensated voltage supply

provided the best performance. The FET gates have both RF and dc present. Special care is taken to provide a well-filtered low source impedance. Otherwise the bias voltage can become RF-modulated resulting in degraded IMD performance.

Although MOSFETs are generally considered to have high impedance characteristics, we have designed the impedance of the bias supply circuit as low as possible. A TL 431 regulator IC provides both voltage regulation and temperature compensation. The thermistor value was determined by a series of cut and try experiments. This compensation may take much time and should be done cautiously. It needs an adequate temperature time constant. If its thermal response is too fast it can lead to over compensation, which will cause distortion. The ideal case is to use a matched pair with the MOSFET V_{th} and g_m parameters matched within ten percent. However, in the ARF1500's construction, the g_m is controlled and you may compensate for V_{th} characteristics of the devices you have obtained by adjustment of the bias controls. A solid state opto-isolator is connected in parallel with the bias supply circuit to obtain a high speed shutdown function as well as a means to remove bias during receive.

Attenuator Circuit

An attenuator on the input provides gain adjustment overall and improves the input SWR. After considering the total gain requirement, 3 dB was chosen. The attenuator must be able to dissipate 50 W. Thin film power resistors in the rugged TO-220 heat sink package were used in this experimental model. Even with all the efforts with feedback and the input attenuator, the input SWR was still unacceptable on 10 m. We added a 10-m impedance matching section inserted by relay between the attenuator and input transformer T1. It is switched at the same time as the 10-m low-pass filter.

Output Harmonics Filter

To remove the unwanted harmonics, six low-pass filters follow the PA stage. Five-element Chebyshev low-pass filters and five-branch elliptic filters were satisfactory for this purpose. Design data are available in the *ARRL Handbook*, *IRE Transaction on Circuit Theory 1958*, and other references.

Final adjustment and trimming of LPF elements are usually required to obtain the best results.

1) To optimize the output power and efficiency.

2) To keep the harmonics within the FCC limits.

3) To keep the in-band output power flatness reasonable.

LPF capacitor elements should be carefully selected for the working voltage and currents. In our experimental model, newly developed chip mica capacitors with 1,000 V rating were used. (These are from Soshin Electric, Japan.)

Printed Circuit Board

The PC board used is glass epoxy, double sided with 1-oz copper foil (4 mil, 105 μm thickness). In designing the circuit pattern, one should carefully design with regard to both RF loss and dc resistance. The island area for source

leads should be as large as possible. The back side should be a continuous ground plane to achieve the maximum amplifier stability.

Heat Sink Design

An aluminum heat sink with a thermal

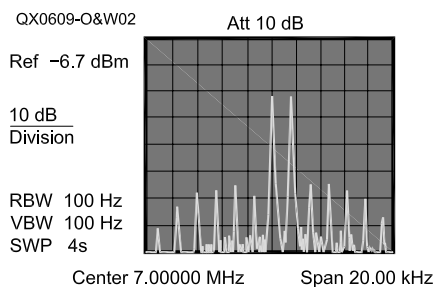


Figure 2 — This spectrum analyzer photo shows the IMD performance of the amplifier.

Test Diagram

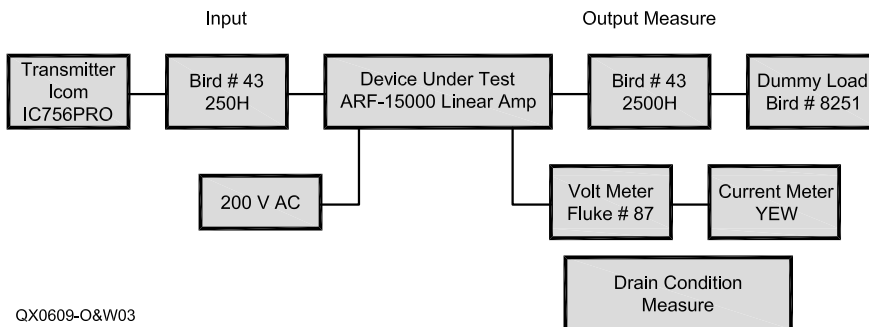


Figure 3 — This diagram shows the test-equipment setup used to measure the performance of the ARF-1500 amplifier.

Table 2
ARF-1500 Linear Amplifier Characteristics
Frequency versus P_{in} - P_{out} Characteristics

Frequency	1.8 MHz	3.5 MHz	7 MHz	10 MHz	14 MHz	18 MHz	21 MHz	24 MHz	28 MHz
Input Power (W)									
10	230	220	220	220	250	280	340	200	300
20	440	400	400	420	490	500	600	380	600
30	638	580	540	650	720	730	860	550	800
40	800	750	700	850	880	950	1050	700	980
50	950	897	850	1000	1060	1080	1250	850	1120
60	1100	1030	990	1160	1220	1200	1400	950	1230
70	1220	1150	1150	1350	1350	1300	1550	1070	1320
80	1310	1280	1300	1600	1520	1480	1700	1200	1430
90	1350	1380	1470	1800	1650	1600	1800	1300	1500
100	1400	1470	1600	2050	1800	1750	1980	1450	1600
Output Power (W)									

Table 3
ARF-1500 Linear Amplifier Characteristics, 1.8 MHz

Input Power (W)	Output Power (W)	Drain Voltage (V)	Drain Current (A)	Drain Input (W)	Efficiency (%)	Drain Dissipation (W)
0	0	127.3	0.6	76.38	0	76.38
10	230	117	7.4	866	27	636
20	440	114	10	1140	39	700
30	638	110	12.6	1386	46	748
40	800	109	14	1526	52	726
50	950	108	16	1728	55	778
60	1100	106	17.8	1887	58	787
70	1220	105	19.5	2048	60	828
80	1310	104	21	2184	60	874
90	1350	103	22.5	2318	58	968
100	1400	101	24.5	2475	57	1075

resistance of 0.05°C/W is forced-air cooled by a high-pressure muffin fan. The sink's tight-pitch bonded fins are relatively thin and a 9-mm ³/₈-inch) thick copper heat spreader is used between the transistors and the alu-

minum heat sink. (Sink area = 170 × 100 mm, 6.7 × 4 inch.)

DC Power Supply

DC power is provided by a simple unregu-

lated supply consisting of a hypersil type transformer, rectifier, and capacitor filter. Because the FETs have a 500-V breakdown voltage spec, we have plenty of voltage margin, so a regulated supply was not required

Table 4
ARF-1500 Linear Amplifier Characteristics, 3.5 MHz

<i>Input Power (W)</i>	<i>Output Power (W)</i>	<i>Drain Voltage (V)</i>	<i>Drain Current (A)</i>	<i>Drain Input (W)</i>	<i>Efficiency (%)</i>	<i>Drain Dissipation (W)</i>
0	0	127.3	0.6	76	0	76
10	220	117	7.6	889	25	669
20	400	113	10.8	1220	33	820
30	580	111	13.2	1465	40	885
40	750	109	15	1635	46	885
50	897	107	16.5	1766	51	869
60	1030	105	18	1890	54	860
70	1150	105	19.4	2037	56	887
80	1280	104	20.8	2163	59	883
90	1380	103	22	2266	61	886
100	1470	102	23.2	2366	62	896

Table 5
ARF-1500 Linear Amplifier Characteristics, 7 MHz

<i>Input Power (W)</i>	<i>Output Power (W)</i>	<i>Drain Voltage (V)</i>	<i>Drain Current (A)</i>	<i>Drain Input (W)</i>	<i>Efficiency (%)</i>	<i>Drain Dissipation (W)</i>
0	0	127.3	0.6	76	0	76
10	220	115	8.9	1024	21	804
20	400	112	12	1344	30	944
30	540	109	14.9	1624	33	1084
40	700	107	16.8	1798	39	1098
50	850	105	18.8	1974	43	1124
60	990	104	20	2080	48	1090
70	1150	102	21.5	2193	52	1043
80	1300	102	23	2346	55	1046
90	1470	100	24.2	2420	61	950
100	1600	100	25.6	2560	63	960

Table 6
ARF-1500 Linear Amplifier Characteristics, 10 MHz

<i>Input Power (W)</i>	<i>Output Power (W)</i>	<i>Drain Voltage (V)</i>	<i>Drain Current (A)</i>	<i>Drain Input (W)</i>	<i>Efficiency (%)</i>	<i>Drain Dissipation (W)</i>
0	0	127.3	0.6	76	0	76
10	220	114	9.8	1117	20	897
20	420	111	13.2	1465	29	1045
30	650	107	16.3	1744	37	1094
40	850	105	18.8	1974	43	1124
50	1000	103.8	20.5	2128	47	1128
60	1160	102	22.2	2264	51	1104
70	1350	101	24	2424	56	1074
80	1600	99	25.5	2525	63	925
90	1800	99	27	2673	67	873
100	2050	97	28.8	2794	73	744

for this application. The filter capacitor is 18,000 μ F / 160 V. A solid state relay switches the primary ac line and a power thermistor solves the inrush current problem.

Cooling Fan

The high air-volume muffin fan is pow-

ered from the dc drain voltage supply. When the ac switch is turned off, the energy in the filter capacitor is bled off by the cooling fan and works as a delayed off-time cooler.

Protection Circuits

If the heat sink temperature reaches the

maximum limit, the T/R system is shut down by a high-temperature thermostat at 70°C. The amplifier is shut down if the reflected RF power exceeds the limit. (270 W $P_{ref} = 2.49$ SWR) The drain current is an important indicator of the amplifier status. The bias voltage supply is shut down if the drain

Table 7
ARF-1500 Linear Amplifier Characteristics, 14 MHz

Input Power (W)	Output Power (W)	Drain Voltage (V)	Drain Current (A)	Drain Input (W)	Efficiency (%)	Drain Dissipation (W)
0	0	127.3	0.6	76	0	76
10	250	112	10.8	1210	21	960
20	490	109	14.8	1613	30	1123
30	720	105	18	1890	38	1170
40	880	103.9	20	2078	42	1198
50	1060	102	22.2	2264	47	1204
60	1220	100.8	24	2419	50	1199
70	1350	99	25.5	2525	53	1175
80	1520	98.8	27	2668	57	1148
90	1650	97	28.5	2765	60	1115
100	1800	96	29.8	2861	63	1061

Table 8
ARF-1500 Linear Amplifier Characteristics, 18 MHz

Input Power (W)	Output Power (W)	Drain Voltage (V)	Drain Current (A)	Drain Input (W)	Efficiency (%)	Drain Dissipation (W)
0	0	127.3	0.6	76	0	76
10	280	114	12.5	1425	20	1145
20	500	110	16.5	1815	28	1315
30	730	107	20.4	2183	33	1453
40	950	105	22.5	2363	40	1413
50	1080	103	25	2575	42	1495
60	1200	101	26.5	2677	45	1477
70	1300	98.6	28	2761	47	1461
80	1480	98	29.8	2920	51	1440
90	1600	97.8	30	2934	55	1334
100	1750	96	32	3072	57	1322

Table 9
ARF-1500 Linear Amplifier Characteristics, 21 MHz

Input Power (W)	Output Power (W)	Drain Voltage (V)	Drain Current (A)	Drain Input (W)	Efficiency (%)	Drain Dissipation (W)
0	0	127.3	0.6	76	0	76
10	340	113	11.8	1333	25	993
20	600	110	15.8	1738	35	1138
30	860	107	19	2033	42	1173
40	1050	105	21.5	2258	47	1208
50	1250	103	23.2	2390	52	1140
60	1400	101	25	2525	55	1125
70	1550	100	26.5	2650	58	1100
80	1700	99	28	2772	61	1072
90	1800	99	29	2871	63	1071
100	1980	96	30	2880	69	900

current exceeds a certain limit (27 A). This is done using a high speed opto-coupler rather than conventional fuses. The dc supply is

protected by 30-A fuses in case of a short circuit. Since the drain voltage supply is not regu-

lated, the supply cannot shut down easily if drain dc voltage exceeds the limit. With a 500-V limit on the MOSFETs, however, the

Table 10
ARF-1500 Linear Amplifier Characteristics, 24 MHz

Input Power (W)	Output Power (W)	Drain Voltage (V)	Drain Current (A)	Drain Input (W)	Efficiency (%)	Drain Dissipation (W)
0	0	127.3	0.6	76	0	76
10	200	115	10	1150	17	950
20	380	111	14	1554	24	1174
30	550	108	16.7	1804	30	1254
40	700	106	19	2014	35	1314
50	850	105	20.8	2184	39	1334
60	950	103	22.1	2276	42	1326
70	1070	102.7	23.8	2444	44	1374
80	1200	100.6	25.5	2565	47	1365
90	1300	99.6	26.5	2639	49	1339
100	1450	99	28.4	2812	52	1362

Table 11
ARF-1500 Linear Amplifier Characteristics, 28 MHz

Input Power (W)	Output Power (W)	Drain Voltage (V)	Drain Current (A)	Drain Input (W)	Efficiency (%)	Drain Dissipation (W)
0	0	127.3	0.6	76	0	76
10	300	115	10	1150	26	850
20	600	111	13.6	1510	40	910
30	800	109	16	1744	46	944
40	980	107	17.5	1873	52	893
50	1120	106	19	2014	56	894
60	1230	105	20	2100	59	870
70	1320	104	21	2184	60	864
80	1430	103	22	2266	63	836
90	1500	103	22.5	2318	65	818
100	1600	102.8	23	2364	68	764

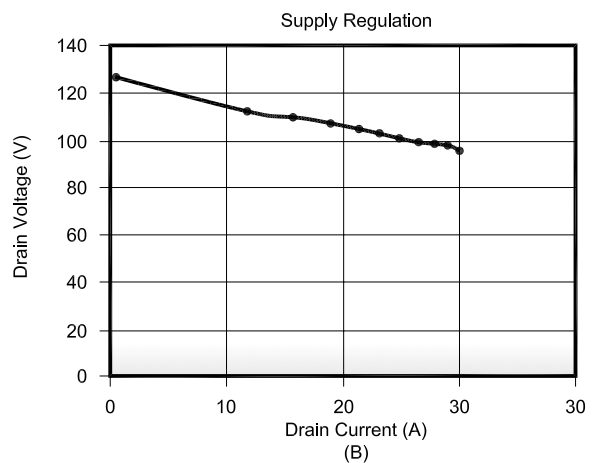
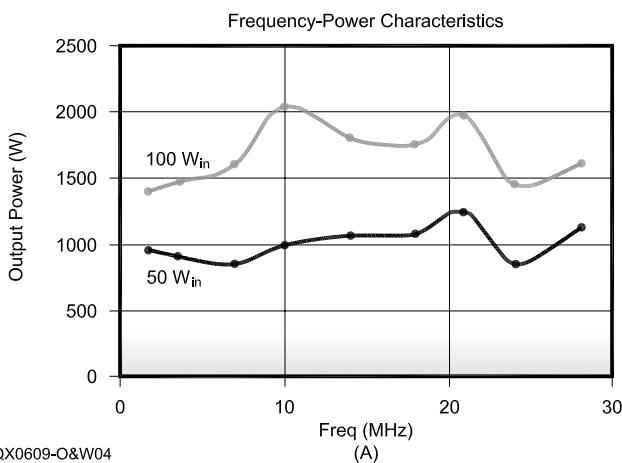


Figure 4 — Part A is a graph of the measured amplifier output power across the amateur bands from 1.8 to 28 MHz. Input powers of 50 W and 100 W are shown. Part B compares the transistor drain current versus drain voltage.

150-V Zener diode clamp is enough to protect the other components from any transient spikes that might come past the supply filtering.

Details of Major Components

T1 Input Transformer

Ferrite core material: Tomita Electric (See

www.tomita-electric.com/enghp or www.tomita-electric.com/pdf/RIB_RIType.pdf), RIB 10 × 21 × 15,

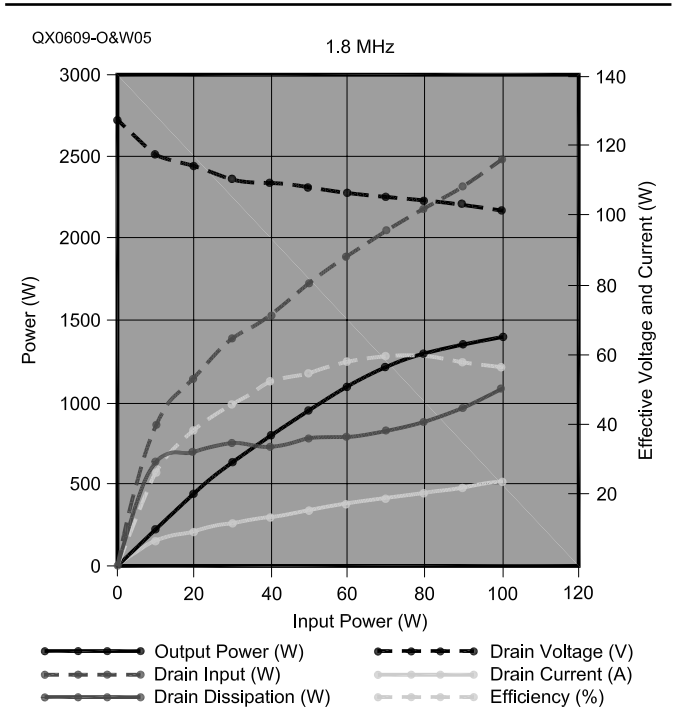


Figure 5 — This graph shows the amplifier characteristics on the 160-m band (1.8 MHz).

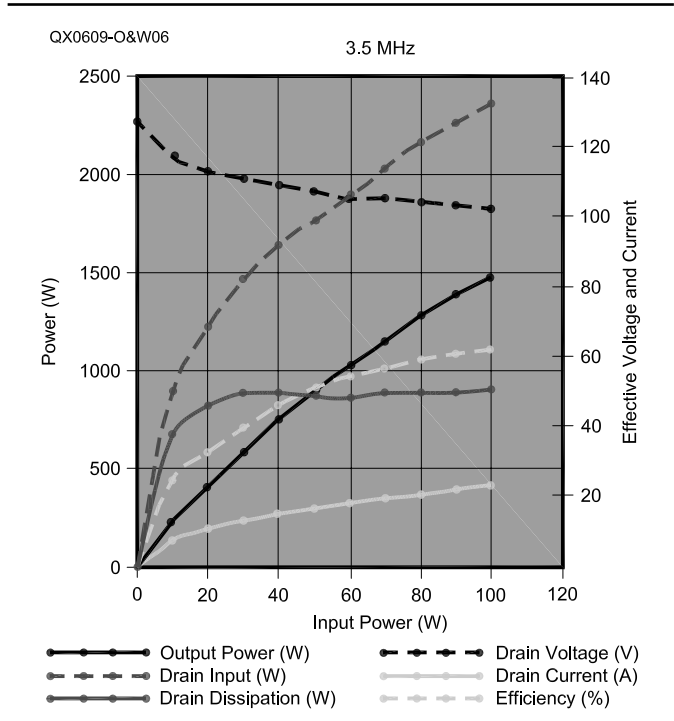


Figure 6 — This graph shows the amplifier characteristics on the 80-m band (3.5 MHz).

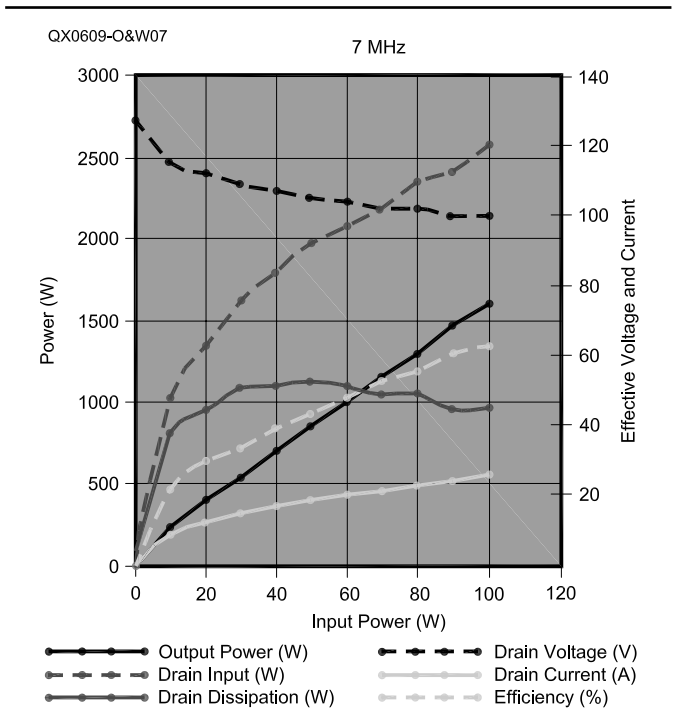


Figure 7 — This graph shows the amplifier characteristics on the 40-m band (7 MHz).

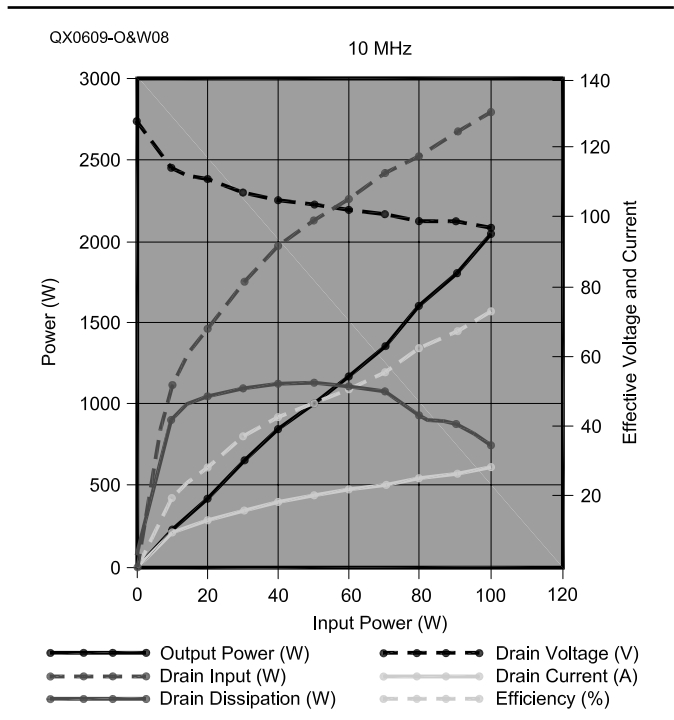


Figure 8 — This graph shows the amplifier characteristics on the 30-m band (10 MHz).

Material D12A, 2-hole balun core.
 Primary winding: 5 turns 0.4 mm diameter (AWG no. 26) Teflon wire.
 Secondary winding: Brass tube 5 mm diameter, 18.5 mm long, 0.3 mm wall.

T2: DC Supply Transformer
 Ferrite core: Tomita RIB 16 × 32 × 16, D12A, 2-hole balun core.
 Drain winding: 4 turns bifilar AWG no. 20 Teflon wire.

NFB winding: Brass tube 8 mm diameter, 21 mm long, 0.8 mm thickness.
T3, T4 Output Transformers
 Ferrite core: Tomita RIB 21 × 42 × 40, D12A, 2-hole balun core.

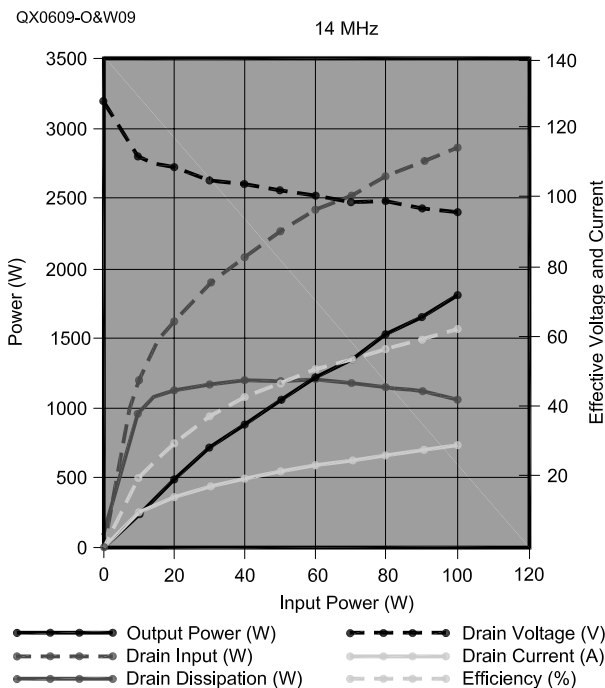


Figure 9 — This graph shows the amplifier characteristics on the 20-m band (14 MHz).

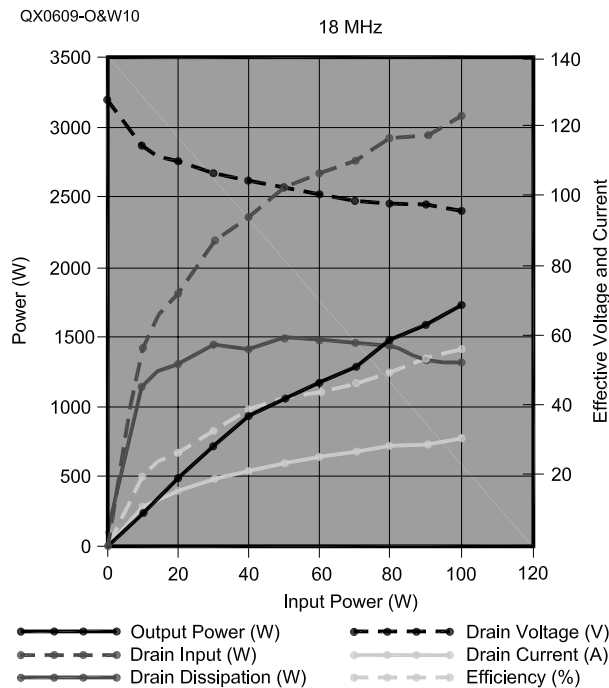


Figure 10 — This graph shows the amplifier characteristics on the 17-m band (18 MHz).

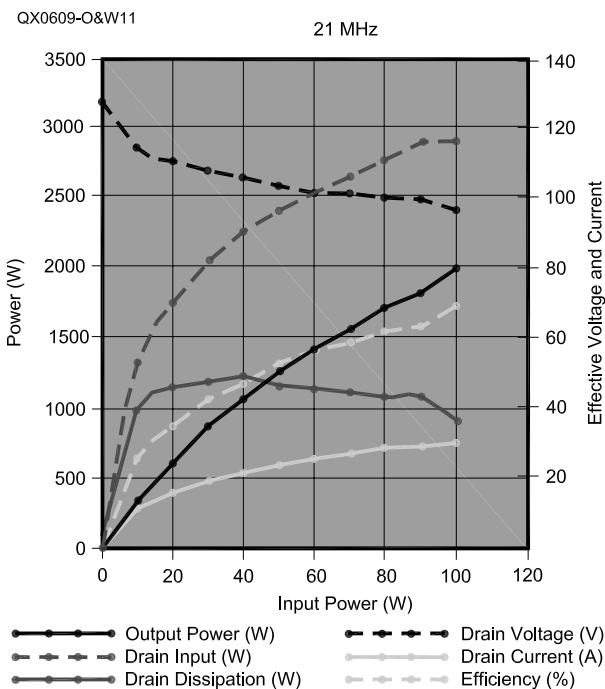


Figure 11 — This graph shows the amplifier characteristics on the 15-m band (21 MHz).

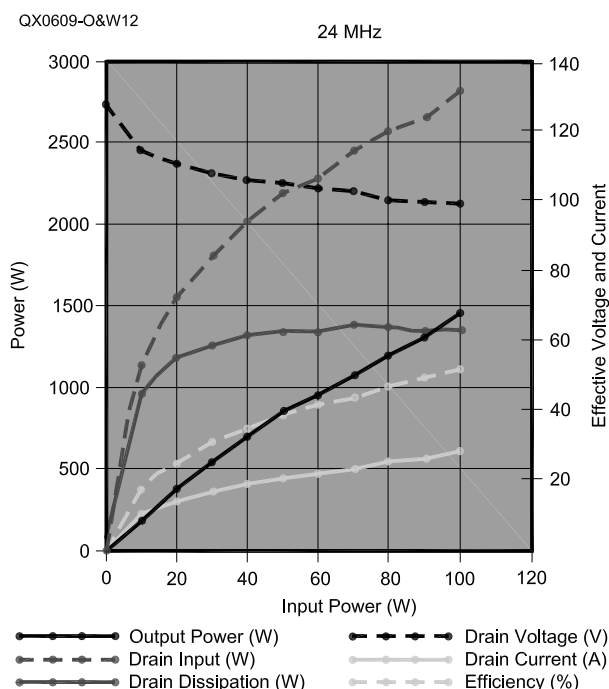


Figure 12 — This graph shows the amplifier characteristics on the 12-m band (24 MHz).

Winding: 3.5 turns of 50 cm long 25 Ω Teflon coaxial cable, DFS014 by Junkohsha, Japan.

T5: Output Balun

Core: 4 pieces Tomita RIB 16 \times 32 \times 16, D12A, 2-hole balun core.
Winding: 2 turns of 50 Ω Teflon coax cable, DFS040 (RG-303).

L2, L3 Choke Coil

Core: Tomita RIB 8 \times 14 \times 13, 4 A material 2-hole bead.
Winding: 1.5 turns of AWG no. 20 Teflon wire.

Capacitors

C3-C6 Input coupling: ATC ceramic chip 900C103MW300.
C9-C14 Output coupling: ATC ceramic chip 900C473MW250.
CC104, all: 0.1 μ F 250 V Murata ceramic chip GHM2145X7R104MAC250.

Conclusion

The circuit described in this article demonstrates a simple 1.5-kW HF amplifier built with a pair of the latest MOSFET devices. Figure 2 shows IMD performance. Table 2 summarizes the input power and output power of the amplifier across the Amateur MF and HF bands. Figure 3 shows the test set-up for the performance measurements we made. Further performance data by band are shown in Tables 3 through 11. Figures 4 through 13 show the corresponding graphs of the performance data.

The authors would like to express a word of gratitude to Mr. Richard Frey, K4XU, and Mr. Bert Butz, DJ9WH, for their kind advice given to us during the experiments.

Notes

¹Helge Granberg, K7ES, "A compact 1-kW 2 - 50 MHz Solid-State Linear Amplifier," QEX, July 1990, pp 3 - 8. (Reprinted as Motorola Application Report AR-347)

²ARF1500 Data sheet, Advanced Power Technology, Inc. www.advancedpower.com.

Toshiaki Ohsawa, JE1BLI, was born in 1956. He graduated from the economics department of Johsai University, Japan in 1978 with a Bachelor's degree in business administration. He is a self-educated electronics and RF communications engineer. A senior research engineer of the research and development department of Tokyo Hy-Power Labs, he is now in charge of developing the pulse RF amplifier for an MRI machine and also a transceiver for NMR studies. Toshiaki has designed a number of power amplifiers during his career. He is an IEEE member and has been a licensed Amateur Radio operator since 1971. He currently holds a Japanese first class Amateur Radio license.

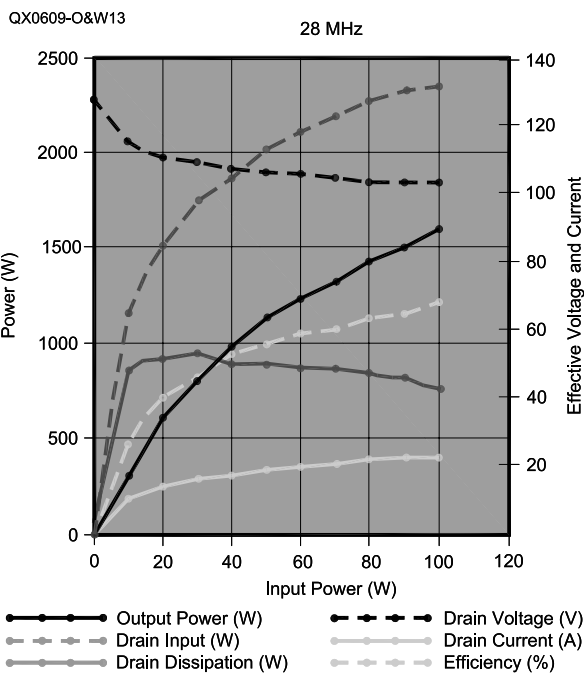


Figure 13 — This graph shows the amplifier characteristics on the 10-m band (28 MHz).

Nobuki Wakabayashi, JA1DJW, was born in 1943. He graduated from the school of engineering, Waseda University, Japan in 1966 with a Bachelor's degree in electrical communications. Nobuki founded Tokyo Hy-Power Labs in 1975 for the purpose of designing accessory items for radio amateurs. He has been President of

Tokyo Hy-Power Labs since 1977. He has designed antenna tuners, HF broadband amplifiers and a 1 kW amplifier using the Eimac 3CX1500A7 triode. He is an ARRL member and has been a licensed Amateur Radio operator since 1959. He currently holds a Japanese second class Amateur Radio license.

QEX

ATOMIC TIME

1010 Jorie Blvd. #332
Oak Brook, IL 60523
1-800-985-8463
www.atomictime.com



ADWA101 - \$49.95

14" LaCrosse Black Wall WT-3143A \$26.95

This wall clock is great for an office, school, or home. It has a professional look, along with professional reliability. Features easy time zone buttons, just set the zone and go! Runs on 1 AA battery and has a safe plastic lens.



WT-3143A - \$26.95




WS-8248 - \$64.95

LaCrosse Digital Alarm WS-8248U-A \$64.95

This deluxe wall/desk clock features 4" tall easy to read digits. It also shows temperature, humidity, moon phase, month, day, and date. Also included is a remote thermometer for reading the outside temperature on the main unit, approx. 12" x 12" x 1.5"

1-800-985-8463
www.atomictime.com
Quantity discounts available!



WS-9412U - \$19.95

Tell time by the U.S. Atomic Clock - The official U.S. time that governs ship movements, radio stations, space flights, and warplanes. With small radio receivers hidden inside our timepieces, they automatically synchronize to the U.S. Atomic Clock (which measures each second of time as 9,192,631,770 vibrations of a cesium 133 atom in a vacuum) and give time which is accurate to approx. 1 second every million years. Our timepieces even account automatically for daylight saving time, leap years, and leap seconds. \$7.95 Shipping & Handling via UPS. (Rush available at additional cost) Call M-F 9-5 CST for our free catalog.

A Simplified GPS-Derived Frequency Standard

Here is a simple and modern approach to a 10-MHz frequency standard.

Bertrand Zauhar, VE2ZAZ

For many reasons, an accurate frequency standard at an Amateur Radio station is desirable. For weak-signal operation such as EME (moonbounce) at microwave

242 Robert-Martial St
Gatineau, Québec J9J 2V1
Canada
ve2zaz@amsat.org

frequencies, you must be transmitting and listening exactly at the right frequency; otherwise the narrow receive filters used will make you miss that weak signal. With such a setup, a 10-MHz frequency reference feeds the frequency synthesizer that generates the radio's operating frequency. An accurate 10-MHz reference is also useful for test equipment adjustment. With an accurate standard, you

can put frequency counters and signal generators on track.

The advent of the Global Positioning System (GPS) has allowed a simplified approach to time and frequency accuracy. Several commercially available GPS receiving units provide a 1 pulse-per-second (pps) signal. This signal typically exhibits a short-term accuracy of ± 1 microsecond (1 ppm or $\pm 1 \times 10^{-6}$).

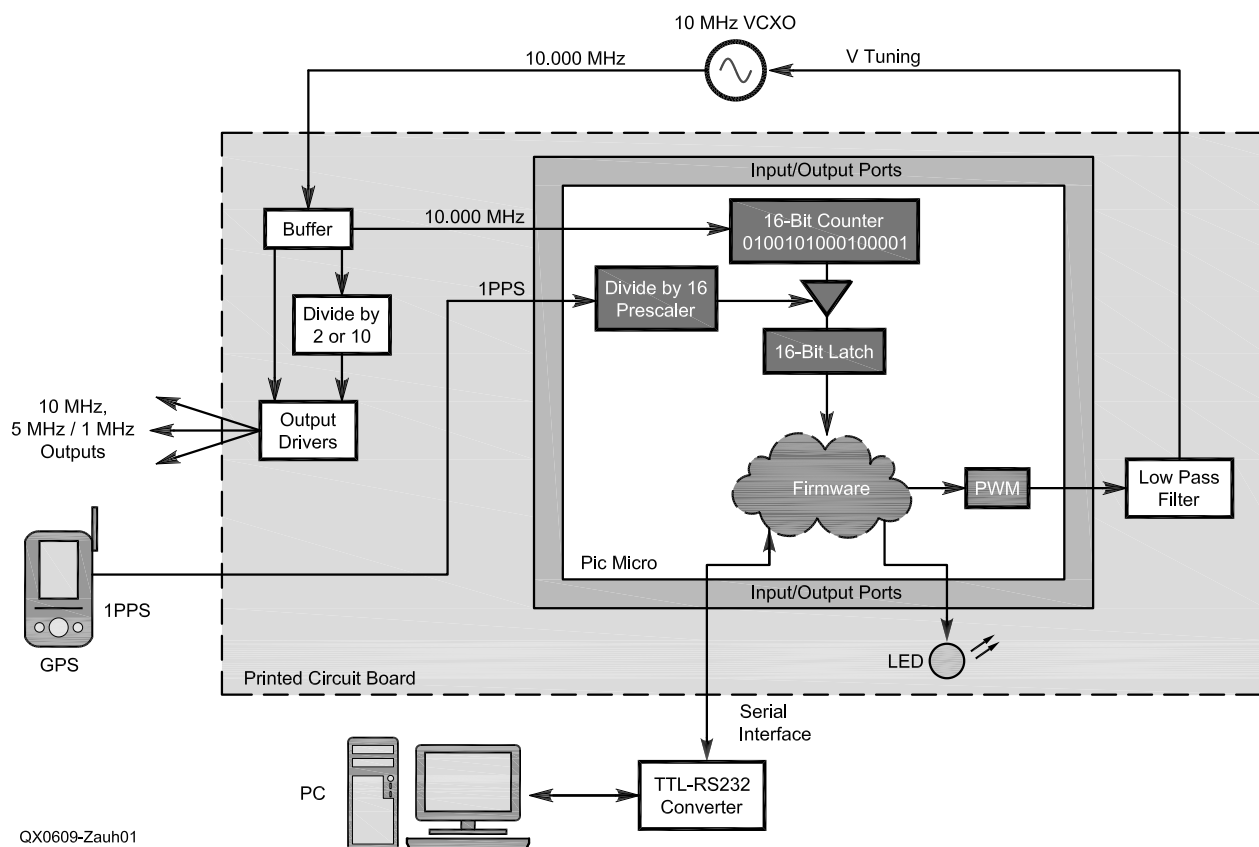


Figure 1 — Block diagram of the GPS-derived frequency standard.

By averaging it over a long period, a much better accuracy can be achieved. This is what this project does: it locks an external 10-MHz voltage-controlled signal source to the 1 pps GPS signal.

The good work of Brooks Shera¹ has generated a lot of interest within a broad community of experimenters who want to increase the level of frequency accuracy available to them at low cost. His system uses a PLL technique to lock an external oscillator to a GPS receiver and obtain an accurate frequency standard.

The project I present here provides a simpler and more modern approach to a ¹Notes appear on page 21.

GPS-derived 10-MHz frequency standard. Improvements found in today's technology offer the following benefits: solid performance, more features and a reduction in the number of components.

This design differentiates itself from other previously published designs because:

- It uses a simpler frequency measurement technique, as opposed to phase measurement.
- It provides on-board reference buffering and fan-out with 50-Ω output impedance.
- It provides the three most common reference frequencies of 10 MHz, 5 MHz and 1 MHz.

- It provides full software control of the frequency acquisition and control processes, without DIP switches.
- It has fewer components and does not require an external DAC or external input counter chips.
- It runs off only one supply voltage: +5 V dc (excluding the VCXO supplies).

Tests have shown that this system consistently produces a short-term reference accuracy in the 1×10^{-10} range. This is derived using standard automotive-grade GPS receivers. That range of accuracy does not rival cesium-based references. It is much better than most of the standard built-in, free-running oscilla-

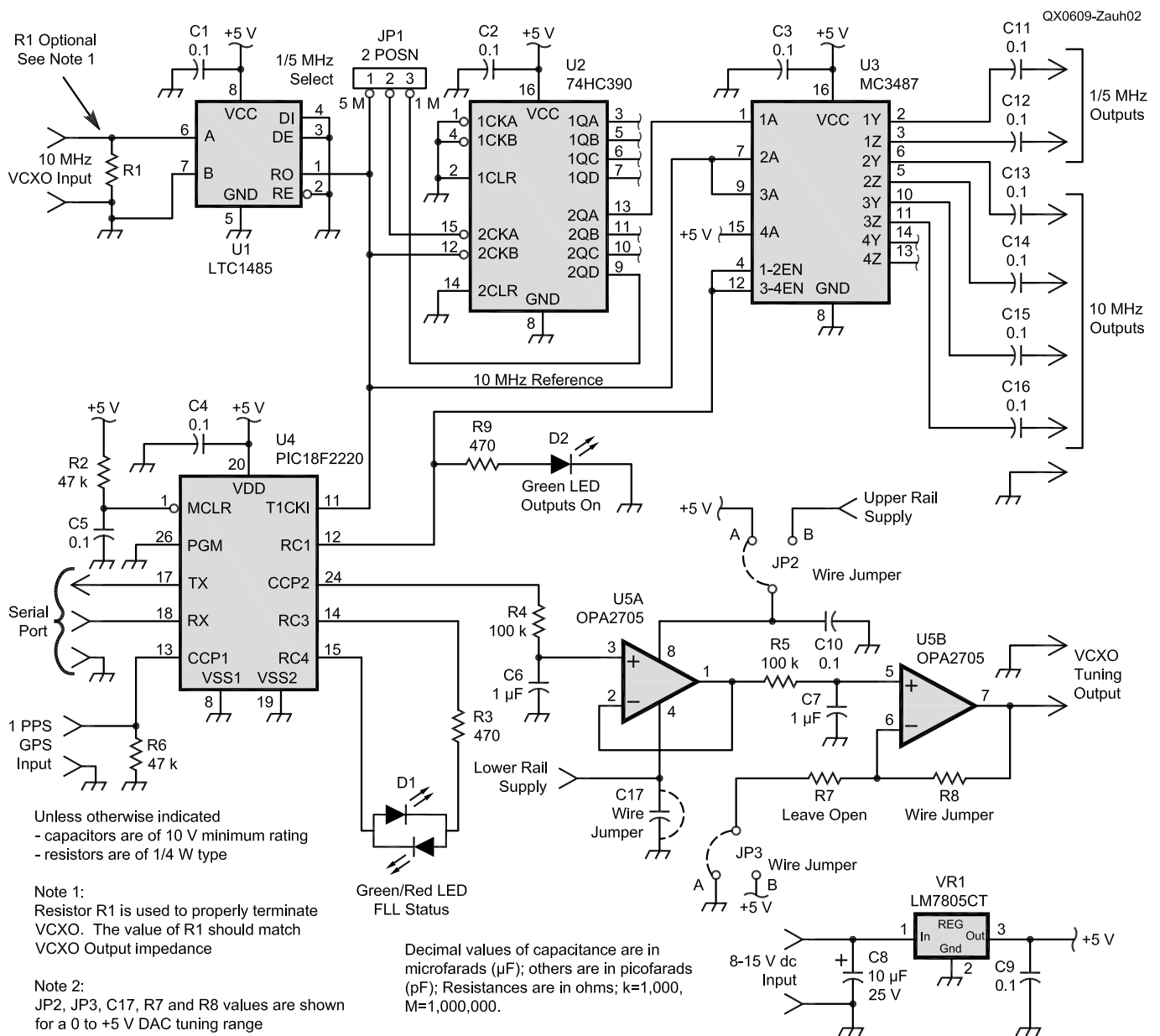


Figure 2 — Schematic diagram of the GPS-derived frequency standard circuit.

tors seen in commercial test instruments, however. Just to give you an idea of the type of accuracy, one part in 10^{10} represents an error of one hertz on a 10 GHz signal!

System Description

Figure 1 shows a block diagram of my GPS-derived frequency standard. The system operates a hardware/firmware frequency-locked loop (FLL). In essence, the system compares a local frequency source (an external oscillator) to a GPS-derived reference. It will adjust the local 10-MHz variable source to match the GPS-derived 1 pps reference. The 10-MHz source is kept aligned with respect to the 1-Hz GPS reference on a real-time basis by the firmware. The resulting 10-MHz reference is fanned out, frequency-divided and provided to the user for high-accuracy applications. System control and monitoring are achieved using a bicolor LED and a serial port connected to a terminal (PC).

Hardware Description

Figure 2 shows the system circuit schematic. The main operation consists of counting the number of rising edges produced by the 10-MHz voltage-controlled crystal oscillator (VCXO) signal over a 16 s period (16 GPS pulses). If the GPS and the VCXO are at the same frequency, exactly 160,000,000 pulses will be counted (± 1 pulse, inherent to counter technology).

Prior to entering the microcontroller, the 10-MHz VCXO signal is buffered and amplified by U1, a receiver chip. An optional input termination resistor R1 can be added if the VCXO's output circuit calls for one. The buffered 10-MHz reference signal is fanned out to several locations on the board.

U4, the Microchip PIC18F2220 microcontroller, has a built-in 16-bit counter incremented by an external source, the VCXO. The counter value is latched by another external signal rising edge, the GPS 1 pps signal in our application. This process is totally autonomous and independent from firmware. The microcontroller's task in this process is to analyze the results and adjust the VCXO frequency accordingly.

VCXO Frequency Control

The Microchip PIC18F2220 microcontroller does not have an integrated digital-to-analog converter (DAC). To produce an adjustable voltage source to vary the VCXO frequency, the built-in 10-bit pulse-width modulator (PWM) is used instead. A continuous rectangular-wave output is produced by the PWM. A downstream external 1-Hz, two-stage low-pass filter (U5A, U5B and discrete components) is used to recover the average dc value of the PWM output. By varying the duty cycle of the PWM, it is possible to produce an accurate analog dc voltage with 2^{10} or 1024 steps over the range.

A DAC of 14-bit resolution is achieved by precisely controlling the duty cycle of the PWM output. This translates to a tuning granularity of 6×10^{-5} Hz for a VCXO that has a 1-Hz tuning range. Achieving a 14-bit DAC using a 10-bit PWM requires additional firmware processing. The idea is to "dither" the pulse width within a 16-cycle window. Those 16 cycles translate into an additional 4-bit resolution. For example, increasing the 14-bit DAC output by one step involves increasing the 10-bit PWM output width by one increment on one of the 16 pulses. Increasing the DAC by two steps means increasing the 10-bit PWM output width by one increment on two of the 16 pulses, and so on.

To add flexibility for interfacing with various VCXOs, the filtering stages have a supply bypass feature that allows you to feed the operational amplifiers with different upper and lower rail voltages. This is done by reconfiguring JP2 and C17. Remember, though, that the maximum voltage difference between upper and lower rails must be kept to 12 V or less. Another feature, the second stage of low-pass filtering, allows for additional gain using R7/R8 if the VCXO operates on a larger tuning voltage range than the more standard 5-V range. A 5-V offset can also be added to the second stage using jumper JP3. This provides support for VCXOs that have a -5 V to $+5$ V tuning range.

Table 1 lists some of the possible configurations on the filtering stages for various VCXO tuning ranges. Finally, the tuning

slope sign can be set in firmware to accommodate both types of VCXOs.

Output References

The system provides up to four 10-MHz reference signals. In addition, it provides up to two references with a selectable frequency of either 5 MHz or 1 MHz. These sub-rates are produced by U2, a synchronous counter. The active sub-rate is selected with an on-board jumper, JP1. All references are of $50\text{-}\Omega$ output impedance and provide an amplitude of greater than 1 V pk-pk with a square wave shape. These signals are provided by U3, a line driver chip.

When the firmware feature is enabled, the reference outputs are inhibited if the FLL goes into its unlocked state. That protection ensures that the user does not use a reference of unknown quality. LED D2 provides an indication of the reference output state.

FLL Status LED

The system provides basic FLL status and alarm conditions with a single bicolor LED (D1). The LED control is designed to allow the user to learn about the current and past FLL status in a lapse of a single second. Being a combined green/red LED pair in a single package, it can produce three colors: green, red and amber. The latter is produced when both green and red LEDs are simultaneously on. Additionally, the LED unit will flash at a 1-Hz rate to provide a 1 pps signal sanity check.

Serial Port

Since the FLL status LED only provides basic FLL status and alarm, a serial port is also implemented. The serial port provides comprehensive control and monitoring of the FLL and other firmware features. When interfaced through a TTL-to-RS232 bidirectional converter, the serial port will connect to a personal computer RS-232 port. Such a converter can be easily assembled using a couple of transistors or can be made using Maxim's MAX23x series of conversion chips. The Internet has several simple circuits documented. It can also be purchased "off-the-shelf."

The serial port is ASCII-character-based

Table 1
Tuning Range Configuration

VCXO Tuning Range	R7	R8	C17	JP2 Upper Rail	JP3 Offset
0 to +5 V	Leave Open	Jumper wire	Jumper wire	Position A	Leave Open
0 to +8 V *	100 k	62 k	Jumper wire	Position B	Position A
0 to +10 V *	100 k	100 k	Jumper wire	Position B	Position A
-5V to +5 V **	100 k	100 k	0.1 μ F	Position A	Position B

*External positive supply required.

**This configuration is used with the HP 10544/10811 series OCVCXO's. External -5 V supply required.

and provides standard status text strings that can be captured and analyzed by the user. The serial port also interprets a series of user commands to control the FLL and other firmware features. Additional information on the text strings and user commands can be found on my Web site.²

+5 V dc Voltage Regulator

To guarantee a stable and clean voltage supply to the board, a separate +5 V dc fixed voltage regulator, VR1, is used. A heatsink is required on the regulator since the board could potentially draw close to 200 mA when all reference outputs are terminated. This would make the voltage regulator excessively hot without a heatsink.

External VCXO

System performance is set to a large degree by the external 10-MHz VCXO selected for this design. It is recommended that an oven-controlled VCXO (OCVCXO) be used to provide better short term stability. Good, second-hand Hewlett-Packard OCVCXOs are readily available on eBay.³ These should be your primary targets.

This project has been tested and proven with OCVCXOs that have a 1-Hz or a 10-Hz tuning range over their entire control voltage. Different tuning slopes may require different firmware parameter settings to achieve optimum performance. The user will want to experiment with these.

GPS Receiving Unit

The GPS receiver used on this system must have a 1 pps TTL-compatible output signal. Accuracy of this signal will influence overall accuracy of the system. Typical accuracy seen on automotive-grade units is in the order of 1 microsecond (1×10^{-6} s) and this is satisfactory for our application.⁴

This design has been tested with the Garmin GPS-35 and the Motorola Oncore GT+ GPS receivers. Both meet the above-mentioned accuracy. The Motorola Oncore GT+ unit is actually specified as having a somewhat better accuracy on the 1 pps output. This did not materialize in better overall system accuracy during evaluation. In fact, the second-to-second "jitter" on the 1 pps

signal happened to be greater than on the Garmin GPS-35, while still meeting the above specification. This jitter gets averaged out, though, by the FLL since many frequency samples are taken before making a VCXO frequency correction.

For better accuracy, I recommend setting the GPS unit to fixed-position (position-pinning) mode. In this mode, the GPS firmware assumes a fixed location. This translates into a more accurate 1 pps signal. Consult the GPS unit documentation for more details on how to set the GPS unit to this mode.

Printed Circuit Board

I designed a double-sided circuit board to integrate the hardware.⁵ Figure 3 shows a top view of the circuit board assembly. Its dimensions are 2.8×3.5 inches. IC sockets are optional, but recommended. This is especially applicable to the microcontroller. A fine-tip soldering iron should be used. I am making the circuit board design files available to the public.⁵

The user may elect to build the circuit using other techniques such as breadboard and point-to-point wiring. The layout is not that critical. Care should be taken in proper dc supply decoupling near the integrated circuits.

Firmware Description

The firmware running on the PIC microcontroller was written in assembly language. It is well documented in the source file. Both the firmware source code and the assembled hex code can be downloaded from my Web site.⁶ (Also see Note 2.) Once assembled, the hex code takes about 3 kbytes of flash memory space.

FLL Acquisition and Control Cycle

A simplified FLL acquisition and control cycle flow chart is shown in Figure 4. The process starts from the left hand side and repeats indefinitely as long as the FLL is enabled. The firmware samples the 10-MHz VCXO signal for a duration of 16 seconds. Based on how close the sample is to the nominal frequency,

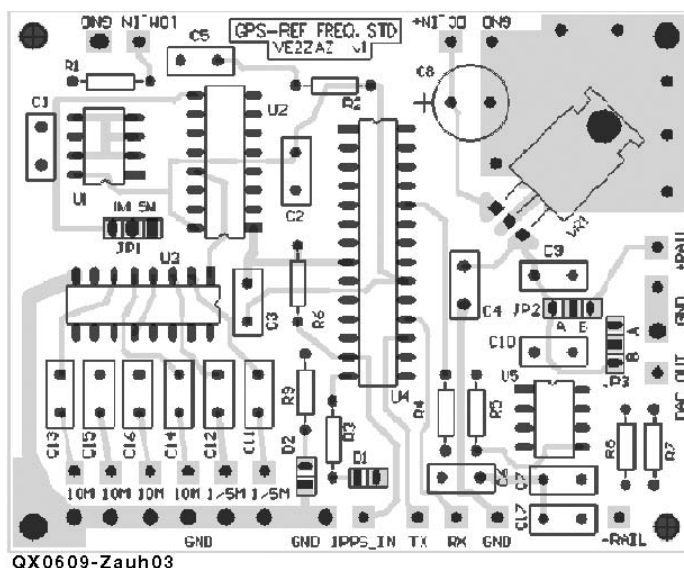


Figure 3 — Circuit board pattern for the GPS-derived frequency standard.

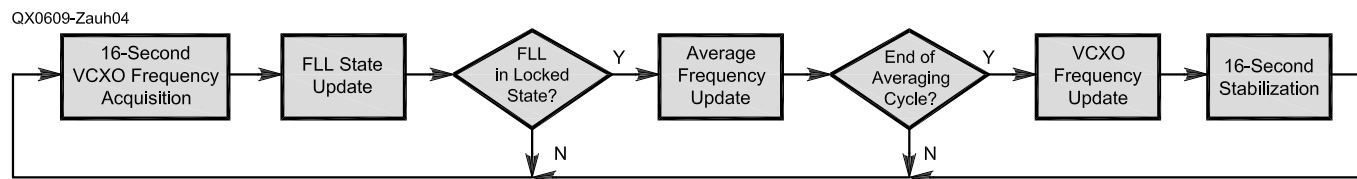


Figure 4 — FLL acquisition and control cycle.

it will update the FLL state. If the sampled frequency is within the specified limits, the firmware will add the sample to the average frequency calculation. Otherwise, it will drop the sample and start another sample acquisition.

After updating the average frequency, the firmware verifies if the frequency averaging cycle has reached the specified number of samples. If it has, the DAC output is updated to reflect the required VCXO frequency change based on the calculated average frequency. Otherwise, the firmware simply starts another sample acquisition.

Whenever the DAC output value is changed, a 16-second pause is inserted to allow the VCXO to stabilize before the next frequency averaging cycle begins.

FLL States and Transitions

Figure 5 illustrates the various states and transitions seen during FLL operation. Under normal “stabilized” conditions, the FLL will be in locked state, with occasional transitions to holdover state to reject GPS receiver timing impairments. The unlocked state is seen at system startup or if the holdover state extends for too long. Finally, the disabled state is initiated by a user command and essentially disables the FLL. In this mode, the FLL merely maintains the last valid DAC voltage.

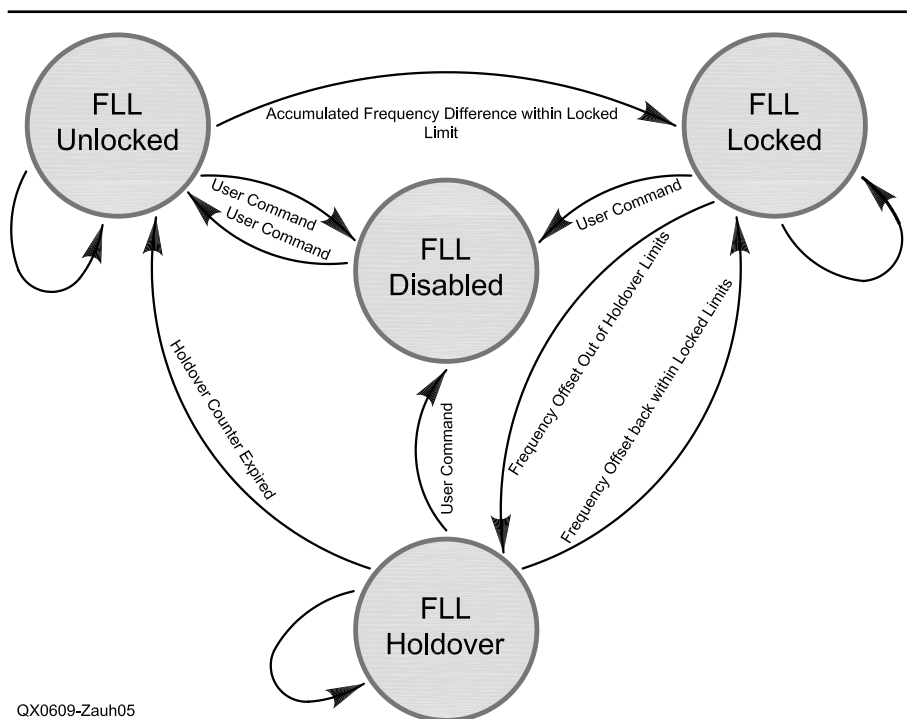
The current FLL state can be clearly identified in the FLL text string sent over the serial port every 16 seconds. It can also be found by assessing the LED color: green for locked, amber for holdover, red for unlocked and disabled. These colors indicate the relative reliability level of the 10-MHz reference output.

Frequency Averaging Modes

Two averaging modes are available to the user. I named them summing mode and voting mode. The summing mode is more effective when the frequency averaging cycle is shorter, for example five minutes. This mode will be helpful in acquiring a lock at a faster pace. The voting mode allows the detection of a trend and is more effective when the frequency averaging cycle duration is large, for example greater than 30 minutes. This mode will be helpful with GPS units that put out a 1 pps signal with significant second-to-second jitter, as the FLL does not care about the size of the frequency difference, but merely the sign. Tests have also shown that this mode yields the best accuracy. The voting mode should be used in conjunction with long frequency averaging cycles. There are more details on how these modes operate in the user manual.

Operation

At power up, the system will display a start-up prompt at the serial port, including firmware version. It will then reload the previously saved FLL parameter settings from



QX0609-Zauh05

Figure 5 — FLL states and transitions diagram.

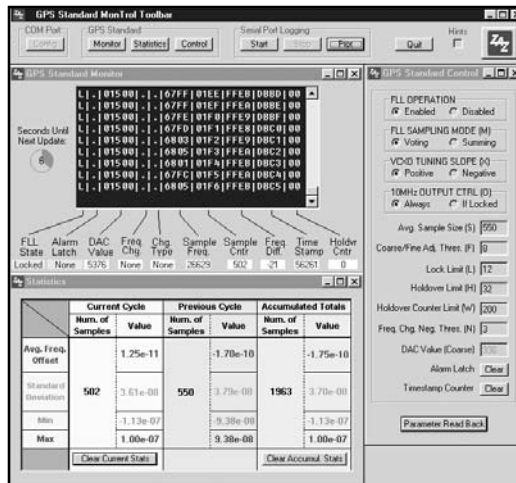


Figure 6 — The Windows GPS Standard MonTrol software provided by the author.

data flash memory. If the microcontroller is powered up for the first time after programming, default parameter values will load.

A few parameters must be set by the user via user commands, because different GPS receivers and different VCXOs require different parameter values. Parameters such as the number of samples taken before updating the VCXO frequency, the number of samples allowed while in holdover state and the tuning slope sign of the VCXO must be set. A detailed description of each of these parameters is included in the systems user manual available on my Web site (see Note 2).

The system FLL will start from the un-

locked state and will try to acquire frequency samples automatically. VCXO frequency adjustments will be made at the end of each averaging cycle. After a period that may span from minutes to hours, the system will transition to locked state. Once the system is set up and in locked state, it should require little maintenance.

Every 16 seconds, and under any circumstances, the firmware sends a status string that provides detailed information on the FLL acquisition process and alarm condition. An example of such status string is shown here:

L|U|01FF6|+|F|67FC|0120|FFFD|007D|03

The definition of each field in the status string is available in the system user manual.

The user will want to accelerate the initial acquisition process by manually tuning the FLL closer to the target DAC value that yields a GPS-to-oscillator lock. This is achieved by zero-beating the 10-MHz oscillator to another known-good reference. The NIST WWV/WWVH or NRC CHU shortwave radio stations are good sources to achieve this.

Once the system is stabilized, the user can increase the averaging cycle duration. The longer the sampling cycle, the more accurate the frequency measurement will be. A typical longer sampling cycle will last from one to four hours. This means that the system will accumulate frequency errors for this period before making a VCXO frequency change. With a good and stable VCXO, the averaging cycle can be made even longer. This will improve system accuracy even further.

To make the man/machine interface even more friendly, I have created a Windows program to monitor and control the system. A snapshot of the software screen is shown in Figure 6. The compiled Windows software is available for download on my Web site.

Results

Figure 7 shows an FLL acquisition phase. The graph illustrates the VCXO DAC value

as a function of time. Initially, the DAC value was intentionally set 0.1 Hz below the nominal value to highlight the acquisition process. The averaging cycle was set relatively short at five minutes between DAC value updates. The

horizontal portion of the curve indicates that the system reached an equilibrium. Under these conditions, the system is considered to be stabilized. At this stage, though, ultimate accuracy may still not be achieved, since long av-

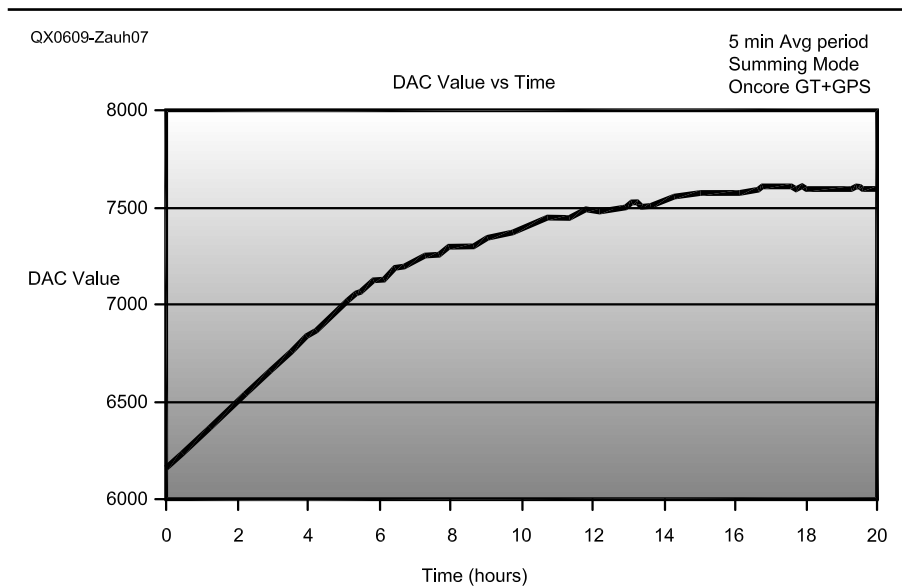


Figure 7 — DAC behavior during FLL frequency acquisition.

Table 2
Parts List

Component Reference	Description	Part Number
C1-C5, C9-C16	0.1 μ F, 10 V or higher, radial	Digikey: 478-2472-ND or equiv.
C17	Piece of wire for a 0-5 V VCXO tuning range.	
	0.1 μ F, 10 V or higher, radial for some other ranges. See text.	Digikey: 478-2472-ND or equivalent.
C6, C7	1 μ F, 10 V or higher, radial	Digikey: 478-2479-ND or equiv.
C8	10 μ F, electrolytic, 25 V or higher	Digikey: P1176-ND or equiv.
D1	Bicolor (Green-Red) LED, two leads.	Digikey: MV6461A-ND or equiv.
D2	Green LED	Digikey: MV5477C-ND or equiv.
JP1	1 \times 3 Header, 0.1 inch spacing, One computer jumper required.	Digikey: S1012-36-ND. Cut to size, or equiv.
JP2	Piece of wire. Selects upper operational amplifier rail. See text.	
JP3	Piece of wire. Adds -5 V offset. See text.	
R1	51 Ω , $\frac{1}{4}$ W, axial. Optional. See text.	Digikey: P51BACT-ND or equiv.
R2,R6	47 k Ω , $\frac{1}{4}$ W, axial	Digikey: P47KBACT-ND or equiv.
R3, R9	470 Ω , $\frac{1}{4}$ W, axial	Digikey: P470BACT-ND or equiv.
R4, R5	100 k Ω , $\frac{1}{4}$ W, axial	Digikey: P100KBACT-ND or equiv.
R7	Optional, do not populate for a 0-5 V VCXO tuning range. See text.	
R8	Piece of wire for a 0-5 V VCXO tuning range. See text.	
U1	Linear Technology LTC1485, DIP-8 package	Digikey: LTC1485CN8-ND
U2	74HC390, DIP-16 package	Digikey: 296-9199-5-ND
U3	MC3487, DIP-16 package	Digikey: 296-1408-5-ND
U4	Microchip PIC18F2220, DIP-28/0.3 inch package, programmed part 5	Digikey: PIC18F2220-I/SP-ND
U5	Texas Instruments OPA2705, DIP-8 package	Digikey: OPA2705PA-ND
VR1	7805 Voltage Regulator, TO-220 package	Digikey: LM7805CT-ND
Sockets for:		
U1, U5	IC Socket, 8-pin, 0.3 inch spacing, low profile, optional	Digikey: ED3108-ND or equiv.
U2, U3	IC Socket, 16-pin, 0.3 inch spacing, low profile, optional	Digikey: ED3116-ND or equiv.
U4	IC Socket, 28-pin, 0.3 inch spacing, low profile, recommended	Digikey: ED3128-ND or equiv.
Heat sink for VR1	TO-220 Compact Heat sink, recommended	Digikey: HS107-ND or equiv.

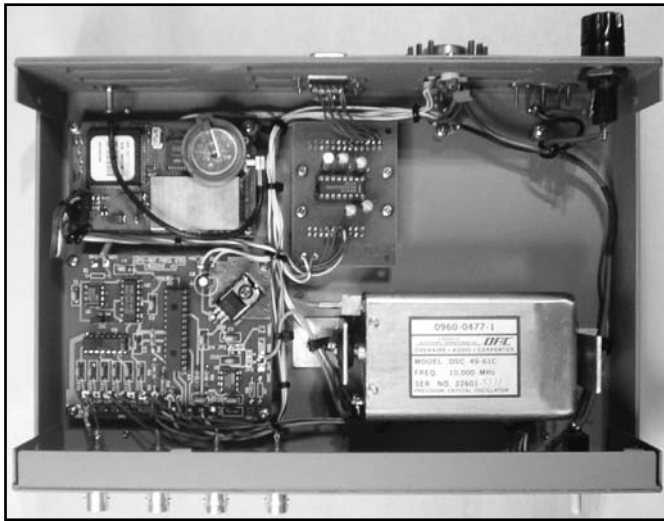


Photo A — The complete frequency standard system integrated into an enclosure. The unit at the top left corner is the GPS board. The bottom-left unit is the FLL controller board and the oven controlled variable crystal oscillator is at the bottom right. The RS232 converter chip and related circuitry is on the board shown at the top center. Also shown in the top-right corner is an 8 V regulator and dc input fuse holder.



Photo B — This photo shows the GPS derived frequency standard connected to an HP frequency counter.

you will be able to assemble and own this high-accuracy 10-MHz standard for less than \$200 US, including VCXO and GPS receiver. This represents a tiny fraction of the cost of atomic-based systems. While using it, you will also learn a lot about frequency accuracy, stability and related measurement techniques. You will no longer have doubts about your transmitted frequency or your frequency counter reading!

Notes

- ¹B. Shera, W5OJM, "A GPS-Based Frequency Standard," *QST*, Jul 1998, p 37.
- ²I maintain a Web site where I provide updates to the project, a detailed user manual, source files and additional comments. Please visit www3.sympatico.ca/b.zauhar for more details.
- ³Look for HP10544A, HP10544-xxxxx, HP 10811A or HP 10811-xxxxx Crystal Oscillator units. These units differ one from the other in their stability and tuning range, but all of them should work in our application. Expect to pay around \$80 for a working unit when purchased on eBay.
- ⁴GPS receivers that provide a 1 pps signal can commonly be found new on eBay for less than \$50. These are OEM versions without display. On such units, settings are entered via a serial port.
- ⁵I distribute high quality, fully-etched bare circuit boards for this project. Please contact me via e-mail if you are interested in purchasing a circuit board. I am also making the circuit board layout files available as PDF files on my Web site. Printing them at a 1:1 scale will give accurate printouts. The layout is made in such a way that component leads pass the signals from one layer to the other. In the case of a hand-made circuit board, all component leads and wires should then be soldered on both sides of the board.
- ⁶For those of you who cannot program Microchip PIC18F series microcontrollers, I make pre-programmed PIC micro-

QX0609-Zauh08

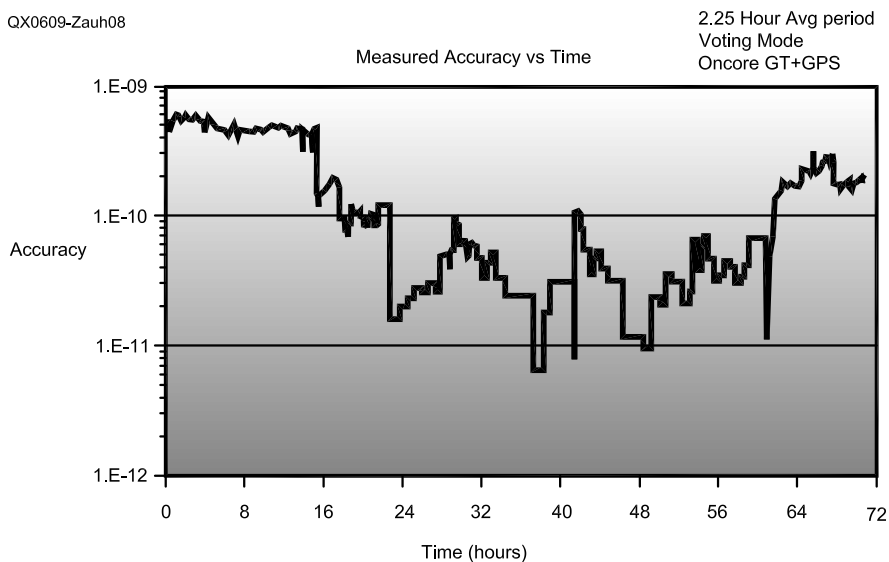


Figure 8 — Frequency accuracy for a 72-hour period.

eraging cycles and fine DAC adjustments are required to achieve higher accuracy.

Figure 8 shows the measured system accuracy as a function of time for a 72-hour period. The reference I used for this comparison is Canada's CHU atomic time radio station.⁷ The graph shows frequency accuracy as a function of time. From the graph, we can conclude that rubidium-like accuracy can be reached, but cannot be guaranteed. This is due to several

factors. One of them is OCVCXO stability over time, voltage, temperature and vibration. When shooting for atomic-like accuracy, the slightest disturbance on the VCXO will make it shift in frequency. This is why I believe that it is difficult to obtain an accuracy better than the 10^{-10} range on OCVCXO-based systems.

Conclusion

Assuming a reasonably stuffed junkbox,

controllers available for purchase. Please contact me via e-mail for more details.

⁷I use the carrier frequency of the 14.670 MHz CHU atomic time radio station for frequency measurement purpose. I basically add (zero-beat) a signal generator synchronized off the GPS-derived 10-MHz standard with the CHU signal into a short-wave receiver. From the duration between two signal nulls, I derive the frequency difference. I compute accuracy using the following formula: Accuracy = $1 / (T_{\text{null-null}} \times 14.67 \times 10^6)$. The National Research Council of Canada maintains three atomic clocks, and the CHU carrier frequency is derived from them. Carrier frequency accuracy is guaranteed at 5×10^{-12} or bet-

ter. I am fortunate to live about 15 km from the transmitters. With such a small station-to-station distance, the propagation mode is ground wave and most certainly surface wave. Since surface wave propagation is very stable (no phase distortion), I can consider the received CHU carrier frequency (and phase) to be virtually as good as the 5×10^{-12} they guarantee at their antenna, and at least one order of magnitude better than the level of accuracy I am trying to measure.

Bertrand Zauhar has been a radio amateur as VE2ZAZ since 1984. He holds an advanced amateur license. Bertrand has

designed for the hobby, amongst other things, an L-band transmit converter (Amsat Journal, May/June 2003), a 1 to 12 GHz frequency counter prescaler, a microprocessor-based repeater controller, several amateur satellite antennas and a RF-sensing alarm (73-Amateur Radio, May 1998). Bertrand received his Electronics Engineering degree in 1989 from École Polytechnique de Montréal. Since then, his professional engineering career has been spent working for Nortel at the Montréal and Ottawa locations. In his current position, he is an electronics hardware design engineer on optical transmission equipment.



Celebrate 25 Years of Digital Innovation!



Come to Tucson, Arizona for the 2006 TAPR/ARRL Digital Communications Conference, September 15-17 at the Clarion Airport Hotel. Join with your fellow hams to celebrate the 25th anniversary of the founding of Tucson Amateur Packet Radio, the group that pioneered amateur digital innovation.

Learn about new digital modes, see live demonstrations and share in the camaraderie that is unique to Amateur Radio. Bring your family, too. Tucson is a desert oasis of beauty and fun!

See the Digital Communications Conference site on the Web at www.tapr.org/dcc/, or call TAPR at 972-671-8277 to make your reservations today.



Installing Vertically Polarized Yagis in the T-Mount Configuration

Getting full performance from that new Yagi? The answer may depend on how you mounted it.

Rick Littlefield, K1BQT



Introduction

T-mounting is a term that describes the practice of installing a vertically polarized Yagi atop a vertical mast. See the lead photo. The practice is commonplace, but it's

probably not a good idea unless steps are taken to decouple the array from its support mast and feed line drop. This article describes what goes wrong and what you can do to fix it.

Impact on SWR

Many hams and commercial installers regard the vertical "T" as an acceptable alternative to end mounting or lateral

stacking for longer Yagis. But, is it really? To measure the actual impact, I ran a series of controlled backyard tests using a Cushcraft 13B2. I positioned this test antenna with the reflector 5 feet off the ground on an end mount with the boom pointing skyward, as shown in Figure 1.

I fed the 13B2 using 25 feet of low-loss foam FEP RG-58U with ten movable 1-inch, 43-mix ferrite sleeves installed over the

109A McDaniel Shore Drive
Barrington, NH 03825
k1bqt@usadatanet.net

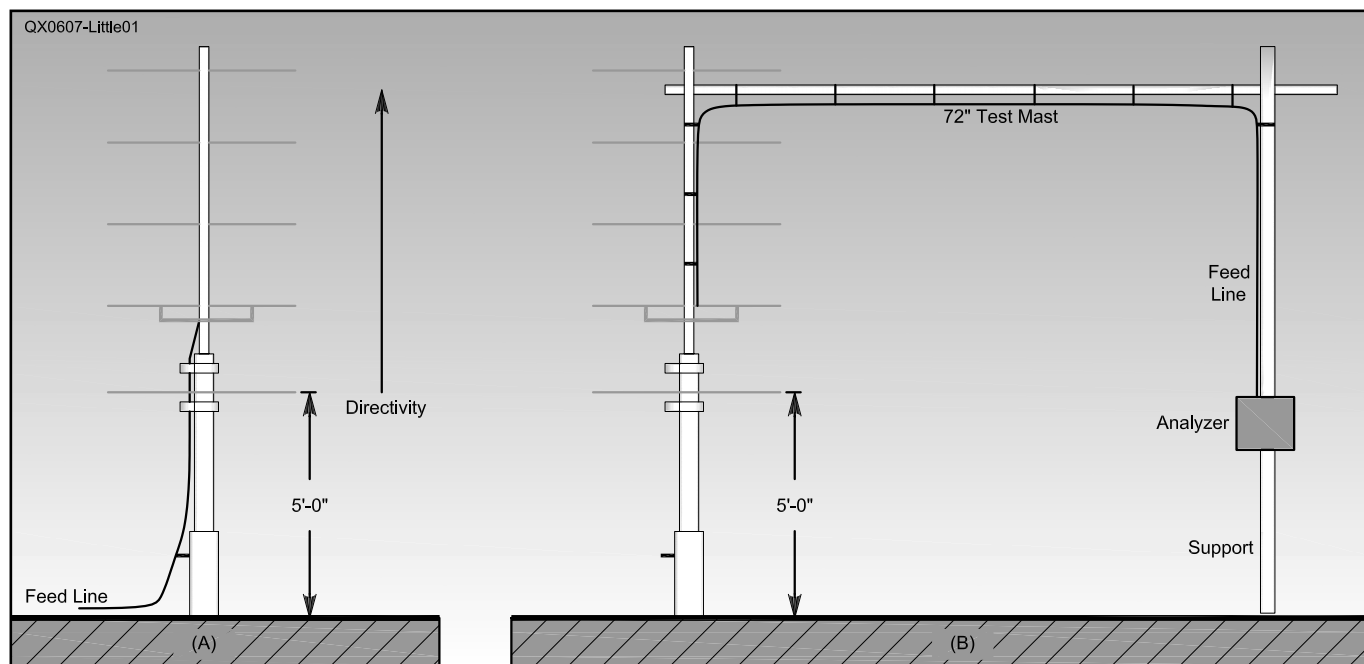


Figure 1 — Test fixture used to test various mast and feed line configurations.

jacket. SWR data for each trial was plotted graphically using an AEA 140-525 handheld analyzer. Two 6-foot test masts were prepared — one being a 1¼ inch aluminum pipe and the other a nonconductive PVC pipe. A wood pole was installed five feet away to support the far end of these test masts. See Figure 2 for SWR plots resulting from my trials.

Plot A represents the baseline SWR performance of the 13B2. Here, the array was pointed skyward with the coax exiting at the rear of the boom and with the ferrites positioned at the analyzer end of the cable. Installing the conductive boom off-axis to the elements, as would be done for horizontal mounting, had no appreciable impact on SWR.

Plot B shows what happened when I created a “T” configuration by rotating the Yagi 90° so the lower half of the array and the mast fell in the same plane. SWR increased significantly — especially toward the low-frequency end of the band. Indeed, resonance appeared to migrate upward in frequency, with the antenna becoming unusable below 145 MHz.

Plot C resulted when I extended the conductive mast up through the array to parallel the full length of the elements — simulating the condition of mounting a Yagi below the top of a vertical mast. SWR performance degraded severely, rendering the array virtually unusable over all but a very narrow portion of the band. Clearly this configuration should be avoided at all cost!

Plot D reflects the outcome when I replaced the aluminum mast with PVC — but left the coax cable drop between the elements in place. As shown, the impact of removing only the mast was minimal because the outer surface of the coax provided a duplicate RF path between the elements.

Plot E illustrates what happened when I repositioned the 43-mix ferrite sleeves at three-inch intervals along the span of the cable drop. The ferrites essentially “broke up” the disruptive current path along the cable and restored the array to original baseline performance.

Impact on Pattern and Gain

Anytime something disrupts the baseline SWR of an otherwise healthy antenna, it's usually a good bet other key parameters will suffer, as well. To test this supposition, I modeled the 13B2 on EZNEC to compare its performance with and without a conductive mast. See Figure 3. With no mast, the model predicted 14.05 dBi gain in free space at 146 MHz, with a sharp symmetrical forward lobe (Figure 3A). I then introduced a 1.25-inch diameter by 72-inch long “wire” in the same plane as the elements, extending

from the boom line between elements 6 and 7. When I ran the 146-MHz patterns again, EZNEC showed a gain loss of approximately 2.5 dB, decreasing the antenna's forward efficiency to nearly the half-power point (Figure 3B). It also showed 8-dB front-to-back degradation and downward squint in the E-plane. At the same time, antenna resonance, defined as the frequency at which the reactive term of the impedance equals zero, migrated up the band by nearly 2 MHz. To check the “universality” of the 13B2 EZNEC prediction, I inserted the same 72-inch conductor into the wire table of two smaller VHF arrays stored in my directory and found proportionate gain losses and parameter shifts. That cross-check made a believer out of me!

Corrective Action

Fortunately, it's not all that difficult to permanently isolate a VHF or UHF Yagi in a T-mount. For my own FM antennas, I use a

configuration similar to the one shown in Figure 4. The insulated mast is made from a 3-foot length of 1-inch OD fiberglass painter's pole — readily available at most hardware or farm-and-garden outlets. I then add a short length of 1⅛ inch OD × 0.058-inch-wall aluminum tubing to each end to prevent the mounting clamps from crushing the fiberglass wall. These tubes may be secured in position with rivets, sheet metal screws, or by splitting lengthwise to provide a friction fit when the clamps are tightened. The antenna's regular mounting hardware is used at the top of the mast and a U-bolt style splice kit is used at the bottom for attachment to the existing metallic mast (RadioShack sells this hardware for smaller mast sizes). Watch out for splinters when working with fiberglass pipe. Those can be painful!

I generally prefer to use a flexible smaller-diameter cable for the initial cable drop from the antenna to a splice-point below the rota-

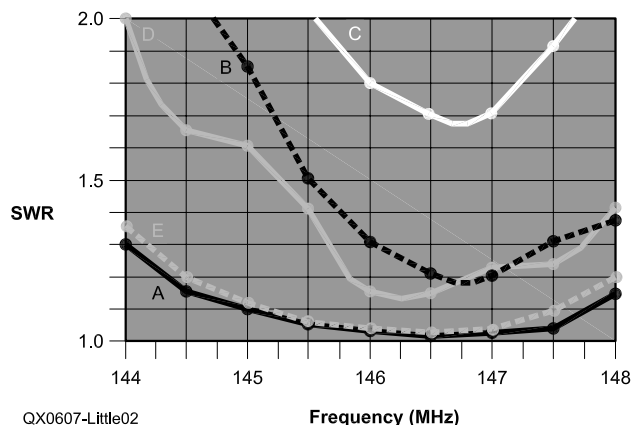


Figure 2 — SWR plots for various test configurations.

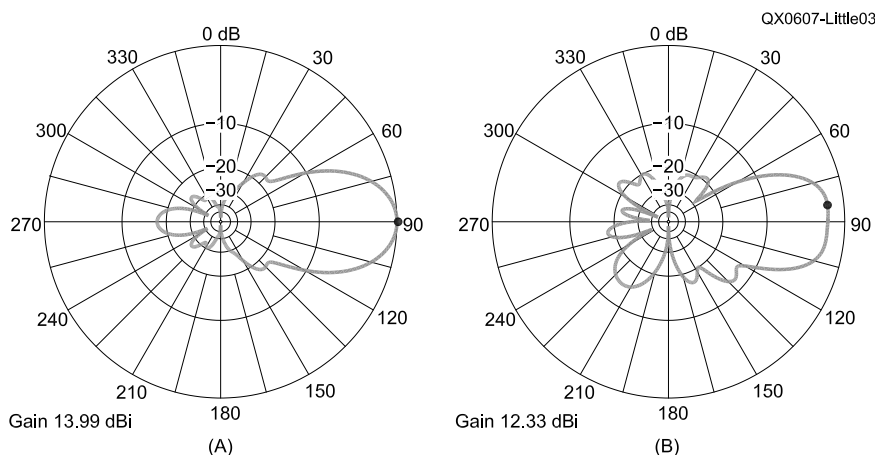


Figure 3 — Part A shows the EZNEC pattern with no mast near the 146 MHz Yagi. Part B shows the EZNEC pattern for the same antenna with a conductive mast included at the mounting point.

We Design And Manufacture
To Meet Your Requirements
*Prototype or Production Quantities
800-522-2253

This Number May Not
Save Your Life...

But it could make it a lot easier!
Especially when it comes to
ordering non-standard connectors.

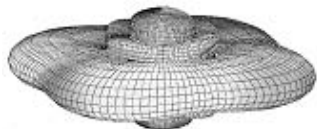
**RF/MICROWAVE CONNECTORS,
CABLES AND ASSEMBLIES**

- Specials our specialty. Virtually any SMA, N, TNC, HN, LC, RP, BNC, SMB, or SMC delivered in 2-4 weeks.
- Cross reference library to all major manufacturers.
- Experts in supplying "hard to get" RF connectors.
- Our adapters can satisfy virtually any combination of requirements between series.
- Extensive inventory of passive RF/Microwave components including attenuators, terminations and dividers.
- No minimum order.



NEMAL ELECTRONICS INTERNATIONAL, INC.
12240 N.E. 14TH AVENUE
NORTH MIAMI, FL 33161
TEL: 305-899-0900 • FAX: 305-895-8178
E-MAIL: INFO@NEMAL.COM
BRASIL: (011) 5535-2368
URL: WWW.NEMAL.COM

A picture is worth a thousand words...



With the

ANTENNA MODEL™

wire antenna analysis program for Windows you get true 3D far field patterns that are far more informative than conventional 2D patterns or wire-frame pseudo-3D patterns.

Describe the antenna to the program in an easy-to-use spreadsheet-style format, and then with one mouse-click the program shows you the antenna pattern, front/back ratio, front/rear ratio, input impedance, efficiency, SWR, and more.

An optional **Symbols** window with formula evaluation capability can do your computations for you. A **Match Wizard** designs Gamma, T, or Hairpin matches for Yagi antennas. A **Clamp Wizard** calculates the equivalent diameter of Yagi element clamps. **Yagi Optimization** finds Yagi dimensions that satisfy performance objectives you specify. Major antenna properties can be graphed as a function of frequency.

There is **no built-in segment limit**. Your models can be as large and complicated as your system permits.

ANTENNA MODEL is only \$90US. This includes a Web site download **and** a permanent backup copy on CD-ROM. Visit our Web site for more information about ANTENNA MODEL.

Teri Software
P.O. Box 277
Lincoln, TX 78948

www.antennamodel.com
e-mail sales@antennamodel.com
phone 979-542-7952

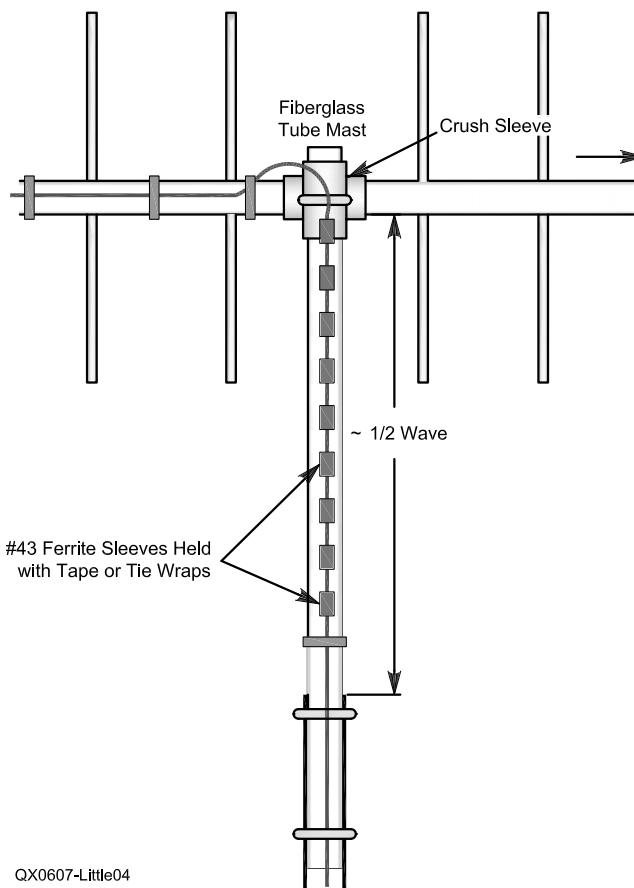


Figure 4 — Recommended T-mount decoupling procedure.

tor. LMR195, low-loss foam-FEP or PTFE-dielectric RG-58, or the slightly larger RG-8X and LMR-240 work well. The loss introduced by a few feet of this thinner and more flexible cable isn't all that significant and the smaller 0.21-inch or 0.25-inch ID ferrites add far less weight to the installation than comparable 0.50-inch ID sleeves.

Be sure to install a sufficient number of ferrite sleeves to do the job, distributing them evenly at 3-inch intervals and securing them in position with tape or a tie wrap (avoid over-tightening tie wraps on foam cable). I usually continue to install sleeves for a few inches beyond the element tips to eliminate all end loading. For RG-58 size cables, you might try Amidon Associates FB-43-5621 or the Fair-Rite Products equivalent. FB-43-5625 should work well for RG-8X and LMR240. Alternatively, I've had very good luck using Fair-Rite Products 4443164251 split sleeves in snap-on carriers. These fit all of the smaller cables and may be snapped in place after coax connectors are installed. Prices vary a lot for ferrite materials, so if you're planning to treat multiple installations, you can save some money by shopping the Web. When buying surplus, however, make sure you're getting 43-mix or your results may not be all that good!

Conclusion

Field testing and modeling of a Cushcraft 13B2 both offer compelling evidence that important performance parameters such as SWR, bandwidth, gain, and resonant frequency are compromised by improperly T-mounting VHF Yagis. Installing a length of non-conductive mast and treating the feed line drop with ferrite sleeves have been shown to reverse this condition and restore baseline performance.

Rick Littlefield, K1BQT, is an Amateur Extra Class ham, first licensed in 1957 at age 13. In 1996, he was inducted into the ARCI QRP Hall of Fame for his work as an avid experimenter and writer. He has over 100 communication-related technical articles to his credit in a variety of electronic hobby magazines and professional journals. Rick's professional resume includes extensive work with familiar amateur-product manufacturers such as MFJ Enterprises, Ten-Tec, and Cushcraft Corporation, where he currently works as a product design engineer. Rick holds a master's degree from the University of New Hampshire and is a member of IEEE. He may be contacted at 109A McDaniel Shore Drive, Barrington, NH 03825 or at k1bqt@usadatanet.net.



An IF Signal Generator

Here is a high-performance 455 kHz signal generator that will assist you in building and testing IF resonators, filters and other circuits.

John Pivnichny, N2DCH

Precise Measurement of IF Filters and Circuits

Those who are experimenting with intermediate frequency (IF) resonators, filters and circuits need a high-performance signal source. Specifically, the signal generator should have:

- 1) very low harmonic content.
- 2) low phase noise.
- 3) a very slow tuning rate.

A typical low-cost signal generator does not meet these requirements and something better is needed.

This article describes an IF signal generator project having high performance in all three areas, which the experimenter can build and use. Photo A shows the front view of the home-built generator and Photo B shows a close-up view of the two frequency tuning scales provided. This unit was designed to have a 450 to 460 kHz scale for tuning through the 455 kHz IF center frequency of many radios, and also a 435 to 445 kHz range for making measurements of ceramic resonators (see below). Any

¹Notes appear on page 27.

3824 Pembroke Lane
Vestal, NY 13850
johnpivn@aol.com

frequency range can be selected and designed in, as will be described.

About six revolutions of the main tuning knob (1.75-inch diameter) cover this 10 kHz range yielding a 1.6 kHz/rev tuning rate.

The Circuit

The oscillator circuit shown in Figure 1 is well known for its excellent stability and low phase-noise characteristics. A JFET circuit in the Hartley configuration drives a bipolar amplifier providing about a 0.5-V RMS signal into a 50-Ω load. Avoid adding a silicon diode from gate to ground. Dr. Ulrich Rohde has shown that this makes the phase noise much worse.¹ The output transformer is constructed by winding 25 turns of AWG 26 gauge copper wire on an FT37-43 ferrite toroid core. The secondary is 5 turns of the same wire.

The circuit is very stable in frequency, provided the frequency determining components are stable themselves. For example, the fixed frequency determining capacitors must all be NP0 or mica. The inductor should be wound on a powdered-iron toroid core. Do not use any type of ferrite core or any slug-tuned coil with a ferrite slug. Ferrites have a high temperature dependence.

A Variable Capacitor

You will need a variable capacitor to tune

the frequency through its range. Although a mechanical variable capacitor may seem outdated, electronic varicaps have severe drift and noise performance problems and must not be used in this application. A 100-pF variable will be about right for tuning a 10 kHz range at 455 kHz center frequency. There are numerous 100 pF variables available from electronic distributors, surplus dealers, and at hamfests. Select one with a ¼-inch shaft.

Use the resonant frequency equation to determine the actual fixed capacitance to put across the variable terminals so that you have your desired tuning range:

$$f = \frac{1}{2\pi\sqrt{LC}} \quad (\text{Eq 1})$$

where C is the total capacitance in the circuit — variable plus fixed.

You can also use frequency ratios to determine the required capacitance ratio. Note that the required capacitance ratio will be the square of the frequency ratio. For example, let's say you want to tune 450 to 460 kHz. This is a frequency ratio of 460 / 450 = 1.02. Then the required capacitance ratio will be the square of this, or 1.045. If the variable tunes 10 to 100 pF, then:

$$(C + 100) / (C + 10) = 1.045 \quad (\text{Eq 2})$$

Solving for the fixed capacitor, C = 1993 pF.

The required inductor, L, is then found using the resonant frequency equation with

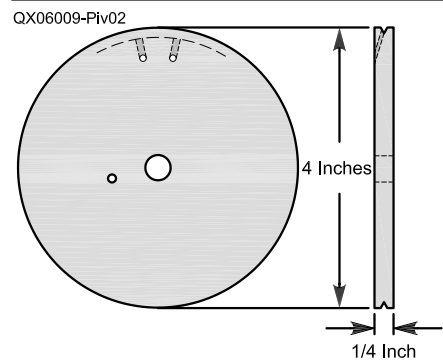
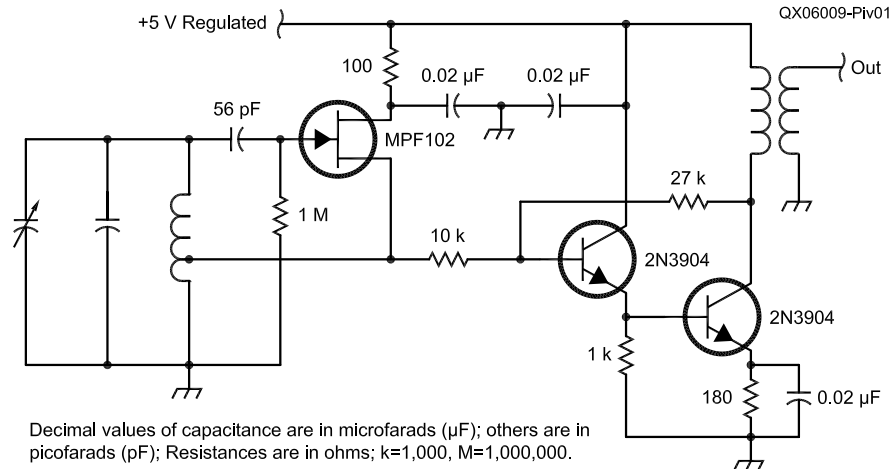


Figure 2 — Mechanical details of the dial pulley.



Decimal values of capacitance are in microfarads (μF); others are in picofarads (pF); Resistances are in ohms; k=1,000, M=1,000,000.

Figure 1 — Oscillator circuit diagram.

450 kHz and $C = 2093 \text{ pF}$:

$L = 59.8 \text{ } \mu\text{H}$

(Eq 3)

The higher the Q of the inductor, the better the stability and phase noise — that is, provided you have a stable inductance value. Select a T68 or larger core. You should be

able to achieve a Q of 140 at 455 kHz with about 100 turns of AWG 30 wire on a T68 core. A larger core with larger wire would be even better. When winding, be sure to leave a tap at $\frac{1}{3}$ of the turns up from the grounded end. The wound inductor should be coated with clear nail polish and mounted

securely with an insulated screw, nut and washer, to the circuit board.

Details of the Mechanical Dial

A 4-inch diameter pulley is cut from $\frac{1}{4}$ -inch thick plastic. Make a groove in the rim with a small round file and then drill two small



Photo A — Front view of the generator.

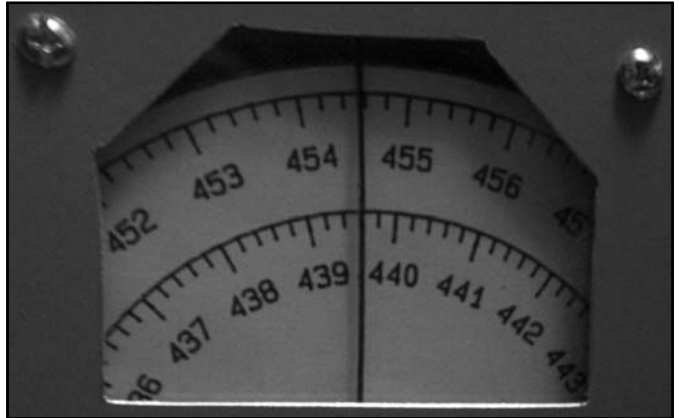


Photo B — Close-up of the dial scale.

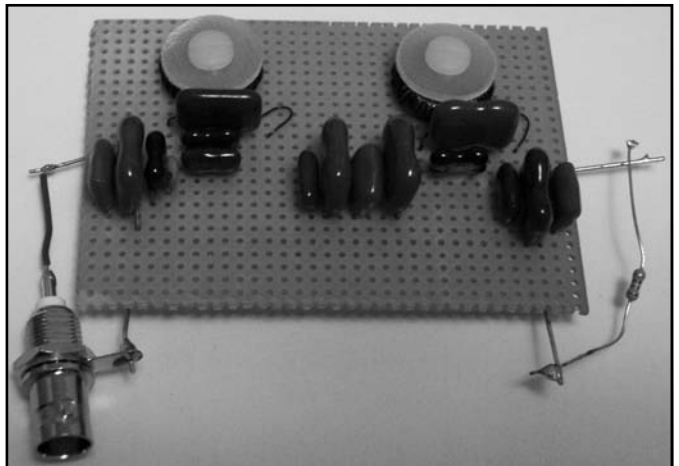


Photo C — The filter circuit board with components.

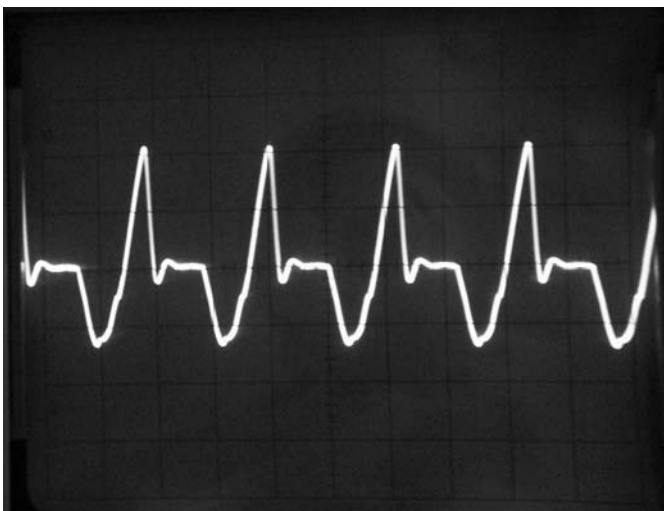


Photo D — The output signal of oscillator circuit before processing with the filter. The horizontal scale is $2 \text{ } \mu\text{s/cm}$ and the vertical scale is 0.5 V/cm .

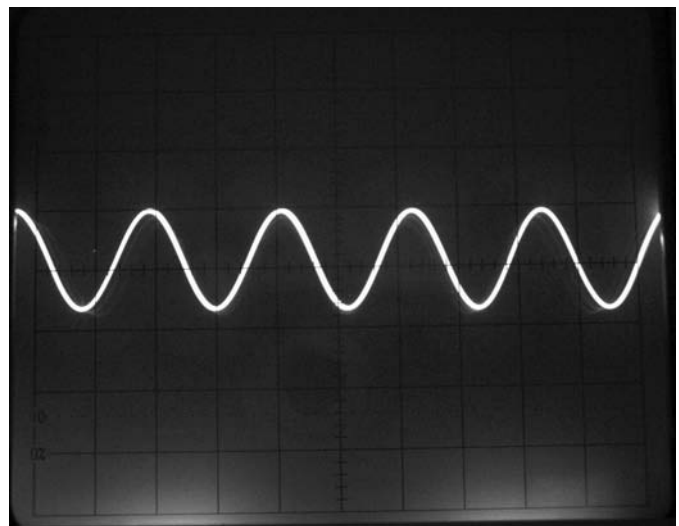


Photo E — The output signal after the filter. The horizontal scale is $2 \text{ } \mu\text{s/cm}$ and the vertical scale is 0.5 V/cm .

holes for the dial cord, through the groove to the back side surface. See Figure 2.

The variable capacitor is mounted on a 5-inch by 1 $\frac{3}{8}$ -inch piece of sheet aluminum. This is supported with size 6-32 machine screws 1 $\frac{1}{4}$ inches long and 6-32 hex nuts placed near the ends of the screws. The 4-inch pulley is fastened to the shaft of the variable capacitor using a $\frac{1}{4}$ -inch locking bearing. Locking bearings are easily made from $\frac{1}{4}$ -inch headphone jacks.

Another $\frac{1}{4}$ -inch bearing is mounted on the front of the 6 by 5 by 3-inch box to support a $\frac{1}{4}$ -inch shaft for the tuning knob. This shaft also drives the dial cord.

Output Signal

The signal produced by the oscillator circuit of Figure 1, although very stable, will have significant harmonic content. See Photo D. A filter is needed to remove the harmonics.

A fifth-order low-pass elliptic filter was designed using the procedure given in *Simplified Modern Filter Design*.⁴ The selected filter is a 1-dB-ripple design with a cutoff of 1.841 times the fundamental frequency, and a minimum of 65 dB attenuation. Transmission nulls are located at 1.920 and 2.952 times the fundamental, providing outstanding attenuation of the second and third harmonics.

The filter circuit is shown in Figure 4. The design has been scaled to 455 kHz and 50 Ω . Fairly high inductance values are needed. These are provided by winding 52 and 56 turns of AWG 26 wire on a T68-2 core. As a check, the 15.76 μ H coil should resonate with a 270 pF silver mica capacitor at 2.44 MHz. Adjust the number of turns if necessary. Likewise the 17.77 μ H coil should resonate at 2.30 MHz with the 270 pF silver mica capacitor. Additional information on constructing high Q inductors can be found in *Radio Components Handbook* published by MFJ.³ Inductances can be accurately measured with instruments described in *Test Equipment* by Guido Silva, I2EO.⁴ Several capacitors are connected in parallel to make up the high values needed. See Photo C.

After passing through the filter, the signal has no discernable harmonic content. (See Photo E.) Measurements were taken with a 50- Ω load on the filter and also with no load (just the oscilloscope). There is no difference in the shape of the output sine wave with either load.

Using the Generator

The generator has many uses. For example, the characteristics of ceramic resonators were accurately measured using the techniques described for crystal measurements found in *Ladder Crystal Filters*, published by MFJ.⁵ Once measured, high quality six- and eight-pole SSB filters were con-

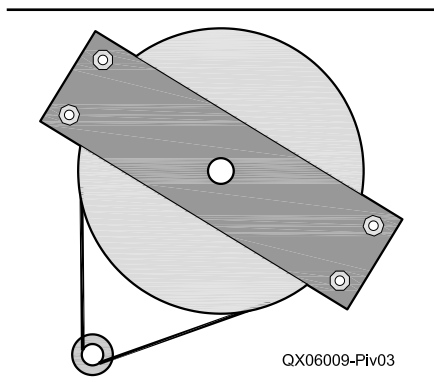


Figure 3 — Mechanical mounting arrangement for the dial pulley.

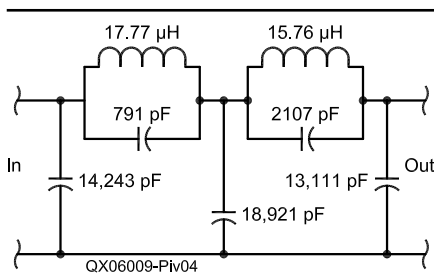


Figure 4 — Filter circuit.

structed for use in commercial short wave radios.

The frequency response of the filters is then easily measured using this generator along with a step attenuator and dBm meter, such as those available in kit form from Unicorn Electronics, 1 Valley Plaza, Johnson City, NY 13790, (800) 221-9454, www.unicornelex.com.

Notes

¹Ulrich Rohde, "Oscillators with Low Phase Noise and Power Consumption," *Communications Quarterly*, Winter 1996, pp 29-54.

²Philip R. Geffe, *Simplified Modern Filter Design*, Rider, NY, 1963.

³Guido Silva, *Radio Components Handbook*, MFJ, Starkville, MS 1998.

⁴Guido Silva, *Test Equipment*, Black Forest, Vestal, NY 2001.

⁵John Pivnichny, *Ladder Crystal Filters*, MFJ, Starkville, MS 1999.

John Pivnichny, N2DCH, has been licensed since 1956. He enjoys operating voice, CW, and digital modes on all the HF and VHF bands. John likes to experiment with circuits for measuring, receiving, and transmitting. He has had a number of articles published in Amateur Radio magazines, and is the author of a book on ladder crystal filters. John has BS, MS, and PhD degrees in engineering, and is currently employed by a large information technology company. You can reach John by mail at his home address or via e-mail at johnpivn@aol.com.

QEX

From MILLIWATTS to KILOWATTSSM
More Watts per Dollar



Quality
Transmitting
& Audio Tubes

Taylor
TUBES



- COMMUNICATIONS
- BROADCAST
- INDUSTRY
- AMATEUR



Immediate Shipment from Stock

3CPX800A7	3CX15000A7	4CX5000A	813
3CPX5000A7	3CX20000A7	4CX7500A	833A
3CW20000A7	4CX250B	4CX10000A	833C
3CX100A5	4CX250BC	4CX10000D	845
3CX400A7	4CX250BT	4CX15000A	866-SS
3CX400U7	4CX250FG	4X150A	872A-SS
3CX800A7	4CX250R	YC-130	5867A
3CX1200A7	4CX350A	YU-106	5868
3CX1200D7	4CX350F	YU-108	6146B
3CX1200Z7	4CX400A	YU-148	7092
3CX1500A7	4CX800A	YU-157	3-500ZG
3CX2500A3	4CX1000A	572B	4-400A
3CX2500F3	4CX1500A	807	M328/TH328
3CX3000A7	4CX1500B	810	M338/TH338
3CX6000A7	4CX3000A	811A	M347/TH347
3CX10000A7	4CX3500A	812A	M382

— TOO MANY TO LIST ALL —



ORDERS ONLY:
800-RF-PARTS • 800-737-2787

Se Habla Español • We Export

TECH HELP / ORDER / INFO: 760-744-0700

FAX: 760-744-1943 or 888-744-1943



An Address to Remember:
www.rfparts.com

E-mail:
rfp@rfparts.com



RF PARTSSM
COMPANY

Magnetic Coupling in Transmission Lines and Transformers

Explore the similarities of these closely-related structures and discard some widespread misunderstandings.

Gerrit Barrere, KJ7KV

During my investigation of transformers and transmission lines and the marriage of the two, a number of questions arose that I could not answer. For instance:

- If the characteristic impedance of a transmission line is the familiar $Z_0 = \sqrt{L/C}$ (square root of inductance per length over capacitance per length), why doesn't this change when the line is surrounded by ferrite, which increases inductance?
- One source stated that the electrical length of a line is increased by adding ferrite, thus extending the low-frequency response. But electrical length also depends on per-length inductance (electrical length is physical length times frequency times \sqrt{LC}), and my measurements showed that neither impedance nor electrical length vary with ferrite loading.
- What exactly are "conventional transformer currents" and what is the difference between this and "transmission line mode"?
- How can "choking reactance" of a transmission line transformer affect differential transmission line signals? This should be strictly a common-mode effect.
- Typically, transmission line transformers are wound with something like a half meter of line. At HF and even VHF this is a small fraction of a wavelength, so how can they be considered transmission lines at all? How can they develop significant longitudinal voltage if they are electrically short lines?

- If two wires carrying differential current pass through a core, the flux they produce cancels, resulting in zero flux in the core. Yet the core has a significant effect on low-frequency behavior. How can this happen with no flux?

I slowly pieced together explanations for those and other aspects of lines and transformers, which I haven't seen in the literature; perhaps you will find them helpful too. Through most of this discussion I will be referring to transmission lines as two wires, but the same ideas apply to any form of line except coaxial cable, which is treated separately.

The Basics

First, I present a review of terminology and the basics. An isolated wire carrying a current, I , produces a magnetic field H external to the wire, as shown in Figure 1. The strength of this field varies as $1/r$, where r is the distance from the center of the wire. It also produces a magnetic field internal to the wire, which goes from $1/r$ at the surface to zero at the center of the wire. For frequencies low enough that skin effect is negligible, the profile of magnetic field strength, H , versus radius, r , inside the wire is linear, as shown by the low-frequency line in Figure 2. Note that the field reaches a peak right at the surface of the wire, at radius r . Also note that a smaller diameter wire will create a larger peak H field at its surface, since the peak is proportional to $1/r$.

The magnetic and electric fields are vector fields [Indicated here in italic boldface type — Ed.] since at every point there is a magnitude and a direction to them. The magnetic field always forms closed paths or loops of magnetic flux, and the electric field always terminates perpendicular to a (perfect) conductor. The lines of flux shown in a field dia-

gram like Figure 1 follow the *direction* of the vector field, and the density of spacing between lines indicates the field magnitude. In general, the *magnitude* of the magnetic field along a given line is not constant; but in a symmetrical case like Figure 1, it is.

Flux is a smooth and continuous phenomenon, like swirling water. The lines in vector field diagrams merely indicate the trends of

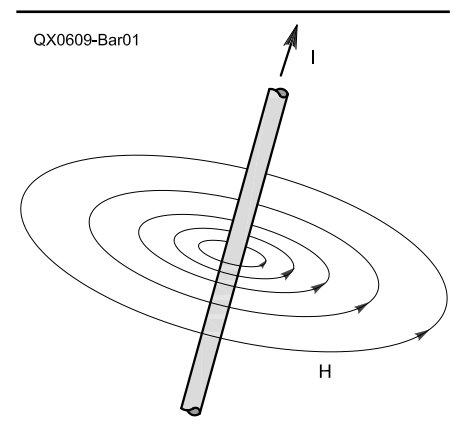


Figure 1 — Magnetic field around a current-carrying wire.

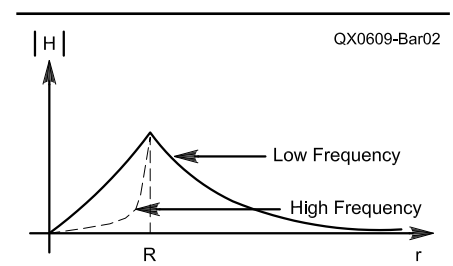


Figure 2 — Magnetic field strength variance with distance from center of wire.

16816 12th PI NE
Shoreline, WA 98155
gerrit@exality.com

the flux field. Flux does not actually occur as discrete lines.

The magnetic field H produces a magnetic flux density field, B , by the relationship $B = \mu H$, where μ is the permeability of the medium in which the flux occurs (μ is the product of the relative permeability μ_r and the permeability of free space μ_0). Thus if a given H field passes through high-permeability material, a greater flux density will result than if it passes through air or copper, which have a μ_r of 1. This flux density may vary along the path of an H field loop, too, depending on the permeability in portions of the path. Keep in mind that flux density is not the same as total flux — when flux density is integrated (summed) over an area, it results in the total flux passing through that area.

Refer to Figure 2 again. Since the wire and air have permeability of 1, this is also a picture of the flux density field, B , because of the current in the wire. The total flux produced is proportional to the integral of this B field, which is the area underneath the line in Figure 2 (between the line and the horizontal axis). The total flux inside the wire is constant for low frequencies, since the area of the triangle from 0 to any R is $0.5 \cdot R \cdot 1/R = 0.5$. The external total flux increases dramatically with shrinking R , however, since each reduction of ΔR results in increased external flux of approximately $\Delta R/R$ (the area under the added slice when R changes to $R - \Delta R$). So, the total external flux produced by a wire at a given current increases greatly as the wire size is reduced.

Inductance is a measure of the magnetic flux linking a conductor relative to the amount of current producing the flux. Flux “links” a wire by circling it, like a link of a chain. Remember that flux always forms closed loops, so if a wire is linked by flux you can imagine pulling on the flux loop and having it tug the wire. This flux may arise from current in the wire itself, leading to self-inductance (also known as simply “inductance”), or from current in another wire, which results in mutual inductance. If more total flux links a wire for a given current, the inductance is greater. This applies to self-inductance or mutual inductance. Self-inductance is increased by using smaller wire, coiling the wire, or by increasing the permeability of the wire’s flux path. Mutual inductance is increased by causing more flux from one wire to link the other, that is, by bringing the wires closer or by increasing the permeability of the path of linking flux. Note that self-inductance is the sum of internal inductance from the flux inside the wire plus external inductance from flux outside the wire. These two components of self-inductance become important in understanding transmission line coupling below.

Bringing a current-carrying wire or coil closer to another increases the total flux link-

ing the two, so mutual inductance increases. In a single inductor, current through it causes voltage to be produced across it. When two inductors are linked by mutual inductance, current in one produces voltage in the other due to the flux from the one, which links the other.

Figure 3 shows two wires in cross section, with current entering the page in wire A and no current in wire B. The current in wire A causes the magnetic flux shown. None of the flux inside loop f_a links with wire B, so it contributes to the self-inductance of wire A only, and not to the mutual inductance between A and B. All the flux outside loop f_b does link with wire B, however, and contributes to both the self-inductance of A and the mutual inductance. Note that the mutual inductance gets much larger as the wires become very close, because of the $1/r$ increase in flux magnitude. The amount of mutual inductance approaches the self-inductance as the wires approach perfect coupling.

Flux from more than one source present in the same region of space adds in a vector fashion at every point. This applies to magnetic or electric fields. The resulting field is still a vector field, and at every point the contributions from the individual fields are added vectorially. This may change the direction and magnitude of the resulting field considerably.

Imagine now that the same magnitude of current is present in both wires of Figure 3, with current coming out of the page in one and into the page in the other. This is simply a differential pair. The H field for one wire will be clockwise and counterclockwise for the other. Now when these wires are brought close together, the H fields add such that an intense line of H field is produced perpendicular to the line joining the centers of the wires, right between the wires. This is the region close to the wires where the individual H fields are the strongest and where the two fields point in the same direction. This H field line drops off rapidly away from the center line of the wires,

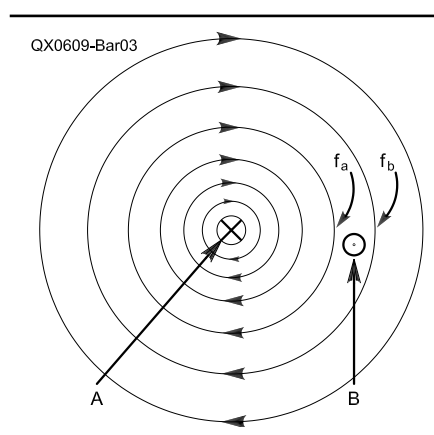


Figure 3 — Flux linkage from wire A to wire B.

since the tightly-curved H lines near the wires rapidly begin pointing in opposite directions. The combined H field is also nearly zero everywhere else, since the fields nearly cancel (they would perfectly cancel if the wires somehow occupied the same region in space).

The combined magnetic field of two close wires carrying differential current is markedly different from a single wire. An intense, short line of magnetic field is created between the wires, and the field is nearly zero everywhere else.

This altered field pattern, however, does not affect the individual inductance of the wires or their mutual inductance, because inductance is a property that exists because of conductor geometry and the permeability of the surrounding medium only, regardless of any current or what the overall magnetic field pattern looks like. That explains how ferrite-loading a coaxial cable can affect its inductance, despite the fact that its external magnetic field is nearly zero (see below).

A final note on inductance: For a particular wire carrying a particular current, a specific total H field is produced. If the permeability of the field path is increased, the inductance of the wire is increased. This is because the B field, and therefore the total flux produced by the current, increases. This is what happens when the wire is passed through a ferrite block, for example. This also distorts the H field, because the ferrite forms a low-reluctance path for the flux, so the field concentrates inside the ferrite since it is an easier path to follow.

Transformer Operation

A transformer is an assembly of inductors (windings) that share flux — often nearly all of their flux. The windings are often wound such that their magnetic field paths are mostly through high-permeability material to ensure that as much flux as possible is shared, but transformers may also be built that use air or low-permeability cores. By adjusting the turns ratio between the windings, voltage and current can be stepped up or down.

The essentials of ideal transformer operation may be summed up as follows: *Changing winding current (ac) produces changing flux, which induces winding voltages related by the turns ratio.* Imagine a transformer core with two windings, and some changing shared flux existing in the core somehow, from some other source. (For now assume that all winding flux is shared and that there is no winding resistance.) These two windings will have a voltage induced across each of them by Faraday’s law.¹ These winding voltages will be locked together at their turns ratio by their common flux. If one winding has twice the turns of the other, it will have twice the voltage, too. If two

¹Notes appear on page 36.

windings share the same changing flux, they *cannot* have a voltage that differs from their turns ratio, or Faraday's law would be violated.

This relationship also holds if one of the windings is producing the flux that links the two. The windings then have a primary/secondary relationship, with the primary creating the flux, but there is voltage induced in both primary and secondary in exactly the same way as before; it doesn't matter that the primary is also creating the flux. Faraday's law holds for both primary and secondary windings. See Appendix A for more on this.

Transformers sometimes appear as common-mode chokes, as in Figure 4. Current in the direction shown will produce flux in the core that adds (points in the same direction) and also links both windings. The result produces four times the inductance of a single side alone, since the mutual inductance adds with the winding inductance in this configuration. This inductance can be used as part of a filter to suppress common-mode currents.

The common-mode choke may also be called a "differential-mode pass-through." For pure differential-mode current, $i_1 = -i_2$ as in Figure 4. That is, the same current enters the dotted side on one winding as leaves the dotted side on the other. In this case, the flux produced by one winding is exactly canceled by the other, resulting in zero core flux, and, by Faraday's law, zero voltage across each winding. A common-mode choke, therefore, simply passes differential-mode currents unimpeded.

In an actual circuit, both common-mode and differential-mode currents may be present. The common-mode choke is excellent for presenting high impedance to the common-mode portion, while not affecting the differential-mode currents.

In real transformers, the windings do not share 100% of their flux. Some amount of flux links one winding but not the other. This flux is accounted for in circuit modeling by "leakage inductance" in series with perfectly-coupled windings, as shown in Figure 5. The mutual inductance is usually many times greater than the leakage inductance, meaning that the great majority of flux produced is shared between the windings. Leakage inductance and winding resistance lead to winding voltages that are not exactly locked together at their turns ratio; but in well-coupled transformers, this is a good approximation.

In high-power transformer applications such as output baluns or matching networks for transmitters, the best possible coupling between windings and low winding resistance is critical to efficiency. The two loss mechanisms in high-power transformers are resistive power loss in the windings and core loss from eddy currents and hysteresis. Either of these will increase heating, sometimes to destructive levels, and reduce transformer

efficiency. Winding loss may be minimized by using large gauge wire or multiple smaller gauges, and core loss may be minimized by proper core material selection and keeping core flux as low as possible. If the windings are separated, the flux that couples them must pass through the core, leading to higher losses. If the windings are intimately wound as twisted pairs or close parallel lines, they will be coupled together with very little of the core required for the coupling flux path.

Transmission-Line Fundamentals

It is important to realize that any pair of conductors carrying a signal and its return is a transmission line, at any frequency. There is no transition between "non-transmission-line" and "transmission-line" behavior. What happens at low frequencies is that the line becomes so electrically short (such a small part of a wavelength) that the line may be lumped into a single equivalent circuit representing its capacitance, inductance, and losses. Signal delay through the line need not be considered. And for many lines, such as the traces on a circuit board carrying moderate frequencies, those equivalent circuit elements have such a tiny effect that they may be neglected entirely. At higher frequencies, where the line length becomes an appreciable part of the signal wavelength (about $1/10$ wavelength for most purposes), the effects of propagation time be-

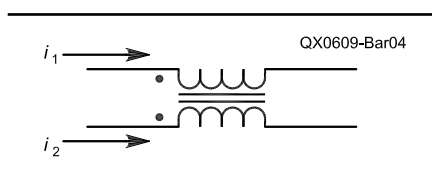


Figure 4 — Common-mode choke.

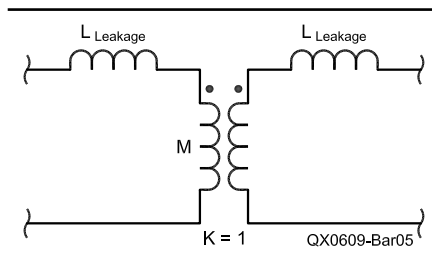


Figure 5 — Transformer model with leakage inductance.

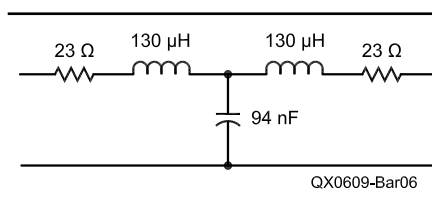


Figure 6 — Lumped-circuit equivalent of 1000 m of RG 58/U.

gin to be seen, which cannot be modeled by lumping the line into single elements. The line must then be represented by its distributed characteristics, and the interaction of forward and reverse waves must be considered.

As an example, consider 1000 m of RG-58 coaxial cable being used to transmit 60-Hz power. The wavelength of 60 Hz is about 3.5 million meters in RG-58, so even 1000 m of line may be lumped, since it is electrically short at the operating frequency. RG-58 cable specs are about 90 pF/m and 260 nH/m (more about what this means later), and it has a total low-frequency resistance of about 0.046 Ω /m. This is 90 nF, 260 μ H, and 46 Ω total for 1000 m, so when it is used to carry 60-Hz power, the cable may be represented as the symmetrical lumped circuit shown in Figure 6. The line resistance is far more than the inductive reactance at this low frequency, which is only about 0.098 Ω . Note that the characteristic impedance is still

$$Z_0 = \sqrt{260 \text{ mH} / 90 \text{ nF}} \approx 53 \Omega$$

(neglecting losses). If the load differs from 53 Ω , the line will be mismatched and both forward and reverse waves will exist, but they will reach equilibrium instantly with respect to 60 Hz. The waves combine exactly as they do at higher frequencies. *The forward and reverse wave analysis of long transmission lines reduces to circuit analysis for short lines, but the same physical phenomena are still taking place.*

Another important characteristic of transmission lines is that current does not "go out and come back." This water-in-a-hose analogy of electrical circuits is useful at dc, but it is not really the way ac electrical energy is transferred. Electrical energy is launched into a transmission line as a power wave of voltage and current, with current *pushed* onto the signal conductor at the same time it is *pulled* on the return conductor. The line is really only a guide for this electromagnetic power wave.

Now recall that any signal and its return forms a transmission line at any frequency and you will realize that even your reading light at 60 Hz receives its power in the form of a wave, guided by the power lines that feed it. An electromagnetic field is set up by your house wiring, and forms the actual medium through which the power is transferred. There is no low frequency limit where a source and return stop acting as a transmission line, but for short electrical lengths line characteristics may be neglected. That means that for all HF work and much VHF, if the transmission line is less than a meter or so, there is negligible distributed transmission-line behavior. Transmission-line transformer windings a meter long become $1/10$ wavelength at 21 MHz (assuming a velocity factor of 0.7), so this is where distributed transmission line effects will *start* becoming

evident. Shorter lines and lower frequencies will see negligible propagation effects and therefore their characteristics may be lumped.

Progression from Loop to Shorted Transmission Line

Now it's time to consider that the ideal isolated current-carrying wire of Figure 1 does not really exist. Every current forms a circuit, so the best approximation we can make for Figure 1 is a large loop where the signal and its return are widely separated. The inductance of this configuration is mostly the self-inductance of the wire, but there is also a small mutual inductance between one side of the loop and the other. The magnetic field from one side of the wire drops off as $1/r$, but it is still present and links the other side eventually.

Now this loop can be pulled straight, forming two closely-spaced wires shorted at the end, with current in opposite directions on each side. This is obviously a shorted transmission line. The wire is still creating the same magnetic field as when it was a loop, the self-inductance of the wire is the same, but almost all the flux from each wire now links the other so the mutual inductance is greatly increased. The capacitance from one side of the line to the other has also increased, thus increasing both electrical and magnetic coupling.

The flux can be separated into two components: the flux that links both wires (contributing to mutual inductance), and the remaining *uncoupled* flux (internal to the wires plus a small shell around each wire). Figure 7 shows the inductance model for either the loop or the shorted line, where L_s means the residual self-inductance due to uncoupled flux and M means the mutual inductance due to coupled flux. In the loop configuration L_s is much larger than M , and in the closely spaced (transmission-line) configuration, M is much larger than L_s .

Now what total inductance, L_{tot} , do we see when we look into the open end of this shorted transmission line? It is clear in Figure 7 that the line is nothing more than a perfect common-mode choke (the mutual inductance) in series with the residual inductance L_s . Common-mode chokes are transparent to differential mode currents as we saw above, so the mutual inductance *does not appear at all* to the purely differential current from the open end.

The only inductance seen at the open end of a shorted transmission line is that caused by the uncoupled portion of the flux from the individual conductors.

This analysis is equivalent to the more common approach that calculates $L_{tot} = L_{indiv} + L_{indiv} - 2M$. Here L_{indiv} is the isolated self-inductance of an individual wire, which does not change as the wires are brought together. The mutual inductance M approaches L_{indiv} as the wires get closer, causing L_{tot} to approach zero. The re-

sult is the same, the only difference is the treatment of the flux that contributes to both L_{indiv} and M . I find it is helpful to consider the flux as composed of two parts: that which links the other wire and that which doesn't.

L_{tot} , resulting only from the uncoupled line flux, is the inductance that is used to compute characteristic impedance, electrical length and so forth. It does not reveal the "hidden" mutual inductance, however, which is typically much larger.

A New Look at the Transmission Line

This leads to a revised model for the transmission line. The familiar model shown in Figure 8 (drawn symmetrically) is the equivalent circuit of a small portion of the line, where the subscript L means per-unit-length. In the limit, a transmission line consists of an infinite number of these infinitesimal sections. This model does not take into account the important quality of mutual inductance, though. The model should be drawn as in Figure 9, showing the distributed mutual inductance M . The inductance per length L_L is now the residual self-inductance due to uncoupled flux, and the mutual inductance in the model is perfectly coupled. Although the coupling is perfect, the mutual inductance is finite.

Now note that the inductive portion of this model is exactly the same as a 1:1 transformer turned sideways (the common-mode choke), shown in the standard configuration in Figure

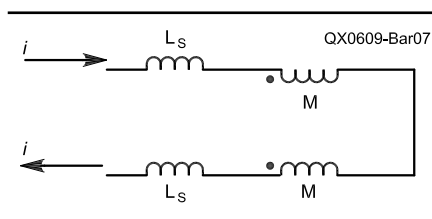


Figure 7 — Inductance of a loop or shorted line.

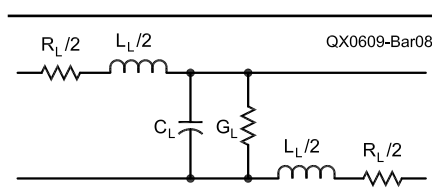


Figure 8 — Standard per-length transmission line model.

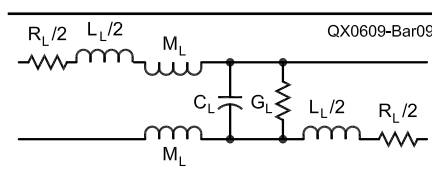


Figure 9 — Transmission line model with mutual inductance included.

5. The line inductance L_L caused by uncoupled flux corresponds to the transformer leakage inductance, and the mutual inductance corresponds to the "ideal-transformer" part of the model, where the coupling is perfect.

A transmission line may now be understood as actually being a transformer with the same flux coupling between windings as a conventional transformer, and with leakage inductance caused by the same phenomenon of imperfect winding coupling.

The main difference is that there is more inter-winding capacitance and less leakage inductance in the transmission line version. In other words, the coupling is better. Also, transmission-line transformer turns ratios are usually limited to small integers, depending on how many individual conductors are incorporated into the line and how they are connected. Both types may be used longitudinally, where input and output are on the ends of the same winding and no dc isolation is provided; or conventionally, where the windings are in separate circuits and share most of their flux.

Now we can understand the invariance of characteristic impedance and electrical length when the line is surrounded by or wrapped around high-permeability material. The total inductance of the transmission line is only due to uncoupled flux. This flux is due to the internal H field of the wires themselves plus a small shell of H field external to each wire. Increasing the permeability of space outside this region does not increase the flux density due to these fields. Therefore the line inductance, L_{tot} , does not change and neither does the characteristic impedance or electrical length.

The magnetic field paths that surround both lines *do* pass through the high-permeability material, however. These external H lines are all lines that link both wires and therefore make up the line mutual inductance. *So placing high-permeability material around or near the entire line increases only the mutual inductance of the line.*

When a two-wire line is wrapped around a ferrite core, L_{tot} will only begin to depend on the core when the wires are separated from each other but make close contact with the core. In this case some of the uncoupled flux passes through the core and increases the wire's self-inductance, and therefore L_{tot} .

If the conductors of the line pass through high-permeability material *individually*, the B field of the uncoupled flux will be increased and the characteristic impedance and electrical length *will* be significantly affected. This will happen if the individual wires of a two-wire line pass through a binocular-type core, or if the dielectric of coax is ferrite-loaded, for example.

The ways this affects the model are twofold. First, there is simply more longitudinal inductance to the coupled portion of the line

because $M = k\sqrt{L_1L_2}$. The coupling factor k is nearly 1, and if mutual inductance M increases, L_1 and L_2 must both increase by the same factor as M . This is *perfectly coupled* inductance, remember, not simple series inductors. The second effect is that the coupling factor k actually increases if the mutual inductance is increased without affecting the inductance due to uncoupled flux. The coupling factor, k , is defined as the ratio of the perfectly coupled inductance of one winding to the uncoupled inductance of the winding. So, k goes from close to 1 because of the close physical coupling of the windings to *very* close to 1, perhaps 0.99, or nearly ideal.

If a transmission line is really a transformer, does the reverse also apply? That is, if a conventional transformer with separated windings is connected longitudinally (sideways, like a common-mode choke), will it behave like a transmission line? A sideways transformer has distributed inductance and capacitance throughout its structure, much like a transmission line. It seems that it would exhibit the same model behavior as Figure 9, so it might be expected to perform like a transmission line. What would be the differences?

First, the winding coupling would be reduced, since the windings would be physically separated and more uncoupled flux would be present. Filling the flux path between the windings with high-permeability material would help the coupling in the same way as with a transmission line, but it would not approach the same values of k . This leads to a higher uncoupled series inductance (leakage inductance), which reduces high-frequency performance.

The distributed inter-winding capacitance would be less, and less uniform. Unless the individual windings were done very carefully, this would also vary somewhat from unit to unit.

There is also a characteristic impedance associated with a sideways transformer, but it is higher because of higher L_{tot} and lower C , and less uniform with frequency because of the variable inductive and capacitive coupling.

There is more self capacitance across each winding relative to the inter-winding capacitance. When the windings are closely coupled as in a transmission line, the capacitance between the coupled wires will be much more than the capacitance between the ends of a given winding. The other winding(s) in a transmission line also act to partially shield a given winding from itself (or to completely shield in the case of a coax transformer). This additional winding self-capacitance leads to reduced high frequency performance and also spurious resonances.

Certainly when the winding lengths are electrically short, the sideways transformer and the transmission line will behave similarly,

given the same cores and winding inductances. The increased leakage inductance of the sideways transformer would cause greater losses and poorer high frequency response, and the less uniform inter-winding capacitance would cause unpredictable resonances also.

Coax: A Special Line Topology

Some interesting line properties arise when one conductor is surrounded by the other, as in coaxial cable. The electric field between the inner and outer conductors is now completely confined to the space between them and perpendicular to both. More interesting is the magnetic field behavior. First note that for currents in the outer conductor (shield) only, there are *no magnetic flux lines* interior to it, as a consequence of Ampere's Law.² All flux lines due to current in the outer conductor are *external* to the outer conductor.

There is a magnetic field created by each conductor, external to the conductor, which varies as $1/r$, the distance from the coax axis. Since the conductors carry opposite currents and generate opposite magnetic fields, external to the outer conductor the magnetic fields are equal and opposite and ideally cancel to zero.

That requires the current to be exactly equal and opposite, the conductors to be exactly coaxial, and for current distribution to be exactly symmetrical, which of course is never actually achieved. Even in practical coax, however, the electric field is well-contained and the external magnetic field is nearly zero. Because of the absence of flux loops from the outer conductor in its interior, *the self-inductance of the outer conductor exactly equals the mutual inductance between the two conductors.*

Every flux line the outer conductor produces is exterior to it and links both the inner conductor and itself. Thus, every flux line from the outer conductor contributes to both its self-inductance and the mutual inductance. This is not true of the inner conductor; some of the flux it produces does *not* link the outer conductor and therefore contributes only to the inner conductor self-inductance. This unlinked flux exists between the inner and outer conductors, and is due to the inner conductor only.

What this means is that *no longitudinal voltage will exist* on the outer conductor due to inductance, if the inner and outer conductor currents are equal and opposite! Any tendency to create longitudinal voltage on the outer conductor due to current through its inductance will be exactly cancelled by the same current on the inner conductor due to the same mutual inductance. As electrical power propagates along the coax, there will be a voltage on the inner conductor relative to the outer and relative to the source (if it is electrically long), but there will be no voltage difference between the source and load ends of the outer conductor due to inductance.

For long lines or high current, a longitudinal voltage can develop on the outer conductor due to finite resistance. This is *not* an inductive effect, however.

With this in mind, coaxial cable should *not* be used in transformers which require the outer conductor to develop a longitudinal voltage, when the inner and outer conductors carry equal and opposite currents. For any use of coax in a transformer this effect must be considered.

Skin and Proximity Effects

Most RF buffs know that wire resistance becomes greater with higher frequency due to skin effect. Skin effect causes high-frequency current in a conductor to move toward the outer regions (skin) of the conductor, so there is greater current density and a larger effective resistance. What is not commonly known is that the skin effect becomes significant at surprisingly low frequencies, and that skin effect also causes total inductance to *decrease*.

Skin effect is caused by variation in inductance across the cross section of the conductor due to the magnetic field *inside* the conductor. The current toward the center of the conductor is linked by more flux than the current toward the outside, so the portion of the conductor toward the center has higher inductance than that toward the outside. The current distributes itself to minimize the total *impedance* it must pass through, so at higher frequencies this means following a path with reduced inductance. The internal inductance difference between the center and the skin is negligible at lower frequencies but becomes very significant as the frequency increases. In the microwave region almost all the current is crowded into a skin only microns thick.

While skin effect causes current to follow the path of least inductance in one conductor, proximity effect causes current to follow the path of *greatest mutual inductance* between two conductors of a transmission line. The general rule for both effects is that *current will tend to distribute itself so that total inductance is minimized.*

As we saw above, when transmission line wires come closer together their total inductance drops due to increasing mutual inductance. This process simply continues with proximity effect, drawing current within the conductors themselves closer. Figure 10 shows how current distributes itself in two close wires of a transmission line, concentrating toward the middle so more flux from one wire couples with the other. Skin effect also accompanies proximity effect, pushing current toward the wire periphery.

The current does not abruptly cut off due to skin effect as the center of the conductor is approached, but it falls off exponentially. The *skin depth* is defined as the point at which

the current has fallen to 1/e or 37% of its maximum at the surface, so most of the current is confined to one skin depth and nearly all of it is within three skin depths.

The radius of three skin depths for copper is shown in Table 1 for various frequencies, with the corresponding gauge of wire this represents.

Table 1 shows that even at 1 MHz, nearly all the current is in a shell the thickness of the radius of AWG 26 wire. The copper near the center of any wire larger than that will not carry any significant current.

That does not mean that high-power transformers at 1 MHz may use AWG 26 wire, however! High-frequency resistance will continue to drop with larger wire since the total cross-sectional area of the skin region will increase. This lower resistance is necessary to keep losses low in high-power applications. The center portion of the wire could be hollowed out, however, and there would be little effect.

Skin effect also causes internal inductance to be reduced at high frequency. Since the current is pushed to the periphery of the conductor, the generation of magnetic flux is too. This causes the H field profile inside the conductor to assume the shape shown in Figure 2 for high frequencies. Since the total flux inside the conductor is the area under this curve between 0

and R , it is clear that less total internal flux is being generated for the same amount of current. Thus the internal inductance drops.

The external field of a conductor is not affected by skin effect, however. With a given transmission line this decrease of internal inductance with the same mutual inductance will cause the coupling factor to increase with frequency due to skin effect.

Skin and proximity effects on inductance are difficult to calculate, but the trends are helpful to understand. They can cause differences in measured values of inductance and coupling of 15 to 20% or so, even in the HF region.

Line Measurements

I measured a 1-m length of RG58-A/U and a 1-m length of twisted pair stripped from some CAT-5 cable (solid AWG 24 insulated wires), treating these transmission lines as if they were transformers. In other words, for the coax the center wire was the primary and the shield the secondary; and for the twisted pair, one wire was primary and the other secondary. I arranged each of these lines in one large loop for the measurements. I measured the coupling factor k , total inductance L_{tot} , the mutual inductance M , and the characteristic impedance Z_0 under two conditions: 1) without any ferrite loading, and 2) with seven blocks of ferrite snapped around the line. These ferrite blocks totaled 22 cm in length, so they surrounded only a small portion of the line length.

The results are shown in Table 2. Mutual inductance between the two conductors of the transmission line is clearly a significant factor, and the coupling factor k and the mutual inductance M both increase significantly with ferrite loading. However, L_{tot} and Z_0 remain the same because the uncoupled inductance

doesn't change. The procedures for this measurement are given in Appendix B.

Analyzing the Transmission-Line Transformer

Now it is clear that the transmission line and the transformer are very closely related. *An electrically-short transmission line is really just another method of constructing a transformer, and winding this transmission line around a ferrite core simply increases the mutual inductance.* It is instructive to examine some transformer configurations using the tools developed here.

There has been a distinction made between the low-frequency behavior of these transformers, where the "...choking reactance becomes insufficient...", and higher frequencies. A separate analysis is made for low frequencies. The analysis of these transformers does not change at the low frequencies, however. From dc until the winding length is no longer electrically short, the analysis is the same: they are treated as lumped-circuit transformers. The distinction instead should be made between lumped and distributed analysis. This transition occurs at 20 to 100 MHz or so, depending on winding electrical length.

Another common error is the failure to recognize the close magnetic coupling between the windings of the transmission line transformer, and the fact that this leads to the winding voltages being equal. Analysis should begin with this fact and derive other voltages and currents from there.

It would be helpful to go through several typical examples to see how these transformers should be approached. This begins with the basic building block circuit as shown in Figure 11. Dots have been added to the figure

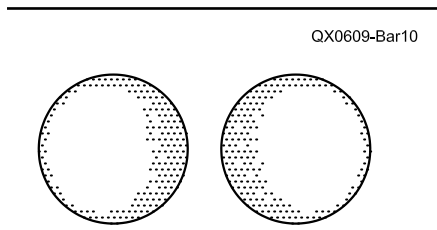


Figure 10 — Current distribution due to proximity and skin effects in a two-wire line.

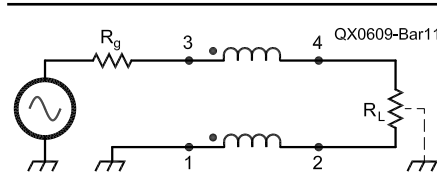


Figure 11 — Basic transmission line transformer building block (and "balun").

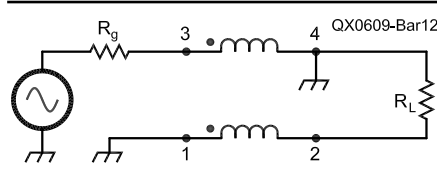


Figure 12 — Phase inverter.

Table 1
Skin Depth Versus Frequency

	100 kHz	1 MHz	10 MHz	100 MHz	1 GHz
Three skin depths (mils)	25	7.8	2.5	0.78	0.25
AWG equivalent	16	26	36	46	—

Table 2
Coupling Factor and Mutual Inductance for Transmission Lines

	k	M (μH)	L_{tot} (μH)	Z_0
Plain coax	0.84	0.86	0.28	52.4 Ω $\angle -1.7^\circ$
Coax plus ferrite	0.98	11.90	0.28	52.5 Ω $\angle -1.7^\circ$
Plain twisted pair	0.78	0.99	0.58	122 Ω $\angle -0.1^\circ$
Twisted pair plus ferrite	0.98	12.20	0.58	121 Ω $\angle +0.1^\circ$

to emphasize the polarity and the transformer-like nature of the two-wire line. I will use the notation V_{xy} to mean the voltage at node x with respect to y , and v_x to mean the voltage at node x with respect to ground. There are four cases to consider: grounding node 4 (phase inverter), as the circuit is shown (“balun”), grounding pin 2 (“delay line”), and connecting nodes 3 and 2 (“bootstrap”).

Phase Inverter, Node 4 Grounded

See Figure 12. First, disconnect the load and examine the magnetizing current (see Appendix A). The source provides magnetizing current directly through R_g and the top winding. There will be a voltage V_{34} across the top winding from voltage divider action between the reactance of the winding and R_g . Because of the flux which couples the two windings, V_{34} always equals V_{12} . Since nodes 1 and 4 are grounded, this places v_2 at $-v_3$ potential and provides a phase inverter.

Now when R_L is connected between nodes 4 and 2, current will be pulled through it because the load voltage is $-v_3$. The lower winding will provide this current since node 4 is grounded, but because of the restoration of magnetizing flux in the transformer (see Appendix A) this same current will be pulled from the source. Note that this is essentially transformer action, drawing load current from the source strictly through flux coupling, and has nothing to do with distributed transmission line behavior.

For frequencies where the line is electrically short, reducing R_L and reducing the winding reactance have the same effect. In both cases there is more current through R_g , either because of transformer-coupled load current or because of reduced reactance (increased magnetizing current) through the top winding. In either case, the drop through R_g causes v_3 to drop and the load voltage to do the same, because the longitudinal winding voltages are locked together by their shared flux. This circuit performs an exact phase inversion down to audio frequencies even with typical RF windings and cores, but the output amplitude falls off because of the decrease in reactance of the top winding.

The low-frequency cutoff of the transformer is the point where the winding reactance equals the parallel combination of R_g and R_L . Remember that the winding reactance is dominated by the mutual inductance which increases with ferrite loading, so the -3 dB frequency can be lowered considerably by adding ferrite.

It is not necessary to require a matched load for this circuit when the windings are electrically short, either for analysis or for operation. Simple circuit analysis is all that is required, remembering that the

winding voltages remain the same.

“Balun”

The circuit of Figure 11 is also known as a Guanella current-mode balun. It is not really a balun, however. Neither currents nor voltages are forced to balance by this circuit. It is, in fact, a common-mode choke. There is no magnetizing current with the load disconnected, so the transmission line currents are fully differential. This means there is no core flux, therefore no longitudinal voltage on the windings, and v_2 is at ground potential. This does not change when ferrite is added to the line, increasing the common-mode choke reactance.

The common-mode choke must have some common-mode impedance following it to affect common-mode signals. The circuit as shown with no ground at the load does not provide that, as it is a purely differential load. Therefore, the load as a whole will become more isolated from the source as the reactance of the choke increases, but in the absence of external ground paths, v_2 will remain at ground potential. If parasitic or direct grounding is placed in the load somewhere, this provides a common-mode impedance and works with the common-mode choke and the source to determine the load voltage. With the choke reactance high enough, the load may be grounded at its midpoint and it will become truly balanced. The choke has not created this balance, however. It has isolated the load enough that it may be made to balance by the midpoint ground connection.

Note that whatever voltage drop V_{34} occurs across the top winding caused by choke reactance, load, or common-mode current will also be induced across the lower winding (V_{12}) by transformer action. This means the total load voltage V_{42} will remain the same regardless of where the ground point might appear in the load.

“Delay Line”, Node 2 Grounded

This is a good example of the importance of mutual inductance in the transmission line model. Without mutual inductance (such as the model of Figure 8), the circuit of Figure 13 does indeed form a delay line. When mutual inductance is considered, however, this is no longer true. Grounding node 2 is then the same as shorting the secondary of a well-coupled transformer. The short is passed directly onto the primary, in this case the top winding.

Here is another way to look at it. Imagine that the transmission line has a large delay, $\frac{1}{2}$ cycle, so when v_3 is at a positive peak, v_4 is at a negative peak. This maximizes the voltage across the upper winding. Now if the lower winding is shorted by grounding node

2, the upper winding is forced to the same voltage, that is, zero. No voltage appears across the upper winding and no delay exists. Once again, remember that the two windings share nearly all their flux and must maintain the same voltage.

This analysis only applies to wire lines. A coaxial line will act as a delay line in this configuration if it is the shield that is grounded at both ends, since the shield does not display any longitudinal voltage. See the discussion on coaxial lines above.

Ruthroff Unbalanced Impedance Transformer

Look at Figure 14A, sometimes called a “bootstrap.” When nodes 2 and 3 are connected together and R_L is connected from node 4 to ground the familiar Ruthroff unbalanced 1:4 impedance converter is obtained. This circuit has been described as “summing a direct voltage with a delayed voltage that traversed a single transmission line.” There is no such thing as a “single transmission line,” meaning one without a return, however, and delay has nothing to do with this circuit except to reduce its performance. It is misleading to analyze it in this way. By looking at the voltages across the nodes, we can see that $V_{43} = V_{21}$ because of flux coupling, so v_4 always equals $2v_2$. The input voltage at nodes 2 and 3 is therefore doubled at node 4, so the configuration is a times two voltage step-up transformer. The power consumed by the load is drawn from the source,

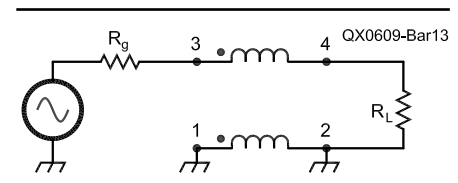


Figure 13 — “Delay line.”

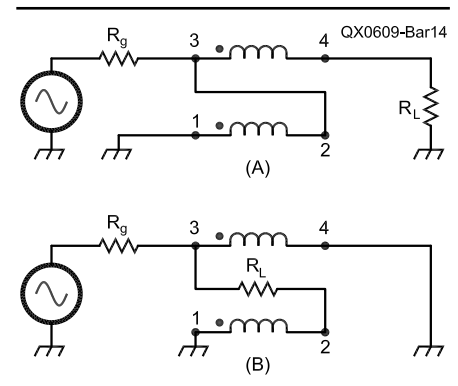


Figure 14 — Ruthroff unbalanced and balanced impedance converters.

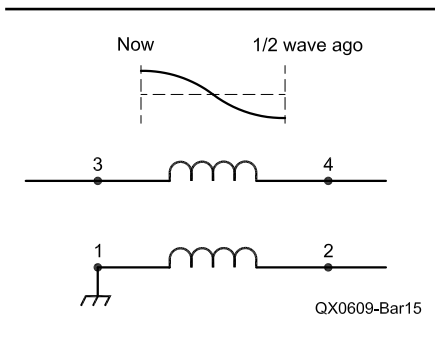


Figure 15 — Delay through a half-wavelength-long transformer.

which is $V_{load}^2 / R_L = (2v_2)^2 / R_L = v_2^2 / (1/4R_L)$ — in other words, as if a load of $1/4R_L$ were connected directly to v_2 without the transformer. Thus the impedance R_L is transformed through $1/4$ its value, as seen at v_2 .

This 1:4 impedance transformation does not depend on load matching as long as the electrical length of the windings is short. Any load will be transformed to $1/4$ its value as seen at v_2 . This effective load will draw current through the source and cause a voltage drop through R_g , depending on the value of the load. When the reactance of the windings is low, there will also be magnetizing current through the lower winding and will cause an additional input-voltage drop.

This transformer (and the next example) actually begins to *degrade* when the windings start acting like transmission lines (that is, when delay starts to become a factor). The voltage wave created by the source at v_3 is connected now the transformer ceases to function, but it will be impaired well before the windings become $1/2$ wavelength long. By this reasoning these configurations should not be considered transmission line transformers at all!

Ruthroff Balun

Figure 14B shows an actual balun, where the voltage across the load is forced to balance with respect to ground. This circuit is very similar to the phase shifter discussed above, where v_3 is seen to equal $-v_2$. So twice the source voltage at v_3 appears across the load, and by the same analysis as the Ruthroff unbalanced configuration above, the load appears as $R_L / 4$ to node 3. So, this is indeed a

1:4 impedance-converting balun. Beware of the performance degradation discussed above as it starts to assume distributed line characteristics.

A Recap

I have answered my original questions and then some:

- Conventional transmission line models are missing a crucial element for transformer analysis: the distributed *mutual inductance*. This is much larger than the uncoupled inductance of the model and has a significant effect on the line's behavior when used as a transformer.
- Transmission line transformers, when the windings are electrically short, are not qualitatively any different from conventional transformers. They are simply very well coupled, which reduces leakage inductance and provides uniform distributed capacitance. There is no distinction between "transmission-line mode" and "conventional-transformer mode" in transformer operation.
- Characteristic impedance and electrical length don't change with ferrite loading because they depend only on the *uncoupled* flux of the individual line conductors. This is almost entirely internal flux when the line is tightly coupled.
- Ferrite loading a line increases the *mutual inductance only*, which also improves the coupling factor. This improves both high and low frequency performance, if the ferrite retains its permeability sufficiently at the high frequencies.
- Using the coupled-windings analysis presented here, a clear distinction is seen between the common-mode choke and the balun. These have been confused in the literature.
- The analysis differs between *lumped* and *distributed* transformer behavior, not between low and high "choking reactance."
- Inductance is a property of conductor geometry and the permeability of the space surrounding the conductor only. It doesn't depend on the fields present.

Acknowledgments

I wish to gratefully acknowledge three of the brightest engineers I know for their helpful review of this article: Larry Brasfield, George Keilman, and Fred Telewski, WA7TZY.

Bibliography

- Cheng, D., *Field and Wave Electromagnetics*, Addison-Wesley, 1989.
 Grover, F., *Inductance Calculations*, Dover, 2004 (orig. Van Nostrand, 1946).
 Krauss, J. and D. Fleisch, *Electromagnetics with Applications*, McGraw-Hill, 1999.
 Ott, H., *Noise Reduction Techniques in*

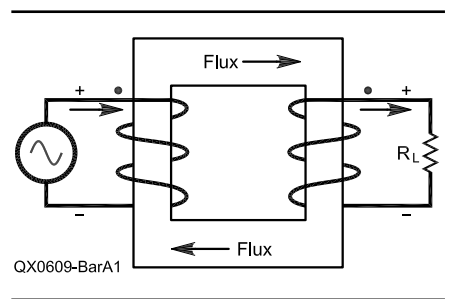


Figure A1 — Voltage, current, and flux relationships in a transformer.

- Electronic Systems*, John Wiley & Sons, 1988.
 Schmitt, R., *Electromagnetics Explained*, Newnes, 2002.
 Terman, F., *Electronic and Radio Engineering*, McGraw-Hill 1955.
 Trask, C., "Designing Wideband Transformers for HF and VHF Power Amplifiers", *QEX*, March/April 2005, pp 3-15.

Appendix A: More Transformer Theory

In conventional transformer operation, ac current from a source passes through a primary winding and generates flux. This flux links with one or more secondary windings, and, in accordance with Faraday's law, induces a *voltage* in the secondary. What is often overlooked is that this flux also generates voltage in the *primary* in exactly the same way. The same flux links both windings, and Faraday's law applies to all windings regardless of where the flux originates.

The polarity of the voltages induced is critical. Lenz's law states that the voltage induced in a conductor by changing flux will be such that it would produce current that would *oppose* the flux that generated it. This sounds rather confusing, but consider Figure A1, showing one instant of time in transformer operation. The voltage source shown produces current into the dotted end of the primary, which produces flux in the direction shown. Check this with the right-hand rule: with fingers curling in the direction of the winding current, the thumb points in the direction of the flux generated. This flux passes through the secondary in the direction shown and induces a secondary voltage as shown. Use your right hand to verify that current from this induced voltage into R_L creates flux in the *opposite* direction from that which produced the voltage.

Now this same flux also creates voltage in the primary which would also tend to create opposing flux. This induced primary winding polarity is the same as the source polarity. Imagine the source replaced by a resistor, and the same flux somehow present

in the core (from some other source). Current would flow *out* of the dotted primary end and thus create flux in the opposite direction of that shown. Thus the primary presents an induced voltage to the source with the same polarity as the source.

So how can there be any current in the primary if a voltage is present on the primary which opposes the source? Wouldn't this result in zero current? Well, imagine that this were so. With no primary current, there would be no flux, and no induced voltage in the primary, which would then produce current! So there is obviously some induced, opposing primary voltage *less* than the source voltage, which allows just the right amount of current to produce the necessary induced voltage. This is really just the regulating mechanism that defines inductive reactance. That is, in any inductor a voltage is induced such that the current that flows is equal to the applied voltage divided by the reactance. For higher frequency or larger inductance, the induced voltage is closer to the applied voltage and therefore there is less current.

This is a complicated introduction to some simple rules that result. There are really only two rules to remember with ideally coupled transformer operation:

- The voltage ratio of each winding (in the absence of winding resistance) will be equal to the turns ratio due to the flux sharing as described above. The polarity is such that the dotted ends (ends entering the core from the same side) will have the same polarity.
- The winding currents need only satisfy two requirements: core magnetization and loss, and load current. These can be determined by disconnecting the load to determine the magnetizing current, and connecting it to determine the effect of the load.

Core magnetization is another term for the current drawn by the finite inductive reactance of the primary winding. Core loss is power drawn from the source to overcome hysteresis and eddy current losses, and applies to ferrite or iron cores. The above rules may be used to determine the behavior of the ideally coupled portion of the transmission line model (identical to a transformer), and the remainder of the model may be added to refine the analysis.

It is also interesting to note that the flux present in the core of a transformer is only that due to core magnetization (neglecting losses), *regardless of load current*. Changing the load current does not change the core flux. To visualize this, refer again to Figure A1, where a voltage source is shown connected directly across the primary. First disconnect the load R_L . Now there is no current in the secondary, and the only primary current is that drawn by the reactance of the primary winding, which depends on the fre-

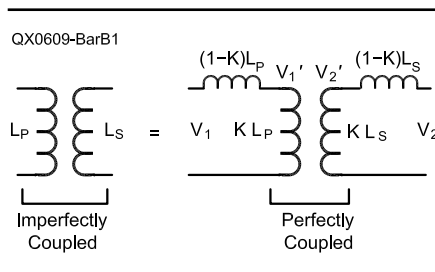


Figure B1—Equivalent circuits for transformer coupling measurement.

quency of operation and the winding inductance. This is the magnetizing current. If the winding reactance is high the magnetizing current will be low, and vice-versa.

Now when a load is connected to the secondary, current is drawn which tries to create flux in the *opposite* direction of the flux established by the magnetizing current. The primary won't allow this to happen, though, since the flux and the primary voltage are locked together by Faraday's law. If the flux changes, the primary voltage must change, but this cannot happen with a voltage source connected to it. Instead, the primary supplies more current, which generates more flux to counteract the flux opposition and thereby restore the flux to the original magnetizing level. This happens effectively instantly (that is, there is no phase shift between primary and secondary currents). So, the load current is immediately drawn from the primary (in proportion to the turns ratio) without changing the core flux. You can think of the flux as a rigid gearbox connecting the windings that transmits the load to the energy source with a fixed gear (turns) ratio.

Appendix B: Transmission Line Measurements

The transmission line measurements above were made on an HP 8151A vector network analyzer with an impedance test fixture. Open/short/load compensation was performed for maximum accuracy. The measurements were made at 2 MHz to avoid excessive skin effect, and a sweep from 1 to 4 MHz was performed to verify that reasonable impedance behavior was seen.

Characteristic impedance Z_0 was determined by measuring Z_{short} and Z_{open} , with the far end of the line shorted and opened respectively. Z_0 is then found from:

$$Z_0 = \sqrt{Z_{open} \cdot Z_{short}} \quad (\text{Eq B1})$$

L_{tot} is determined from the imaginary part of Z_{short} .

Transformer coupling was determined by the following means, illustrated in Figure B1:

L_p = measured midrange inductance of primary, secondary open

L_s = measured midrange inductance of secondary, primary open

$\frac{v_2}{v_1}$ = measured midrange voltage ratio, secondary open, v_1 actual loaded voltage across the primary.

For the voltage ratio test, v_1' is divided from v_1 by the series primary inductors.

$$v_2' = \sqrt{\frac{kL_s}{kL_p}} \cdot v_1' = \sqrt{\frac{L_s}{L_p}} \cdot v_1' \quad (\text{Eq B2})$$

The coils are perfectly coupled, and there is no voltage drop across the secondary leakage inductor.

$$v_1' = \frac{kL_p}{kL_p + (1-k)L_p} \cdot v_1 = k \cdot v_1 \quad (\text{Eq B3})$$

$$v_2' = v_2 = \sqrt{\frac{L_s}{L_p}} \cdot v_1' = kv_1 \sqrt{\frac{L_s}{L_p}} \quad (\text{Eq B4})$$

so

$$k = \frac{v_2}{v_1} \cdot \sqrt{\frac{L_p}{L_s}} \quad (\text{Eq B5})$$

and by definition


$$M = k \sqrt{L_p L_s} = \frac{v_2}{v_1} \cdot L_p \quad (\text{Eq B6})$$

Notes

¹Faraday's law is one of Maxwell's equations, and states that voltage is induced in a conductor in proportion to the rate of change of the total flux linking it. That is, higher amplitude or higher frequency current will result in a higher induced voltage, as will more total flux linkage — by coiling the wire around the flux path, for example.

²Ampere's Law is another of Maxwell's equations, and states that the net magnetomotive force in any closed loop (that is, the summation of the tangential H field around the loop times the loop length) is equal to the net current passing through the loop. Any flux line has a non-zero magnetomotive force since it points in the direction of H for the entire loop (that is, H is always tangential to it and in the same direction). So any closed loop which does not enclose net current cannot be a flux line, thus no flux lines exist in the interior of the coax outer conductor due to current in the outer conductor. An H field *may* exist inside a loop which encloses zero net current, but this field cannot produce a magnetomotive force around the loop.

Biographical Notes

Gerrit Barrere, KJ7KV, is a consulting electronic engineer (www.exality.com) living in Shoreline, near Seattle, WA. He was first licensed in 1995. His professional and Amateur Radio interests include transformers, RF amplifiers, receivers, and signal processing, and he has done much work in medical ultrasound and sonar applications. Gerrit enjoys volunteering, music, reading, and cooking. 

Easy Microwave Filters Using Waveguides and Cavities

The authors show us how to design filters for a microwave station.

Paolo Antoniazzi, IW2ACD, and Marco Arecco, IK2WAQ

Waveguide band-pass filters are frequency-selective devices that perform valuable functions in microwave equipment used in communications. They are most compatible with waveguide antenna feeds and are required for high-power applications and precision performance. They are primarily used at frequencies from 8 GHz to more than 100 GHz.

The main function of a waveguide signal filter is to provide adequate stop-band selectivity without introducing unacceptable insertion loss and frequency distortion. When constructed, the modeled prototype ideally achieves all the desired characteristics; but in practice, this does not automatically happen. Prior to the PC-simulation era, the recourse was to build and modify a prototype to achieve the desired filter characteristics. This is still a good way for amateurs to build many filters, as in the microwave field, when using small copper cavities realized using standard “pipe-cap” techniques.¹ See Figure 1.

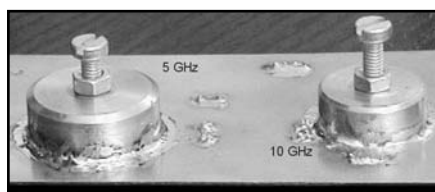
Cavity Filters

The simplest filter for microwave is a single-cavity resonator. A cavity enclosed by metal walls has an infinite number of natural frequencies at which resonance will occur. Different resonance modes can be used with a cavity.² Most interesting for Amateur Radio use is the TM_{010} mode, where the resonant frequency depends only on the inner diameter (D) of the cavity. A practical formula for the resonant frequency is $f = 229.5 / D$, where D is in mm, and f is in GHz. Figure 2 shows the E (electric) and H (magnetic) fields in cylindrical

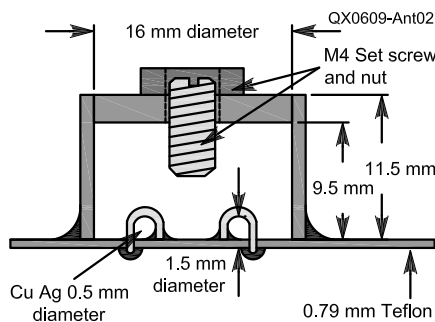
cavities resonating in modes TM_{010} and TE_{011} .

We can see also from the Figure 3 graph that, with $D/L = 1$, high values of Q are theoretically possible; but that is not compatible with the necessity of avoiding spurious modes (as the TE_{111}) because the adjustment screw normally used (see example in Figure 1B) acts in a different manner for modes TM_{010} and TE_{111} .

As an example, with $L = 14$ mm (cylindrical



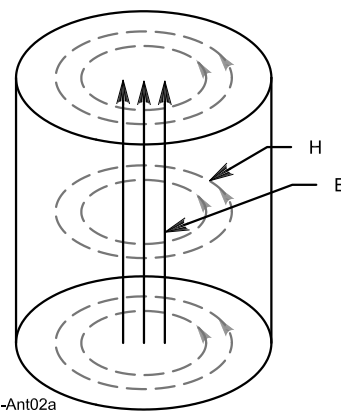
(A)



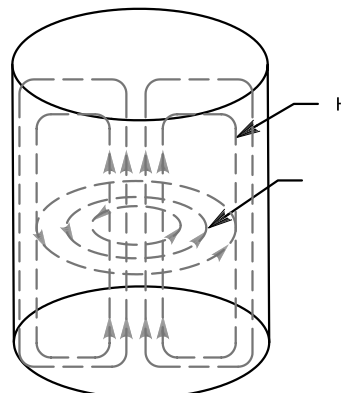
(B)

Figure 1 — Part A shows a typical pipe-cap resonator. Part B shows the dimensions for one example of a 10-GHz resonator.

drical cavity height) and $D = 20$ mm we have: $f_{TM_{010}} = 11.48$ GHz and $f_{TE_{111}} = 13.85$ GHz, with the spurious mode TE_{111} only 2.37 GHz away. Unfortunately, the highest Q of resonator cavities can't be reached when using a



(A)



(B)

Figure 2 — Part A shows electric and magnetic fields in a TM_{010} cavity resonator. Part B shows electric and magnetic fields in a TE_{011} cavity resonator.

¹Notes appear on page 42.

Via Roma 18
20050 Sulbiate MI
Italy
paolo.antoniazzi@tin.it

Via Luigi Einaudi 6
Cologno Monzese MI
Italy
ik2waq@alice.it

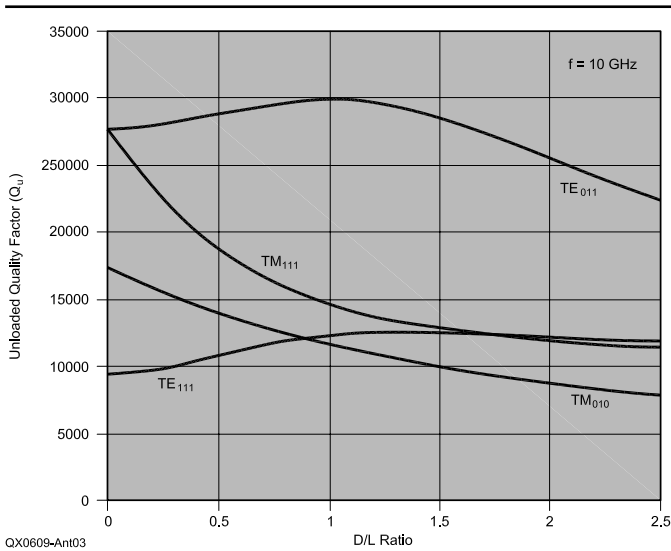


Figure 3 — Unloaded Q of microwave cavities.

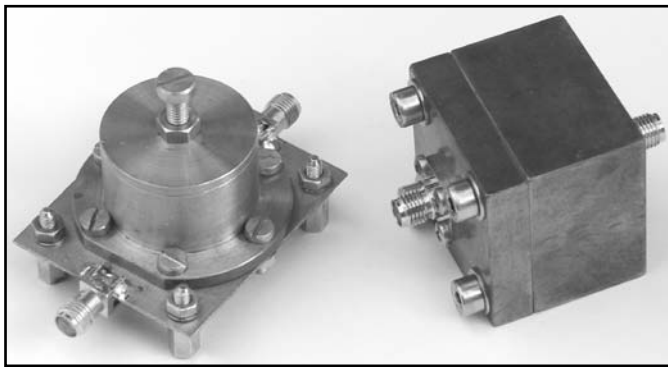


Figure 4 — Two TM_{010} laboratory cavities for “Q” tests.

small cavity height, and therefore the selectivity of the filters is lower. A suggested, but expensive, way is to use a precision TM_{010} machined cavity with a tuning screw limited to the Fine Tuning function. In a copper cavity with $D = 21.5$ mm and $L = 14$ mm the resonance (TM_{010}) is at ~ 10.7 GHz with a calculated $Q_U \approx 9500$ (see Note 2). The nearest TE_{111} spurious mode is at about 13.5 GHz.

We have measured the Q and bandwidth of the two TM_{010} copper cavities of Figure 4 with $D = 21.5 \pm 0.05$ mm and $L = 14$ mm. The ratio between the loaded Q (Q_L) and unloaded Q (Q_U) starting from the resonant bandwidth and the insertion loss of the single cavity with 50- Ω attenuators at the input and output was obtained as shown in Figure 5. For the first cavity (left in Figure 4) excited using small probes (about 2 mm height) or loops on the printed circuit, we measured (with specific microstrip circuits) about 0.8 dB insertion loss because of the feed lines only, and a very bad final unloaded Q_L of 450.

For the second cavity (right in Figure 4) the driving probes are realized using micro-

wave SMA connectors with *only 1.0 mm* of pin height. The measured insertion loss was only 0.6 dB and the resonance bandwidth = 31.6 MHz, with a final $Q_L = 336$ and $Q_U = 4804$. This is a very interesting value for a TM_{010} cavity where the theoretical maximum Q_U (perfectly polished internal walls) is about 9500. The measured resonant frequency was 10.627 GHz.

It is useful to be able to predict the spurious mode frequencies to gain insight into the spurious performance of a cavity filter. The easiest way to predict these modes is to use a Mode Chart as shown in Figure 6.³ The dominant mode of a cavity is the lowest frequency

at which it can resonate.

To prevent the secondary (or spurious) mode resonances, the TM_{010} mode cannot be excited over the entire D/L range reported in Figure 3, but only in the part of the graph where the ratio $D/L > 1$. At $D/L \leq 1$, the dominant mode becomes TE_{111} . Practical values of the D/L ratio to be used are 1.4 to 2.4 for TM_{010} and 0.45 to 0.5 for TE_{111} modes. Frequently, the tuning screw is very long and the cavity is reduced to a standard coaxial resonator in T_{EM} mode.

Another interesting mode is TE_{011} , which is not a dominant mode, so care must be used to choose a coupling system that does not

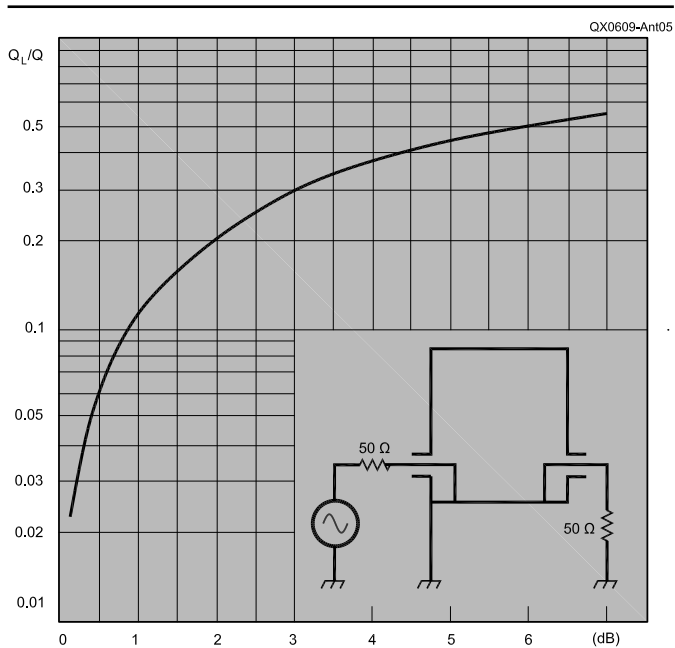


Figure 5 — Ratio of loaded to unloaded Q versus insertion loss in a cavity.

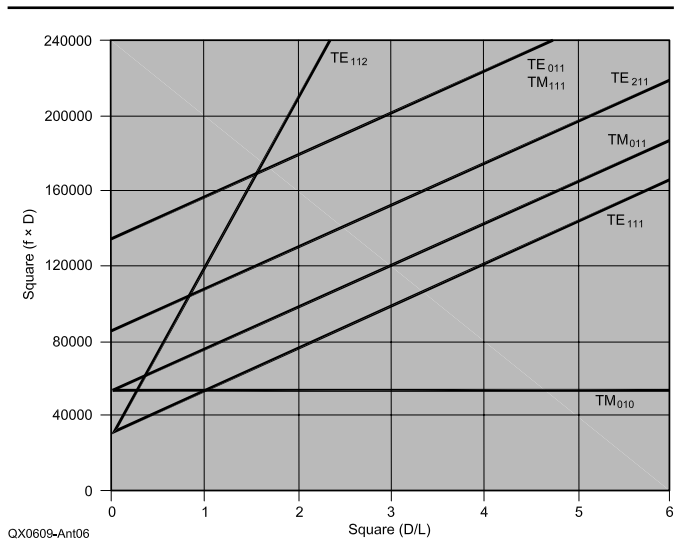


Figure 6 — Mode chart for microwave cavities (frequency in GHz and D&L in mm).

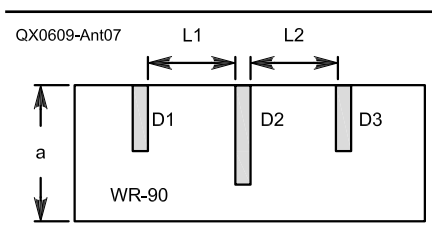


Figure 7 — Layout of a simple two-pole microwave iris filter.

excite the other possible modes that could resonate within the frequency tuning range of the cavity.

To couple power into or out of a resonant cavity, either waveguide or coaxial loops, probes, or apertures may be used. An inductive loop is inserted in the resonator at a desired point where it can couple to a strong magnetic field. The degree of coupling may be controlled by rotating the loop. A capacitive probe is inserted in the resonator at a point where it is parallel to, and can couple to, a strong electric field. The degree of coupling is controlled by adjusting the length of the probe.

The TE_{011} mode is very interesting for its very high quality factor Q_U that is about *three times greater* than that of TM_{010} or TE_{111} cavities. Another advantage of TE_{011} is that there is no axial current. This means that the end plate can be free to move to change the resonant frequency without significant loss due to the current that is parallel to the circular caps of the cylinder. With $D/L = 1.5$, the diameter of the TE_{011} cavity is about two times that of a TM_{010} cavity. For a more professional filter design in X-band, the solution is probably a waveguide filter.

Waveguide Band-Pass Filters

There are several types of filters that can be used to perform the job of separating RF and LO or image frequencies, but most are either difficult to construct or have losses that are unacceptable. The waveguide approach is attractive from the construction point of view and, at 10 GHz, is relatively simple and small.

Waveguide band-pass filters originated in Bell Telephone Laboratories and the MIT Radiation Laboratory of World War II. In 1957, a milestone paper introduced direct-coupled waveguide band-pass filters that quickly evolved into a preferred configuration.⁴ For the waveguide filter structures and design see also a classic reference from 1964 (mentioned in the text of Note 3), the RSGB Microwave Handbook, Vol. 2, and an interesting method of verifying the realized filter on-line.^{5,6} Typical band-pass structures consist of propagating sections of standard waveguide (WR-75 and WR-90 for the 10-GHz band) acting as half-wavelength resonators, which are coupled via discontinuities in the guide such as iris (see Figure 7) or posts.

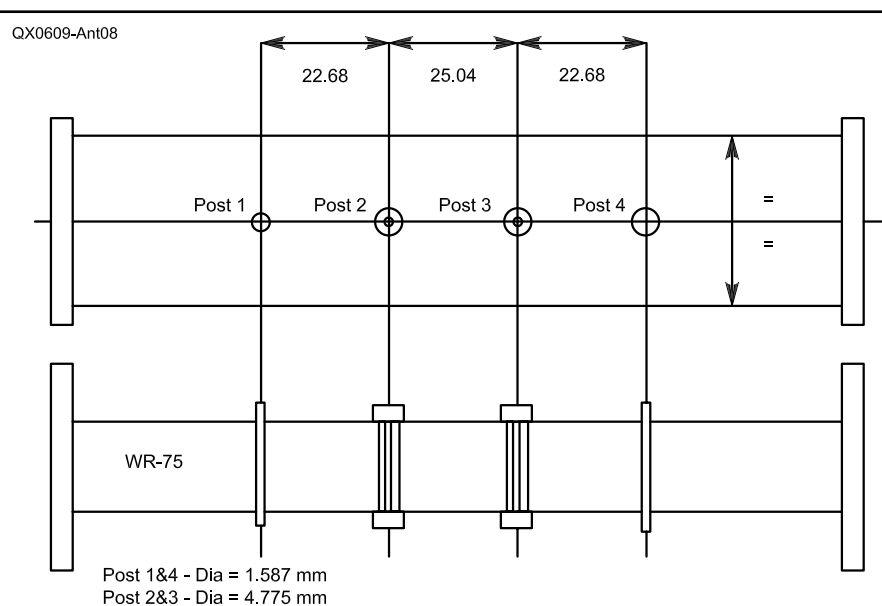


Figure 8 — Mechanical data of a simple “no-tune” post filter with a WR-75 guide.

Filters Using Posts

For the filters using posts, we include only a three-pole 10.315 GHz example from a W1VT design.⁷ The most important mechanical dimensions of this no-tune filter using four inches of WR-75 copper waveguide are shown in Figure 8. The measured performance is very interesting and our proposed idea is for a quasi-no-soldering solution. This is very important because the soldering phase in waveguide is not simple and not without problems. The tested filter is shown in Figure 9.

The main advantage of the no-tune design is the ease of home construction without the need for expensive test equipment. Reliability is also enhanced because of the impossibility of going out of alignment (no screws) if the filter is a part of a transverter at the top of a tower submitted to vibration. Remember that this kind of filter must be carried out with a suitable mechanical accuracy (better than 0.1 mm) to meet performance goals.

To receive the frequency $f_o = 10.368$ GHz and using $f_{IF} = 144$ MHz, the LO frequency becomes $f_{LO} = f_o - f_{IF} = 10.224$ GHz, since most people prefer a lower LO frequency. In the case of our filter, composed of three waveguide resonators ($n = 3$), if an attenuation $A = 30$ dB is requested at the image frequency, the bandwidth can be calculated by:

$$BW = (2 f_{IF}) / (10^{A/(20n)}) = 91 \text{ MHz} \quad (\text{Eq 1})$$

Our test filter was designed *for laboratory use only* at $f_o = 10.315$ GHz to verify the no-tune precision.

The measured performance was:

Insertion Loss = 1.4 dB

SWR < 1.3:1 in-band

BW = 74 MHz (–3 dB) and 250 MHz (–20 dB)

For the complete frequency response, see Table 1. Two homemade waveguide WR-75 to SMA adapters are used for testing the waveguide filter. If the mechanical errors are < 0.1 mm (post positioning), the results are quite good (calculated $f_o = 10.315$ GHz and measured $f_o = 10.294$ GHz).

Iris-Coupled Filters

In waveguide filters that employ iris-coupled resonant sections, we see a pattern similar to that of capacitively coupled resonator filters. If, in rectangular waveguide capable of propagating the dominant mode only,

**Table 1
Measured Response of the No-Tune Three-Pole Filter Designed for $f_o = 10.315$ GHz**

Frequency (GHz)	Attenuation (dB)
10.166	–20
10.228	–10
10.248	–6
10.266	–3
10.273	–2
10.282	–1
10.300	0
10.328	–1
10.334	–2
10.340	–3
10.346	–6
10.368	–10
10.414	–20

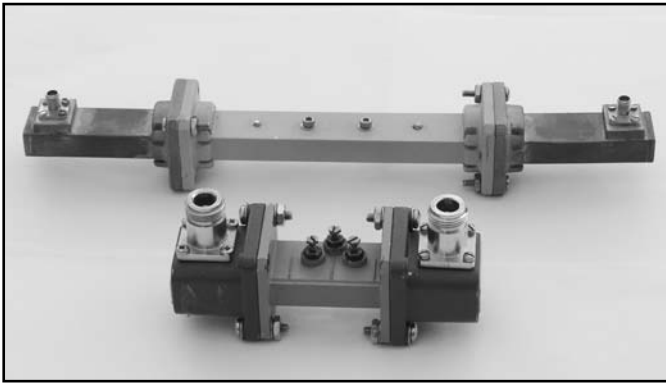


Figure 9 — Photo of the two waveguide band-pass filters (no-tune and iris).

a thin metal partition is inserted in such a way that the edge of the partition is parallel to the electric field, the iris so formed is equivalent to a shunt inductance.⁸ The value of the susceptance has been accurately calculated.^{9, 10}

The waveguide can be cut with a saw, and the iris material soldered on, before plating. As with other metallic filters, it is not unusual for a designer to take advantage of the opportunity to have tuning screws to accommodate small tolerance variations in the filter.

The unloaded Q may be substantially reduced by losses in the loading capacitance. If the capacitance is realized as a simple brass screw, the threads exposed within the waveguide should be removed and the remaining smooth metal should be plated with a highly conductive material such as copper, silver or gold. A low-resistance contact should be insured at the grounded end of the tuning screw.

The layouts of Figure 7 and Table 2 are used as an example to verify, via the Web, the performance of the filter. In our case, the filter is designed for a 10.368 GHz nominal frequency, but the on-line software gives a 10.8 GHz center frequency because the tuning screws are not considered. After the final adjustment the filter is tuned exactly at 10.368 GHz. From the layout data in Figure 7, it's clear that the filter is asymmetric: realized with iris reactances only in one side of the waveguide and with a guide WR-90,

where side a is 22.86 mm. The Java real-time software available free at Guided Wave Technology (see Reference 6) uses a mode-matching simulation method with 13 modes considered in the analysis. The frequency response and the input/output matching ($S_{11} = S_{22}$) of the filter are shown in Figure 10.

Design of a Two-Pole Filter Using Asymmetrical Iris

The first things to be defined are the lower and the upper frequencies at which the filter must operate. To define the filter working frequencies, the values will be 3 to 5% higher to permit fine tuning using suitable screws placed at the center of each resonator. In our case the two frequencies are: $f_1 = 10.805$ GHz and $f_2 = 10.895$ GHz. The tuning screws, to shift the resonant frequency, are simple brass M4 machine screws.

At this point, we select the waveguide to be used: WR-90, with a cut-off frequency of 6.56 GHz ($\lambda_c = 45.72$ mm), is a good candidate to satisfy our requirements (see Table 3).

We have all the elements to calculate both the free-space and the corresponding guide wavelengths:

$$\lambda_1 = 299.8 / f_1 = 27.75 \text{ mm}$$

$$\lambda_2 = 299.8 / f_2 = 27.52 \text{ mm}$$

Table 3
Waveguide Data (Standard WR-90 and WR-75)

Waveguide Designation	Inner Dimensions (mm)	Dominant Mode	λ_c (mm)	f_{cutoff} (GHz)	Frequency Range (GHz)
WR-90	22.86 × 10.16	TE ₁₀	45.72	6.56	8.2 – 12.5
WR-75	19.05 × 9.53	TE ₁₀	38.10	7.87	9.8 – 15.0

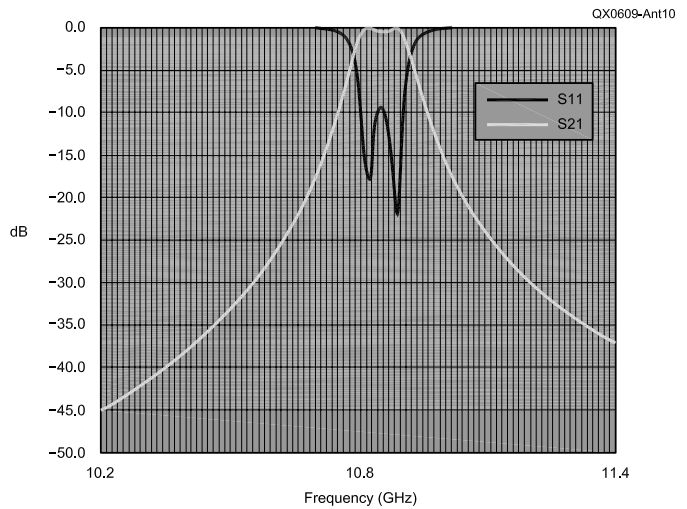


Figure 10 — On-line calculated response of the two-pole filter.

$$\lambda_{g1} = \frac{\lambda_1}{\sqrt{1 - \left(\frac{\lambda_1}{\lambda_c}\right)^2}} = 34.91 \text{ mm}$$

$$\lambda_{g2} = \frac{\lambda_2}{\sqrt{1 - \left(\frac{\lambda_2}{\lambda_c}\right)^2}} = 34.46 \text{ mm}$$

where f_1 and f_2 are in GHz; λ_1 , λ_2 and λ_c in mm.

Table 2
Design Data for the 10.4-GHz Two-Pole Iris Filter

a	Waveguide Width (mm)	22.8
W	Iris Thickness (mm)	0.5
d ₁	Iris no. 1 Length (mm)	13.2
L ₁	First Resonator Length (mm)	16.4
d ₂	Iris no. 2 Length (mm)	16.5
L ₂	Second Resonator Length (mm)	16.4
d ₃	Iris no. 3 Length (mm)	13.2

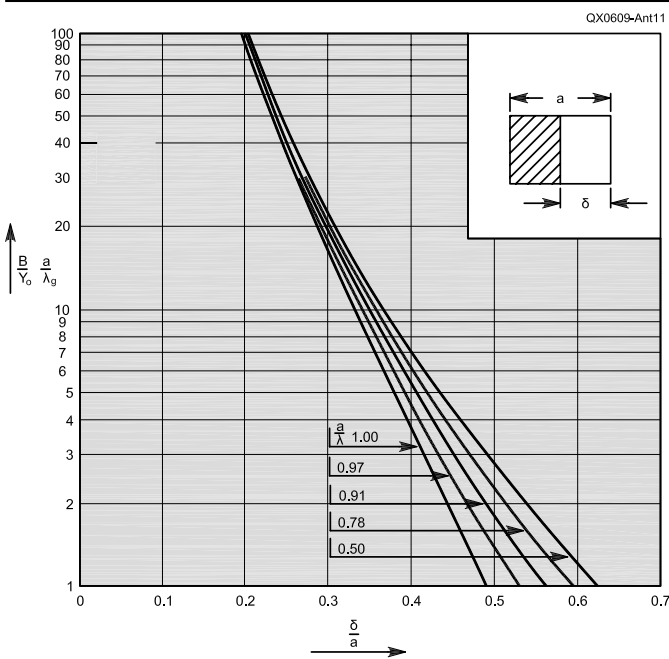


Figure 11 — Susceptance of asymmetrical iris in waveguide.

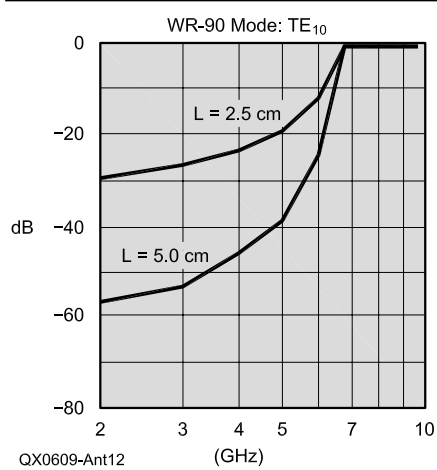


Figure 12 — Calculated response of a high-pass filter using WR-90 in the cutoff zone.

The center waveguide wavelength can be computed by the following:

$$\lambda_{g0} = (\lambda_{g1} + \lambda_{g2}) / 2 = 34.68 \text{ mm} \quad (\text{Eq 2})$$

This corresponds to the free-space wavelength $\lambda_0 = 27.63 \text{ mm}$.

Now we determine the fractional bandwidth from the waveguide wavelength with the equation:

$$\Omega_\lambda = (\lambda_1 - \lambda_2) / \lambda_0 = 0.01307 \quad (\text{Eq 3})$$

It is not the same thing as the fractional bandwidth calculated in terms of frequency. This is related to the dependence of the guide wavelength to the guide physical dimensions.

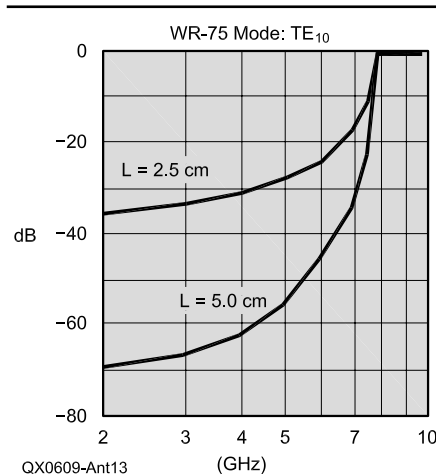


Figure 13 — Calculated response of a high-pass filter using WR-75 in the cutoff zone

At this point, we define the filter response required by our application. We assume to realize a two-pole filter ($N=2$) that will work with a 0.2-dB-ripple Chebyshev response. Table 4 gives the g -value normalized elements that allow us to calculate the coupling coefficients. The values to be used are: $g_0 = 1$, $g_1 = 1.0378$, $g_2 = 0.6745$, $g_3 = 1.5386$:

$$K_{01} = \sqrt{\frac{\pi\omega_\lambda}{2g_0g_1}} = 0.14064 \quad (\text{Eq 4})$$

$$K_{12} = \frac{\pi\omega_\lambda}{2\sqrt{g_1g_2}} = 0.02453 \quad (\text{Eq 5})$$

$$K_{23} = \sqrt{\frac{\pi\omega_\lambda}{2g_2g_3}} = 0.14064 \quad (\text{Eq 6})$$

Note that, in case of a filter with three or more cells, the equation to be used for the whole central element is similar to the one of the second coefficient K_{12} (with a suitable index).

Then we calculate the normalized reactances, to $Z_0 = 1 \Omega$, needed at each iris plate position.

The results, without the relevant units, are pure numbers due to the normalization:

$$X_{01} = X_{23} = K_{01} / (1 - K_{01}^2) = 0.14348 \quad (\text{Eq 7})$$

$$X_{12} = K_{12} / (1 - K_{12}^2) = 0.02455 \quad (\text{Eq 8})$$

We can see that $X_{01} = X_{23}$ and so there is no need to work with the whole values, but only with the first two. The asymmetric iris (layout of Figure 7) appears as an inductor across the guide. After the calculation of the reactances, we are able to compute the spacing between iris into the waveguide (about a $\lambda/2$ cell) both in terms of electric angle (radians) and in millimetres:

$$\theta_1 = \theta_2 = \theta = \pi - [\arctan(2X_{01}) - \arctan(2X_{12})] / 2 = 3.0264 \text{ radians} \quad (\text{Eq 9})$$

$$L_1 = L_2 = (\theta\lambda_{g0}) / (2\pi) = 16.71 \text{ mm} \quad (\text{Eq 10})$$

The iris sizes are obtained through the normalized susceptances:

$$B_{01} = 1 / X_{01} = 6.97 \quad (\text{Eq 11})$$

$$B_{12} = 1 / X_{12} = 40.73 \quad (\text{Eq 12})$$

With the graph of Figure 11 for the iris design, we calculate the value of the ordinate:¹⁰

$$(B_{01} a) / \lambda_{g0} = 4.59 \quad (\text{Eq 13})$$

$$(B_{12} a) / \lambda_{g0} = 26.85 \quad (\text{Eq 14})$$

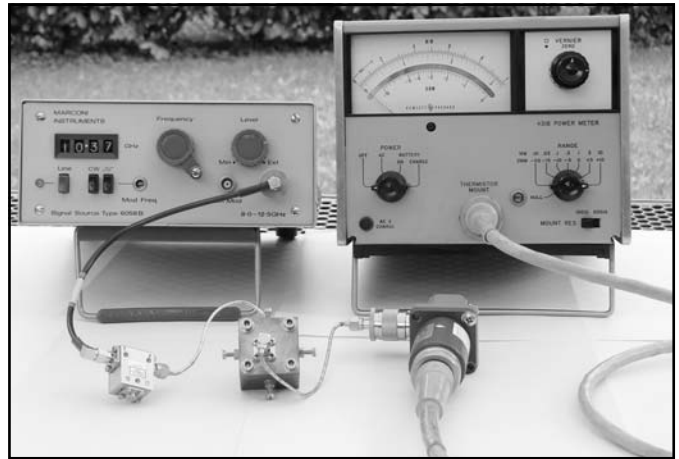


Figure 14 — Test setup: a Marconi 6058B generator, a Narda 7 to 12 GHz circulator and the HP 431B power meter plus thermistor mount

and the ratio $a/\lambda_0 = 0.83$ for a correct choice on the diagram:

$$\delta_1/a = \delta_3/a = 0.42 \quad (\text{Eq 15})$$

$$\delta_2/a = 0.28 \quad (\text{Eq 16})$$

The asymmetric iris (0.5 mm metal sheet) lengths can be obtained by:

$$d_1 = d_3 = a(1 - 0.42) = 13.26 \text{ mm} \quad (\text{Eq 17})$$

$$d_2 = a(1 - 0.28) = 16.46 \text{ mm} \quad (\text{Eq 18})$$

At the end of the computation phase, the filter was also simulated using the on-line software (see Note 6). The relevant results are reported in Figure 10: $f_0 = 10.75$ GHz, $BW = 104$ MHz at -3 dB, insertion loss < 1 dB, return loss > 15 dB, attenuation > 25 dB at $f_0 \pm 250$ MHz. From our laboratory tests: $f_0 = 10.368$ GHz, $BW = 98$ MHz at -3 dB. The differences between simulation and measurements are related to the tuning screws that cannot be simulated.

In Figure 9, note the two band-pass filters analyzed in the paper [three-pole with posts (rear) and iris two-pole (front)] with the waveguide-to-coax adapters (WR-90 and WR-75) used in the tests.

High-Pass Filters

A very easy method to realize a high-pass filter consists in the use of a standard waveguide, of defined length, in the cut-off region. If the involved guide has a different size than the used one, suitable adapters are used to match source and load.

The equation that describes the shape of the waveguide attenuation, in decibels, under cutoff frequency is:

$$A = 54.58 \frac{d}{\lambda_c} \sqrt{1 - \left(\frac{\lambda_c}{\lambda}\right)^2} \quad (\text{Eq 19})$$

where λ_c is the cutoff, λ the working wavelength and d is the guide length. To apply Equation 19 correctly, all dimensions must be expressed using the same units. Take note that the total attenuation obtained (in dB) is directly proportional to the guide length.

The cutoff wavelength can be calculated using the formula applicable to the rectangular guide:

$$\lambda_c = 2a \quad (\text{Eq 20})$$

where a is the largest dimension of the guide cross section considering operation in the TE_{10} mode. A new equation is applied for the circular waveguides operating in the TE_{11} dominant mode:

$$\lambda_c = 3.412a \quad (\text{Eq 21})$$

where, in this case, a becomes the waveguide radius.

Two examples are shown in Figure 12 using a WR-90 waveguide (X-band = 8.2 to 12.4 GHz) and in Figure 13 using a WR-75

Table 4
Chebyshev 0.2-dB Ripple

N	g_0	g_1	g_2	g_3	g_4
1	1.000	0.4342	1.000		
2	1.000	1.0378	0.6745	1.5386	
3	1.000	1.2275	1.1525	1.2275	1.000

(9.8 to 15 GHz). See also Table 3. The considered lengths are about one and two inches (25 and 50 mm).

Simple Measurements

In the photo of Figure 14, see the simple setup used for our measurements, which includes a Marconi 6058B microwave generator and a well known HP 431B power meter with waveguide thermistor mount X486A. Two waveguide to coax adapters, a 7 to 12 GHz SMA Narda isolator and a fixed 7 dB SMA attenuator are the only other components of the tests circuit. An HP waveguide attenuator model X382A and a 10 dB waveguide directional coupler model X752C (with 40 dB directivity) was used to analyze the input/output matching. A high-stability counter with 13-GHz prescaler is used to obtain high-precision frequency measurements. All these components are available today at very low cost on the surplus market.

Appendix:

Cavity Resonating Modes

The general classification of transverse electric (TE) and transverse magnetic (TM) modes is true both for cylindrical and rectangular cavities. The denomination derives from the one already used for the waveguide. In the transverse electric mode, the entire electric field is in the transverse plane, which is perpendicular to the length of the waveguide (direction of energy travel). Part of the magnetic field is parallel to the length axis. In the transverse magnetic mode, the entire magnetic field is in the reverse plane and has no portion parallel to the length axis.

In the rectangular waveguide resonators the modes are named TE_{mnp} or TM_{mnp} where the integer "m" designates the number of half waves of electric or magnetic field in the "x" direction (the bigger dimension of waveguide cross section), while "n" denotes the number of half cycles in the "y" direction (the smaller dimension of waveguide cross section) and "p" indicates the number of half wave in the "z" direction (perpendicular to the waveguide cross section).

In cylindrical resonators the same type of index system is used, but changes the meaning of its subscripts: "m" represents the number of half waves variation along the circum-

ference that constitutes the base of the cylinder (as a function of its angle at the centre), "n" express the number of half cycles change along the base radius direction, "p" define the number of half wave change along the cylinder symmetry axis.

Notes

¹H. J. Meise, DK2AB, *Complementation of Cylindrical Resonator Cavities*, Dubus, 2/1987, pp 95-97.

²*Reference Data for Engineers*, SAMS, Seventh Edition, 1989, pp 30-20 to 30-22.

³G. Matthaei, L. Young and E. M. T. Jones, *Microwave Filters, Impedance-Matching Networks and Coupling Structures*, Artech House, 1980.

⁴S. B. Cohn, "Direct-Coupled Resonator Band-Pass Filters," *Proc of IRE*, pp 187-195, Feb 1957.

⁵*RSGB, Microwave Handbook*, 1991, Vol. 2, pp 12.23 to 12.27.

⁶www.guidedwavetech.com/IRISHTML/iris2p.htm

⁷Zack Lau, W1VT, "A No-Tune 10 GHz Filter", *QEX*, May/June 2000, pp 52-55.

⁸C. G. Montgomery, *Principles of Microwave Circuits*, 1948, pp 163-167.

⁹N. Marcuvitz, *Waveguide Handbook*, 1951

¹⁰*Microwave Journal Handbook*, Feb 1968, pp 26.

Paolo Antoniazzi was licensed as IW2ACD and became a member of the Associazione Radiatori Italiani (ARI) in Italy in 1961. He worked for Siemens, GTE, Sprague and ST Microelectronics in the fields of RF and telecommunications marketing and applications until his retirement in November 2003. Paolo is particularly interested in simulation and measurements (and writing papers) about narrow-band LF, 2.4 GHz, and more recently, the 10 GHz band. Space communications with the future P3E and P5A satellites is a priority interest for 2006 - 2007.

Marco Arecco, IK2WAQ matured his professional experience in semiconductor manufacturing, working for STMicroelectronics for more than 35 years. His last position, before retirement in early 2004, was as the Nonvolatile Memory Product Engineering Team leader. Marco is a member of ARI. He has been licensed 12 years and his Amateur Radio interests include LF operation and VHF, UHF and microwave antenna simulations and measurements.



Q Calculations of L-C Circuits and Transmission Lines: A Unified Approach

Calculate the Q factor of any circuit based on its complex impedance data. These computations allow easy simulation and optimization of stub resonators. They apply to RLC circuits, transmission lines and antennas.

Jacques Audet, VE2AZX

Q factor calculations of reactive circuits are of interest since the Q factor relates directly to the circuit selectivity: The higher the Q , the better the selectivity and the lower the insertion loss of the filter. For oscillators, higher Q also means that lower phase noise is produced. In the case of antennas, a lower Q is generally preferred, giving a larger SWR bandwidth.

This paper attempts to clarify the various methods that can be used to calculate Q factor. I will show how to calculate the Q factor using general methods for simple RLC circuit configurations and will show that the same methods can be used to compute the Q factor of stub resonators and antennas operating outside their resonant frequencies. It allows computing the SWR bandwidth of antennas once the Q factor is known.

The calculations for transmission line stubs may be carried out using *Mathcad* files (described later in the article) with attenuation data provided by freeware programs available on the Web. Simulation results will be presented as well as measured Q values on a length of RG-58 cable.

Simple RX Circuits

When the internal circuit configuration or

7525 Madrid St
Brossard, QC J4Y 1G3
Canada
ve2azx@amsat.org

equivalent circuit is known, we can measure the complex impedance at a single frequency and calculate the Q of that impedance using the classic relation:

$$Q = \frac{|X|}{R_s} = \frac{R_p}{|X|} \quad (\text{Eq 1})$$

where X is the reactance, R_s the series resistance and R_p the parallel resistance.

The simple series model $R_s - jX$ assumes that the impedance consists of a resistance R_s in series with a *single* reactance X , coming from a perfect inductance or from a perfect capacitance. Note that the measurement of R_s and X only needs to be done at a single frequency. Examples of this are the Q of an ideal inductor or capacitor. In this model, only two elements are used to describe the impedance.

Since real capacitors all have some series inductance, we add it in series with the capacitor. At some frequency the reactances of the L and C will cancel and the impedance is reduced to the series R_s . Using Equation 1 to compute the Q factor yields a value of zero, since the total reactance is zero. In general, the above equation cannot be used to compute the Q factor when multiple reactances are involved. The Q factor as obtained from Equation 1 is called the apparent Q , since it is not generally related to the resonator selectivity.

In this last case the Q cannot be simply calculated by Equation 1. The equation does not tell us the selectivity of our circuit since

we now have a resonator. A resonator requires a minimum of two reactive elements that have opposite signs.

Q Factor of Series RLC Circuits

A simple RLC circuit — series or parallel — can be used as a resonator. We will first consider the series RLC configuration. Here we are interested in the Q factor at resonance and at other frequencies.

The impedance Z of the RLC circuit shows zero reactance at resonance. Then clearly Equation 1 cannot be used to compute the Q factor at resonance.

Equation 2 shows how to calculate the Q factor *at resonance and below*. Note that the derivative term

$$\frac{dX}{d\omega}$$

implies that the reactance X is effectively calculated (or measured) at two frequencies:^{1,2}

$$Q_a = \frac{-X + \omega \frac{dX}{d\omega}}{2R_s} \quad (\text{Eq 2})$$

where

$$Z = R_s + jX,$$

$$R_s = \text{Re}[Z]$$

and

$$X = \text{Im}[Z]$$

¹Notes appear on page 51.

R_s and X are the real and imaginary components of the RLC circuit impedance Z and $\omega = 2\pi f$.

Equation 2 may be simplified as:

$$Q_a = \frac{F_r}{R_s f} \sqrt{\frac{L}{C}} \quad (\text{Eq 3})$$

where Q_a is the Q factor below the resonant frequency F_r , and f is the frequency at which Q_a is calculated.

The resonant frequency may be expressed as:

$$F_r = \frac{1}{2\pi\sqrt{LC}} \quad (\text{Eq 4})$$

After substituting Equation 4 into Equation 3, we get:

$$Q_a = \frac{1}{2\pi f C R_s} \quad (\text{Eq 5})$$

This equation is valid at resonance and below.

Equation 5 simply represents the ratio of the capacitive reactance to the series resistance, R_s .

An equation similar to Equation 2 may be used *above resonance*:

$$Q_b = \frac{X + \omega \frac{dX}{d\omega}}{2R_s} \quad (\text{Eq 6})$$

The sign of the first term of the numerator, X , is now positive. As before, Equation 6 may be simplified:

$$Q_b = \frac{f}{R_s F_r} \sqrt{\frac{L}{C}} \quad (\text{Eq 7})$$

After substituting Equation 4 into Equation 7, we get:

$$Q = \frac{2\pi f L}{R_s} \quad (\text{Eq 8})$$

This equation is valid at resonance and above.

Equation 8 simply represents the ratio of inductive reactance to the series resistance, R_s .

Equations 2 and 6 may be combined by taking the absolute value of X in the first numerator term. Equation 9 gives the Q factor of a series RLC circuit, below and above the resonant frequency.

$$Q = \frac{|X| + \omega \frac{dX}{d\omega}}{2R_s} \quad (\text{Eq 9})$$

This equation is for computing the Q factor above and below series resonance.

Figure 1 shows an example of the Q factor variation versus frequency as computed from Equation 9 or from Equations 5 and 8. Note that the Q factors calculated by Equations 5 and 8 are equal at the resonant frequency of

10 MHz, since the reactances are also equal. Above and below 10 MHz, the reactances increase, causing a corresponding increase in the Q factor. The “off resonance” Q factor gives the selectivity obtained when a lossless reactance is used to recover resonance.

Q Factor of Parallel RLC Circuits

The Q factor of RLC parallel circuits may also be calculated with the general formulas given by Equations 2 and 6 above. In this case, we need to use the admittances instead of the impedances, since the reactance goes to \pm infinity at resonance, with a negative reactance slope. We then substitute $1/Z$ for Z in these equations.

As in series RLC circuits, the Q factor may also be calculated:

$$Q = \frac{-\text{Im}\left[\frac{1}{Z}\right] + \omega \frac{d}{d\omega} \text{Im}\left[\frac{1}{Z}\right]}{2\text{Re}\left[\frac{1}{Z}\right]} \quad (\text{Eq 10})$$

where Re and Im are the real and imaginary operators.

This equation is for use below resonance, after substituting $1/Z$ for Z in Equation 2.

Equation 10 may be simplified:

$$Q_a = \frac{R_p}{2\pi f L} \quad (\text{Eq 11})$$

This equation is for calculating the Q below resonance. R_p is in parallel with L and C .

Above resonance:

$$Q = \frac{\text{Im}\left[\frac{1}{Z}\right] + \omega \frac{d}{d\omega} \text{Im}\left[\frac{1}{Z}\right]}{2\text{Re}\left[\frac{1}{Z}\right]} \quad (\text{Eq 12})$$

This equation is for calculating the Q above resonance.

Equation 12 may be simplified:

$$Q_b = 2\pi f C R_p \quad (\text{Eq 13})$$

This equation is for calculating the Q above resonance.

Equations 10 and 12 may be combined by taking the absolute value of

$\text{Im}\left[\frac{1}{Z}\right]$ in the first numerator term. Equation 14 gives the Q factor of a parallel RLC circuit, for use below and above the resonant frequency.

$$Q = \frac{\left| \text{Im}\left[\frac{1}{Z}\right] \right| + \omega \frac{d}{d\omega} \left| \text{Im}\left[\frac{1}{Z}\right] \right|}{2\text{Re}\left[\frac{1}{Z}\right]} \quad (\text{Eq 14})$$

This equation computes the Q factor for parallel resonance.

Transmission Line Stub Resonators

The transmission line stub resonator always includes three distributed elements: inductance, capacitance and resistance. Taking a single measurement of the complex impedance at the stub terminals only allows us to represent the line as a simple two-element model, with an apparent Q value as given by Equation 1. It does not allow Q factor predictions under resonant conditions. While this is sufficient for some uses, very often one needs to know the stub Q factor when the stub is used as a resonator, with or without a compensating (loading) reactance. In particular, it is interesting to know the Q factor of a quarter wavelength resonator, versus one that is less than a quarter wavelength long and brought back to resonance by using capacitive loading at its open end. In some cases, the shorter resonator will have a higher Q . Thus it is useful to know how the resonator unloaded Q varies versus frequency, length,

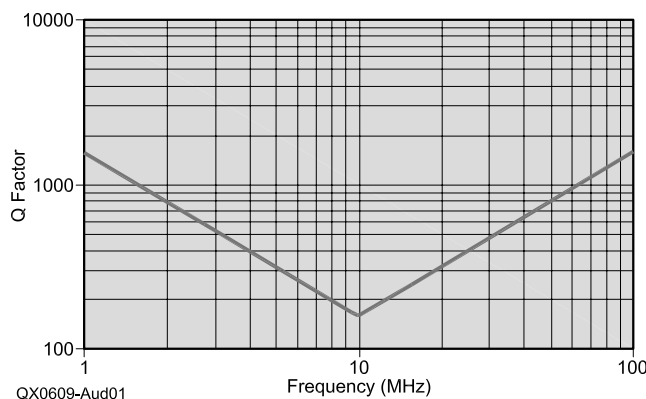


Figure 1 — Q factor of a series RLC circuit.

line attenuation and resonator loading such as capacitive or inductive loads in both open and short configurations.

Estimating the Q factor of a "Short" Unloaded Resonator

In general, Equation 1 above can't be used to compute the Q factor for a quarter-wave resonator, since the reactance value X is zero or infinite at resonance, and will set the Q to zero or infinity. We also expect a short line (say 1% of wavelength) to behave as lumped inductance in the case of a shorted line and a lumped capacitance in the case of an open line, and with a Q factor that can be approximated by Equation 1.

Computing the Q Factor of a Quarter Wavelength Unloaded Stub, Open or Shorted — The Easy Way

The simplest way to calculate the Q factor of a quarter wavelength unloaded stub is to use Equation 15.

$$Q = \frac{8.686 \pi}{A_o \lambda} \quad (\text{Eq 15})$$

where A_o is the attenuation in dB/100 ft and λ is the wavelength in hundreds of feet.

Equation 15 may also be written in a more practical form as:

$$Q = \frac{2.7743 F_o}{A_o VF} \quad (\text{Eq 16})$$

where F_o is the quarter wave resonant frequency in MHz, A_o is the attenuation in dB/100 ft at F_o and VF is the velocity factor. Equation 16 may also be derived from the attenuation coefficient α and the phase coefficient β :³

$$Q = \frac{\beta}{2\alpha} \quad (\text{Eq 17})$$

I have found that Equations 15 to 17 apply to all unloaded resonators — open or shorted — whose length is an integer multiple of a quarter wavelength. Note that these equations do not distinguish between open and shorted quarter wave resonators. It was found that open and shorted resonators have equal Q factors for a given resonance mode, no matter their conductor and dielectric losses, as long as we use the same loss values for both lines.

From Equation 16, given constant values for A_o and VF , the Q factor is proportional to the frequency. In real life, the attenuation factor A_o will increase with frequency, causing the Q to increase less rapidly.

The line losses, A_o , are the total losses. Transmission lines have two loss mechanisms, however: conductor losses, which are caused by skin effect, and dielectric losses, which occur in the dielectric material.

In practice, in the HF and VHF ranges,

the dielectric losses are much lower than the conductor losses for coaxial lines. For those lines, we expect the Q factor of opened lines (subjected to dielectric losses) to be higher than their shorted equivalent (subjected to conductor losses) only when their length is much below a quarter wavelength.

Computing the Q Factor When the Stub Length is Below or Equal to a Quarter Wavelength

Computing the Q factor of a line requires knowledge of the attenuation due to conductor losses: $A_o c$ in dB/100 feet and the attenuation due to dielectric losses — $A_o d$ in dB/100 ft. The frequency term, f , is in MHz.

$$A_o c = K_1 \sqrt{f} \quad (\text{Eq 18})$$

$$A_o d = K_2 f \quad (\text{Eq 19})$$

where K_1 and K_2 are respectively the conductor and dielectric losses in dB/100 ft at 1 MHz.

The K_1 and K_2 loss coefficients may be obtained from the TLDetails.exe program.⁴ It gives the coefficients for most coaxial cables. An accompanying Microsoft Excel file also allows K_1 and K_2 calculations for user-entered attenuation data.

For printed circuit lines such as microstrips, it is convenient to express the losses as follows:

$$A_o c = A_o cr \sqrt{\frac{f}{f_r}} \quad (\text{Eq 20})$$

This equation calculates attenuation due to conductor losses.

$$A_o d = A_o dr \frac{f}{f_r} \quad (\text{Eq 21})$$

This equation calculates attenuation due to dielectric losses.

$$A_o = A_o c + A_o d \quad (\text{Eq 22})$$

This equation calculates the total losses.

A_o is the total attenuation in dB/100 ft, $A_o cr$ is the conductor loss attenuation in dB/100 ft at frequency f_r , f is the frequency, $A_o dr$ is the dielectric loss attenuation in dB/100 ft at the same frequency, f_r .

Note that the conductor losses vary in proportion to the square root of the frequency, and the dielectric losses are proportional to frequency. The program TXLine.exe may be used to compute the PCB line attenuations for various configurations.⁵

Note that $A_o d$ may also be derived from the loss tangent, $L \tan$, of the dielectric. VF is the velocity factor and f is the frequency in MHz.

$$A_o d = 2.78 L \tan \frac{f}{VF} \quad (\text{Eq 23})$$

We need to compute the attenuation co-

efficient, α , and the phase coefficient, β :

$$\alpha = \frac{\ln(10)}{2000} A_o \quad (\text{Eq 24})$$

(Attenuation in neper/foot)

$$\beta = \frac{2 \pi f}{VF c_e} \quad (\text{Eq 25})$$

(Phase coefficient in radians/foot)

VF is the line velocity factor, c_e is the velocity of light in million feet/sec, A_o is the total attenuation in dB/100 ft and f is the frequency in MHz. The complex propagation coefficient, γ , may now be calculated:

$$\gamma = \alpha + j\beta \quad (\text{Eq 26})$$

To properly model the lossy transmission line, we must compute the complex line impedance, Z_o , using Equation 27. Here the term R represents the series conductor losses due to the skin effect and dc conductor resistance. G is a conductance term representing the parallel dielectric losses. Both R and G are a function of the frequency, f , thus making Z_o a complex value, which is also a function of the frequency.⁶

$$Z_o = \sqrt{\frac{R + j2 \pi f L}{G + j2 \pi f 10^{-6} C}} \quad (\text{Eq 27})$$

In Equation 27, R and G are in ohms per foot and siemens per foot, respectively. The L and C are the distributed inductance in $\mu\text{H}/\text{foot}$ and capacitance in pF/foot , respectively. The frequency, f , is in MHz.

The R , L , C and G components will be calculated as follows (See Note 6.):

$$L = \frac{\text{Im}[\gamma Z_o]}{2 \pi f} \quad (\text{Eq 28})$$

L is in μH per foot.

$$C = \frac{\text{Im}\left[\frac{\gamma}{Z_o}\right]}{2 \pi f 10^{-6}} \quad (\text{Eq 29})$$

where C is in pF per foot.

$$R = 2 \alpha \text{Re}[Z_o] \quad (\text{Eq 30})$$

where R is in ohms per foot.

$$G = \frac{2 \alpha \text{Re}[Z_o]}{|Z_o|^2} \quad (\text{Eq 31})$$

where G is in siemens per foot

Computing R and G requires the knowledge of Z_o and to compute Z_o we need the R and G values. To get around this problem we use an iterative process where we first use a real value of $Z_o + j 0$ ohms for Z_o (the cable nominal impedance). We then calculate R , L , G and C . These values are then used to recalculate a new complex value for Z_o . This

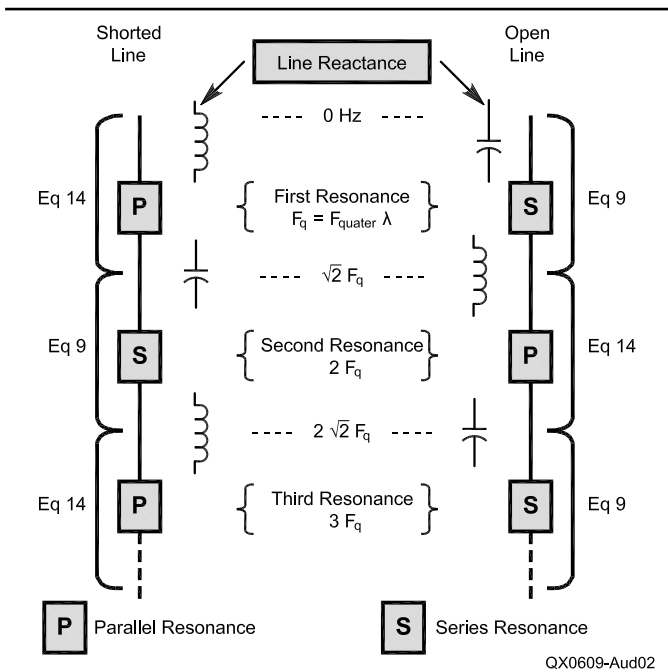


Figure 2 — Resonant modes for shorted and open lines along with the relevant equations for Q calculations.

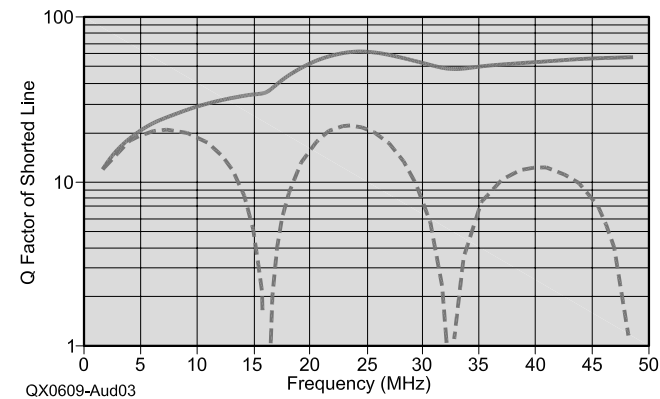


Figure 3 — Q factor of a shorted line. Q factor versus frequency for a 10 foot length of RG-58C, giving first resonance at ~16.229 MHz (f_q). Solid line is resonator Q, dotted line is the apparent Q.

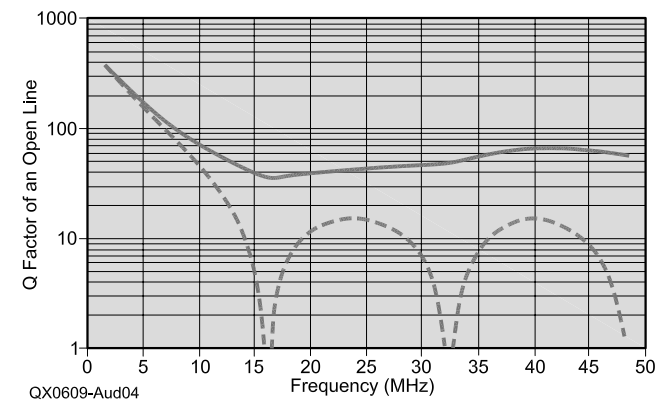


Figure 4 — Q factor of an open line. Q factor versus frequency for a 10 foot length of RG-58C, giving first resonance at ~16.229 MHz (f_q). Solid line is resonator Q, dotted line is the apparent Q.

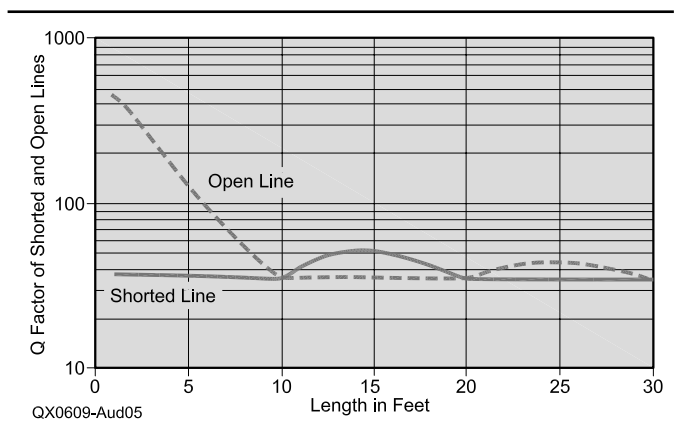


Figure 5 — Q factor versus line length for RG-58C, at 16.229 MHz.

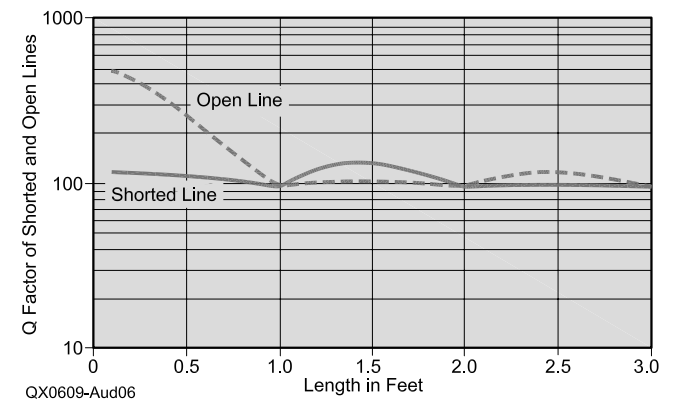


Figure 6 — Q factor versus line length for RG-58C, at 162.29 MHz.

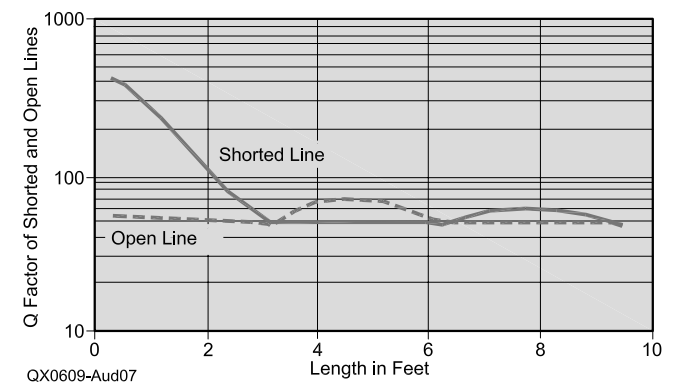


Figure 7 — Q factor versus line length at 500 MHz for a 50 Q microstrip, 114 mil wide, above a 62 mil thick FR4 substrate.

process is repeated twice until we get a final value for Z_o .

We are now ready to calculate the stub impedances, using the complex value of Z_o , for both open and short lines. Equation 32 or 33 will be used to calculate the stub impedances.

$$Z_{s,open} = \frac{Z_o}{\tanh(\gamma len)} \quad (\text{Eq 32})$$

where len is the line length in feet and Z_o the stub line complex impedance.

The shorted stub impedance may be calculated as:

$$Z_{s,short} = Z_o \tanh(\gamma \text{ len}) \quad (\text{Eq 33})$$

The stub Q factor may now be calculated as a function of frequency or length using Equation 9 for an open stub, since it behaves like a series resonant circuit. For a shorted stub, we use Equation 14 to calculate the Q factor, just like in the case of the RLC parallel circuit. These calculations are valid below and above the quarter wave resonant frequency.

Resonant Modes

Figure 2 shows the resonant modes for

shorted and open lines. Equation 14 is used when the line exhibits parallel resonance and Equation 9 when it exhibits series resonance, just like for discrete RLC resonators. Note that the shorted line presents an inductive reactance below the first quarter wave resonance while the open line is capacitive below resonance.

The *Mathcad* spreadsheets TRL_Q_Calc1.mcd for use with the TLDetails.exe program on coaxial lines and TRL_Q_Calc-PCB1.mcd for use with TXLine.exe program on PCB lines show all above calculations in detail.^{4,5,7}

Examples of Calculated Q factors versus Frequency for Shorted and Opened Lines of Identical Lengths

Figures 3 and 4 show the resonator Q factor for shorted and open lines (a 10-foot length of RG-58C). The solid curves were computed from Equations 14 and 9 as per Figure 2, while the dotted curves show the ratio of reactance to resistance as computed by Equation 1. This is the apparent Q . In general, the resonator Q cannot be computed just by taking the ratio of reactance to resistance as in Equation 1. This

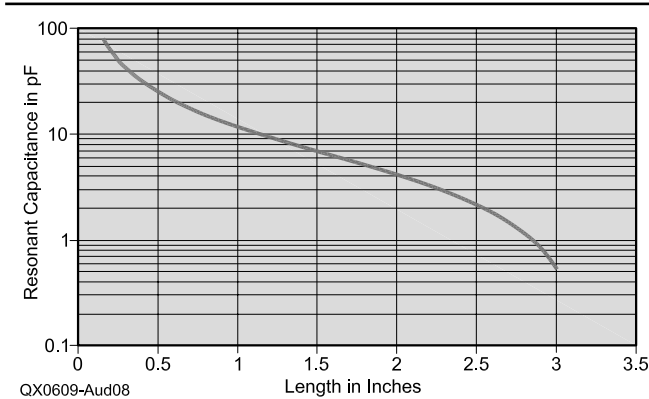


Figure 8 — Capacitance in pF required to keep the resonant frequency at 500 MHz.

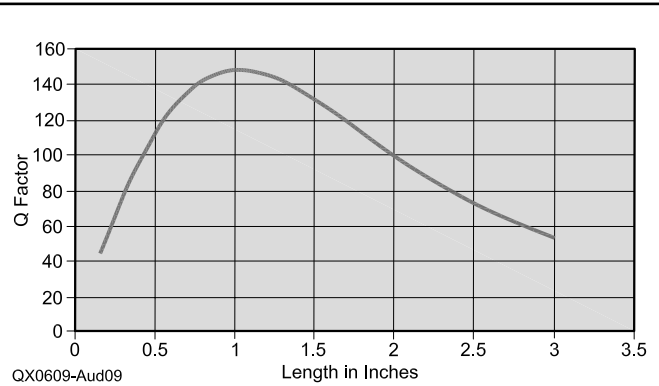


Figure 9 — Shorted stub Q factor versus length with the microstrip resonated with a capacitor having an ESR of 0.08 Ω .

Table 1

Mode	Freq (MHz)	Shorted Line			Open Line			Conductor Losses dB/100 ft	Dielectric Losses dB/100 ft
		EQ. Used	Calc Q	Q error	EQ. Used	Calc Q	Q error		
1X	10	14	28	<0.1%	9	79	<0.1%	1.0	0.1
1X	16	14	18	0.2%	9	29	<0.1%	2.0	0.02
1X	16	14	16	0.2%	9	14	<0.1%	1.0	1.00
1X	16	14	166	<0.1%	9	142	<0.1%	0.1	0.10
1X	18.5	14	15.5	0.1%	9	22.8	0.1%	2.0	0.02
1X	19	14	10	0.5%	9	11	0.6%	4.0	0.02
1X parallel	19.8545	14	20.3	0.2%				2.0	0.02
1X series	19.8773				9	20.4	<0.1%	2.0	0.02
2X	21	14	23.4	0.1%	9	21	0.2%	2.0	0.02
2X	28	14 or 9	36.9	0.3%	9 or 14	24.3	0.6%	2.0	0.02
2X	28	14 or 9	14.1	2.4%	9 or 14	17.5	1.6%	1.0	1.0
2X	28	14 or 9	143.7	<0.1%	9 or 14	177	<0.1%	0.1	0.1
2X parallel	39.729	9	28.6	0.3%				2.0	0.02
2X series	39.71				14	28.6	0.2%	2.0	0.02
3X	41	9	29	0.3%	14	30.8	0.2%	2.0	0.02
3X	50	14	15.7	4.0%	9	13.4	5.3%	1.0	1.0
3X	50	14	139.6	<0.1%	9	162.4	<0.1%	0.1	0.1
3X parallel	59.5863	14	34.6	0.4%				2.0	0.02
3X series	59.609				9	34.6	0.2%	2.0	0.02

approximation is valid for frequencies below 25% of the quarter wave resonant frequency (~16.229 MHz), however. For both shorted and open stubs, Equation 16 may be used to calculate the Q factor at all integer multiples of a quarter wavelength.

Using a constant real value for the line impedance makes the Q factor versus frequency equal for both open and shorted lines. This method makes calculations much faster and simpler, but as shown in Figures 3 and 4, it will give very large errors in the Q and in the complex stub impedance. I also discovered that the common transmission line models used in my professional RF-microwave circuit simulator use this shortcut too.

Note the Q factor behavior below the quarter wave frequency F_q . At frequencies below F_q , the Q factor goes down for the shorted line while it goes up for the open line. This tells us that the line losses are mostly in the conductors (~1.8 dB/100 ft while the dielectric losses are ~0.14 dB/100 ft. at the quarter wave resonant frequency).

It is also interesting to compute the Q factor versus line length at a fixed frequency. Figure 5 shows the Q factor at 16.229 MHz for a 10-foot length of RG-58C cable. Again the open line has a much higher Q factor below the quarter wave resonant length of 10 feet.

Figure 6 shows the Q factor versus line length for a 1 foot length of RG-58C line. Decreasing the line length by a factor of 10 has increased its resonant frequency by the same factor and the Q at self resonance goes from 36 to 100, a factor of ~3. This is possible since the losses are mainly conductor losses: 5.77 dB/100 ft and the dielectric losses are 1.36 dB/100 ft at 162.29 MHz. Note also that the loss tangent of the dielectric is 0.002.

In contrast, PCB losses will be much higher with say, FR4 which has a typical loss tangent of 0.02

The Q factor for a 50- Ω microstrip trace has been computed in Figure 7. The PCB loss tangent is 0.02 and the trace length is 3.469 inches to obtain quarter wave resonance at 500 MHz. At that frequency, the conductor losses are 5.7 dB/100 feet and the dielectric losses are 47.5 dB/100 feet.

Note that the open line now has its Q factor almost constant below quarter wave resonance. The Q factor of the shorted line is now much higher, in fact the shorter the line the higher the Q . The shorted stub becomes attractive as a resonator by using shorter lines with the higher Q . Then a low loss capacitor will be required to bring the line back to resonance at 500 MHz.

Figure 8 shows the required stub loading capacitance versus line length to resonate at 500 MHz. When the line length approaches a quarter wavelength, the required loading capacitance decreases toward zero.

Real capacitors have a series resistance that limits their Q factor, however. In the next example, a series resistance of 0.08 Ω is assumed. The effective Q factor of the stub and the capacitor may be computed by recalling that the Q factors add like parallel resistors. There is now an optimum length that will provide the highest Q , which is around 1 inch or about 25% of the original self resonant length. See Figure 9.

The highest Q will generally be obtained by paralleling multiple capacitors to decrease the effective series resistance. Note that wider PCB traces will provide higher Q factors, even if the line Z_0 is lower.

Substituting RG-174 coax gives a maximum Q of 100 at 2.5 inches, while a length of RG-213 shows a maximum Q of 394 at a quarter wavelength (3.9 inches). This means that a low to very-low-loss line will have its highest Q at a quarter wavelength and above. I have measured the unloaded Q of a 6-inch-diameter quarter-wave resonator at 145 MHz in quarter-wave mode and 430 MHz in $3/4$ -wave mode. At 145 MHz, the unloaded Q was 5324 and 9065 at 430 MHz: an increase by a factor of 1.7. This is also predicted by the models presented here.

Note that adding a lossless reactance in parallel (or series) with the stub — to modify its resonant frequency — does not change its Q versus frequency as calculated from Equations 9 or 14. Only its resonant frequency is changed.

So far from these simulations, Equations 9 and 14 make sense for calculating the resonator unloaded Q for resonator lengths ranging from 1% of the wavelength to many wavelengths. At low frequencies where the resonator is less than $1/16$ wavelength, we get the same results by simply taking the reactance-to-resistance ratio to compute the Q factor instead of using the more complex Equations 9 and 14.

Validating the Computed Resonator Q from the Calculated Stub Impedance

A second method of calculating the resonator Q factor has been used to determine the limits of validity of Equations 9 and 14 as applied to transmission lines. The resonator Q may be determined by finding the two frequencies f_1 and f_2 around the stub resonance that yield a stub impedance with a phase angle of $\pm 45^\circ$. The exact stub resonant frequency is f_r , where its input reactance is zero in the case of series resonant lines. For lines that are parallel resonant, we use admittances and note the frequency where the susceptance goes to zero. For Q factors above 10, f_r can be taken as the average of f_1 and f_2 .

The stub Q factor can then be calculated from:

$$Q = \frac{f_r}{f_2 - f_1} \quad (\text{Eq 34})$$

Note that the stub impedance measurements may be done at either end of the line, without affecting the Q value.

This method may also be used to compute the Q factor at frequencies other than at resonance by adding a lossless frequency-dependant series reactance (L or C) in the case of a series resonant line. Similarly, parallel resonant lines require the addition of a susceptance in shunt with the line. This method was used to verify the accuracy of Equations 9 and 14 with the help of *Mathcad* to do the calculations.

Table 1 summarizes the results for a line length of 8.17 feet. The frequency for the losses is 5 MHz. The Q error was derived by using Equation 34 to compute the resonator Q from the impedance/admittance data and comparing the values obtained with Equations 9 or 14.

At 28 MHz, we are about halfway between resonances, and either Equations 9 or 14 may be used, for both shorted and opened lines. This value is the geometric average between the first and second resonances.

As it can be seen from Table 1, the error is largest for Q values below 20 or so. The worst errors occur at the highest resonance modes having the lowest Q s. Below quarter wave resonance, the Q error is below 1% for Q s above 10.

Computing Resonator Q from Bandwidth Measurements at Multiples of Quarter Wavelength Resonance

Another way to verify the resonator Q factor is to build a band-pass filter and measure its selectivity by measuring its -3 dB points on an S21 display. To precisely determine the resonator Q_u (unloaded Q), the coupling of the stub under test to the source and detector will have to be very small. Equation 34 is used to compute the resonator Q factor. Figure 10 shows the circuit that I have used for my simulations on a line, which behaves as a parallel LC resonator.

In Figure 10, the source and detectors have low impedance (50 Ω). The stub is coupled to the source-detector via 0.1 pF capacitors. This method is useful to determine the resonant frequency of a shorted quarter wave line, since it presents the highest impedance at resonance. Again, Equation 34 is used to compute the stub unloaded Q factor, where f_1 and f_2 are the -3 dB frequencies, as measured from the resonant frequency f_r . Note that the source and load resistive impedances will decrease the Q factor somewhat. Equation 35 may be used to calculate the unloaded

Q , based on the measured attenuation at the resonant frequency and percent bandwidth.

Computing Resonator Q from Bandwidth Measurements below Quarter Wavelength Resonance

Figure 11 shows the setup that may be used with series resonant RLC elements when the resonant line is inductive or capacitive. The total reactance is cancelled, leaving the series R_s at resonance. This series R_s is easily determined by doing an attenuation test (S21) in a 50-to-50 Ω circuit at the series resonant frequency. The equivalent L and C lumped elements must also be determined by doing two more attenuation tests, before one can calculate the Q factor. I have developed an *Excel* file that does these calculations: Calc_SeriesRLC.xls.⁷ Note that the C element has to be replaced by an inductor when the stub impedance is capacitive.

Tests were done on a 100-inch length of RG-58 cable, by measuring the complex reflection coefficient over 201 frequency points, using a lab-quality vector network analyzer (HP 8753D). See Figure 12. The measured coefficients were then converted to impedance data using *Mathcad*. The Q factor was calculated as per Equations 9 and 14 (solid curves) and as per Equation 1 (dotted curves). These dotted curves show the cable resonant frequencies; for example, where the reactance is zero: 19.4 MHz and 38.8 MHz.

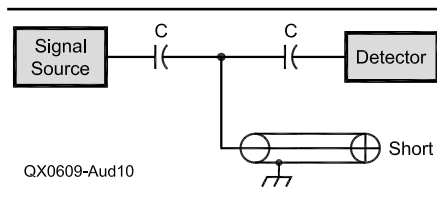


Figure 10 — Measuring and computing resonator Q from bandwidth measurements.

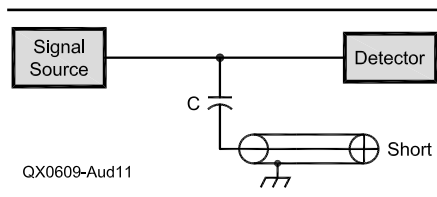


Figure 11 — Measuring and computing resonator Q below quarter wavelength resonance.

Table 3

Shorted Line		Open Line			
Frequency (MHz)	Calculated Q (Eq 14)	Measured Q	Frequency (MHz)	Calculated Q (Eq 9)	Measured Q
19.375	35.3		19.375	36.36	
19.106		34.43	19.334		30.95

Shorted and Open Line Measurements

In Figure 12, the shorted line exhibits parallel resonance at 19.4 MHz, and Equation 14 is used to compute the resonator Q factor up to 27 MHz. Equation 9 is used from 27 MHz up to 50 MHz, since we have a series resonance at 38.8 MHz.

For the open line of Figure 13, the equations are used in the reverse order. Note that the open line has a higher Q factor. The above Q curves are representative of a line that has much less dielectric losses than conductor losses as in Figures 3 and 4. Note the Q curve sloping down below 3 MHz. This is possibly caused by the inaccuracies in the measurements, especially for resistive impedance values below 5 Ω .

Measured Q Values versus Computed Values

Table 2 shows the percentage error between measured Q factors versus the computed values at three frequencies. Notice that there is good agreement between the two. The measured Q was computed directly from attenuation measurements, as per Figures 10 and 11. A series inductor was used to resonate the line when its reactance is capacitive and vice-versa.

The Q of the inductor was measured and its series resistance was subtracted from the total series resistance to obtain the actual stub series resistance. This data was then used to correct the resistive part of the VNA measurements, by calculating the offset between the two measurements. This correction is only valid around the test frequency. Then the Q was computed using the corrected VNA measurements, with Equations 9 and 14.

Table 3 shows the calculated and measured Q factors at the (approximate) quarter wave frequency. The calculated values were obtained from the Equations 14 and 9, while the measured values were done by impedance measurements, using Equation 34. Keep in mind that the measured Q value for open line has probably more errors, since the resistive part of the impedance is around 1 Ω .

The conductor losses are dominant here and we can also use equation 16 to compute the resonator Q based on the measured stub attenuation in dB/100 ft. The Q value obtained is 32.00 at 19.375 MHz.

Using the Resonator as a Bandpass Filter

Knowing the unloaded Q , as calculated

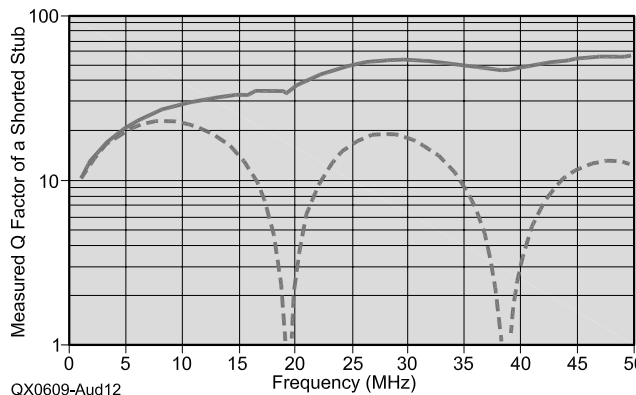


Figure 12 — Measured Q factor of a shorted line. Computed Q factor versus frequency (solid lines, from impedance measurements) for a 100 inch length of RG-58, giving first resonance at ~19.4 MHz. Compare these to simulations in Figures 3 and 4. The dotted lines show the apparent Q .

Table 2

Shorted Line		Open Line	
Frequency (MHz)	% Q error	Frequency (MHz)	% Q error
9.33	2.7	4.92	2.9
28.93	2.1	28.93	1.5

above, allows us to compute the insertion loss of a single resonator bandpass filter based on the percent bandwidth.

$$Loss = 20 \log \left[1 - \frac{100}{K Q_u} \right] \quad (\text{Eq 35})$$

Equation 35 shows the relation between the unloaded Q (Q_u), K the percentage bandwidth (ratio of bandwidth to center frequency in %) and the resonator losses in dB.⁸ For instance, a 2% bandwidth with a Q_u of 200 will give an insertion loss of 2.5 dB.

Q Factor of Antennas

Equations 9 (for open circuit antennas) and 14 (for closed loop antennas) may also be used to calculate the Q factor of antennas, based on their impedance data. I have provided a *Mathcad* file that does impedance calculations on a monopole for various lengths.^{7,9} The monopole is treated as a transmission line whose average impedance Z_a is given by:

$$Z_a = 60 \ln(hd) \quad (\text{Eq 36})$$

where hd is the length-to-radius ratio. Here, the radiation resistance is proportional to the frequency to the power 1.7. It is added to the conductor losses.

Figure 14 gives the simulated monopole Q factor. Once the Q factor is known, the bandwidth, BW , may be easily calculated using Equation 37. The bandwidth obtained gives the frequencies where the impedance phase angle is $\pm 45^\circ$.

$$BW = \frac{f_r}{Q} \quad (\text{Eq 37})$$

where f_r is the center frequency.

This bandwidth, as calculated from the Q factor, corresponds to the 7 dB return loss

points or to an SWR of ~ 2.62 . For a 2:1 SWR, the bandwidth is 70% of the above. This assumes that the SWR is 1:1 at resonance.

Conclusion

In this paper I have shown that a single general equation may be used to calculate the Q factor of RLC circuits and transmission lines as it relates to circuit selectivity. I have shown that series resonances are taken care by Equation 9 while Equation 14 takes care of parallel resonances. The difference between the two is the use of impedances for the first and admittances for the second equation. By using the provided *Mathcad* files and the associated public domain programs, it is easy to compute the Q factor of coaxial and microstrip or stripline resonators for any length and frequency. The calculated Q factor agrees very well with the measured data and with the Q values computed by the impedance measurement method. When simulating stub resonators, it is very important that the full $RLGC$ transmission line models be used. The *Mathcad* files show how to optimize the Q factor of PCB microstrip and stripline resonators. The same files also show the calculations of $RLCG$ functions and coefficients to be incorporated into any RF simulation software. It is interesting to note that these four frequency dependent parameters fully describe the transmission line. I found that the Q values predicted from Equations 9 and 14 fully agree with the values obtained in the simulation software.

The simulations presented here show that it is possible to get higher Q factors on low-loss lines by using higher-order modes, such as $\frac{3}{4} \lambda$. For PCB resonator traces, the optimum Q is generally below a quarter wavelength.

Note that the models presented here do

not take into account the radiation losses and surface roughness of microstrips. The line dc resistance has been included in the PCB line models, since its contribution is not negligible at narrow trace widths. For coaxial lines, the dc resistance has been omitted to keep the models simpler and relieve the user from searching for the resistance data. This makes the coaxial models less accurate below approximately 5 MHz. The dc resistance may be added to the ac conductor resistance by taking the square root of the sum of the squares of the dc and ac resistances, as done in the file: *TRL_Q_Calc-PCB1.mcd*.

Thanks to Chase Hearn and Yan Gunmar for triggering this study and providing various helpful references and comments.

Appendix

An intuitive view of the general function for calculating the Q factor is derived here.

The general equation for computing the Q factor of RLC circuits, transmission line resonators and antennas operating in the series resonant mode is given by the source at Note 1. This equation is valid from low frequencies, though series resonance and for frequencies much above series resonance.

$$Q = \frac{\omega}{2R} \left(\frac{dX}{d\omega} + \frac{|X|}{\omega} \right) \quad (\text{Eq A1})$$

Where $\omega = 2\pi f$, the radian frequency, R and X are respectively the real and imaginary parts of the impedance.

Equation A1 may be written in terms of the frequency:

$$Q = \frac{f}{2R} \left(\frac{dX}{df} + \frac{|X|}{f} \right) \quad (\text{Eq A2})$$

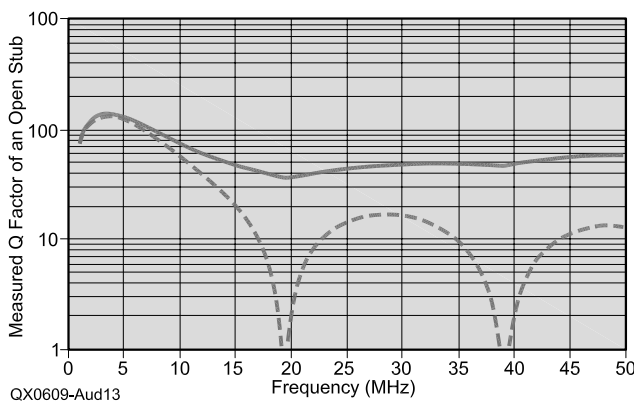


Figure 13 — Measured Q factor of an open line. Computed Q factor versus frequency (solid lines, from impedance measurements) for a 100 inch length of RG-58, giving first resonance at ~ 19.4 MHz. Compare these to simulations in Figures 3 and 4. The dotted lines show the apparent Q .

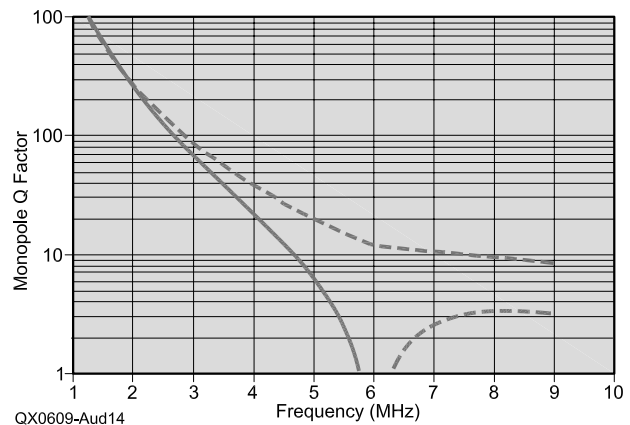


Figure 14 — Monopole Q factor (solid curve) as calculated from the *Mathcad* file: *Monopole-Ralph.mcd*. The quarter wave resonance is at 6 MHz, as shown by the dotted line curve (apparent Q) which was calculated from the reactance to resistance ratio. Note the steep increase in Q as the frequency is lowered. This comes from the fact that the radiation resistance decreases approximately as frequency to the power 1.7. At 1 MHz and below we have a low-loss air insulated capacitor!

Notice that the first term of Equation A2 represents the Q factor at resonance, when $X = 0$.

$$Q = \frac{f}{2R} \left(\frac{dX}{df} \right) \quad (\text{Eq A3})$$

This equation gives the Q Factor at resonance, as very often seen in textbooks.

Applying Equation A2 for a series resonant circuit, for frequencies well above the resonant frequency, we get:

$$\left(\frac{dX}{df} \right) = 2\pi L \quad (\text{Eq A4})$$

Recall that the reactive component comes from the inductance.

$$Q_{hf} = \frac{f}{2R} \left(2\pi L + \frac{|2\pi f L|}{f} \right) \quad (\text{Eq A5})$$

where Q_{hf} is the Q factor for frequencies well above the resonant frequency. This simplifies to:

$$Q_{hf} = \frac{2\pi f L}{R} = \frac{X_L}{R} \quad (\text{Eq A6})$$

where X_L is the inductive reactance. This is the same as Equation 1 in the main text — valid well above the resonant frequency.

For frequencies well below the resonant frequency, where the reactance component comes from the capacitance, we get:

$$\left(\frac{dX}{df} \right) = \frac{1}{2\pi f^2 C} \quad (\text{Eq A7})$$

$$Q_{lf} = \frac{f}{2R} \left(\frac{1}{2\pi f^2 C} + \frac{1}{2\pi f C f} \right) \quad (\text{Eq A8})$$

Q_{lf} is the Q factor for frequencies well below the resonant frequency.

After simplification:

$$Q_{lf} = \frac{1}{2\pi f R C} = \frac{X_C}{R} \quad (\text{Eq A9})$$

where X_C is the capacitive reactance — valid well below the resonant frequency. This is the same as Equation 1 in the main text.

Notes

¹Peter Vizmuller, *RF Design Guide*, Artech House, Norwood, MA, 1995, p. 235.

²The Small Koch Fractal Monopole: Theory, design and applications, p 6. See www-personal.engin.umich.edu/~lschulwi/koch.pdf

³Professor Niknejad, Lectures on Lossy Transmission Lines and the Smith Chart, University of California, Berkeley. Course EECS 117, Lecture 6: www-inst.eecs.berkeley.edu/~ee117/sp04/lect/lecture6.pdf

⁴The program TLDetails.exe may be downloaded from Dan Maguire, AC6LA. Download from www.ac6la.com/tldetails.html e-mail: ac6la@arrl.net

⁵The program TXLine.exe may be downloaded from www.mwoffice.com/products/txline.html (you will need to register.)

⁶Frank Witt, AI1H, "Transmission Line Properties from Manufacturer's Data," *ARRL Antenna Compendium Vol. 6*, ARRL, 1999, pp 179 - 183 and related *Mathcad* files on the accompanying CD-ROM.

⁷The *Mathcad* files TRL_Q_Calc1.mcd and TRL_Q_Calc-PCB1, Monopole-Ralph.mcd and the *Excel* file: Calc_SeriesRLC.xls may be downloaded from the ARRL Web at www.arrl.org/qexfiles/. Look for **9x06_Audet.zip**.

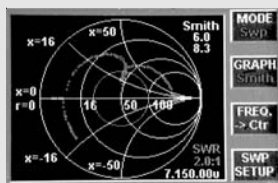
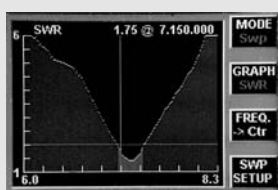
⁸Randall W. Rhea, *HF Filter Design and Computer Simulation*, section 5.5, Noble Publishing.

⁹Ralph Holland, "Impedance of Wide Regular Structures," antennex.com/archive3/archive3.htm. You must be an antennex subscriber to view this article.

Jacques Audet, VE2AZX, became interested in radio at the age of 14, after playing with crystal radio sets and repairing old receivers. At 17, he obtained his first ham license. In 1967 he obtained his B Sc degree in electrical engineering from Laval University. He then worked in engineering functions at Nortel Networks, where he retired in 2000. He worked mostly in test engineering on a number of products and components operating from dc to light-wave frequencies. His areas of interest are in RF simulations, filters, duplexers, antennas and using computers to develop new test techniques in measurement and data processing. **QEX**

Introducing the... AntennaSmith™!

Check Our New Line-up:



Patent Pending

TZ-900 Antenna Impedance Analyzer

2 Sec Sweeps, Sweep Memories, 1 Hz steps, Manual & Computer Control w/software, USB, low power. Rugged Extruded Aluminum Housing - **Take it up the tower!**

- Full Color TFT LCD Graphic Display
- Visible in Full Sunlight
- 0.2 - 55 MHz
- SWR
- Impedance (Z)
- Reactance (r + jx)
- Reflection coefficient (ρ, θ)
- Smith Chart



Now Shipping!

**Check Your Antennas and Transmission Lines
Once you use the TZ-900 -
you'll never want to use any other!**



651-489-5080 Fax 651-489-5066

sales@timewave.com www.timewave.com

1025 Selby Ave., Suite 101 St. Paul, MN 55104 USA

- HamLinkUSB™ Rig Control
TTL Serial Interface with PTT
- HamLinkBT™ Remote Control
- U232™ RS-232-to-USB Universal Conversion Module replaces PCB-mount DB-9 & DB-25
- PK-232 /USB Multimode Data Controller (upgrades available)
- PK-96/USB TNC (upgrades available)

Timewave - The Leader in Noise & QRM Control:

- DSP-599zx Audio Signal Processor
- ANC-4 Antenna Noise Canceller

From the Timewave Fountain of Youth - Upgrades for many of our DSP & PK products!

Some Thoughts About the Quality Factor of a Coil

As frequency increases, various factors affect the Q of a real inductor, beyond the ideal inductive reactance.

Pierre Desjardins, VE2PID

The quality factor Q at a particular frequency in the case of a coil is generally measured using one of the following two methods. We add to it a variable capacitor to form a series RLC circuit. Using a frequency generator having the lowest internal resistance possible:

1) We bring that circuit to resonance, take the corresponding frequency and divide it by the -3 dB bandwidth. The upper and lower limiting frequencies of that region are the points where the voltage has dropped to 70.7% of the voltage measured at resonance, which in turn, corresponds to a power consumption of 50% of the power value observed at resonance; or

2) At resonance, take the maximum voltage across the inductor and divide it by the excitation ac voltage applied.

They give the same result, but to see exactly why, some mathematics is needed.

Passive circuit elements like a resistance R, an inductance L or a capacitance C are defined by the manner in which voltage and current are related for the individual element. If the voltage is proportional to the time derivative of the current, then the element is an inductance; L is the constant of proportionality, and:

$$V = L \frac{dI}{dt} \quad (\text{Eq 1})$$

Consequently, the power, P, developed is:

$$P = VI = L \frac{dI}{dt} I = \frac{d}{dt} \left(\frac{LI^2}{2} \right) \quad (\text{Eq 2})$$

The energy stored in a time interval $\Delta t = t_2 - t_1$ is:

$$W_L = \int_{t_1}^{t_2} P dt = \int_{t_1}^{t_2} LI dI = \frac{L(I_2^2 - I_1^2)}{2} \quad (\text{Eq 3})$$

So, if the current has a maximum value of I_{\max} , the maximum energy stored will be:

$$W_L = \frac{LI_{\max}^2}{2} \quad (\text{Eq 4})$$

If the frequency is ω , the energy dissipated per cycle by the resistive part R is:

$$\left(I_{\text{eff}}^2 R \right) \left(\frac{2\pi}{\omega} \right) = \left(\frac{I_{\max}}{\sqrt{2}} \right)^2 \left(\frac{2\pi R}{\omega} \right) = \frac{\pi R I_{\max}^2}{\omega} \quad (\text{Eq 5})$$

For a component or a complete circuit, the quality factor, Q, is defined as:

$$Q \equiv 2\pi \left(\frac{\text{maximum energy stored}}{\text{energy dissipated per cycle}} \right) \quad (\text{Eq 6})$$

Using the preceding results and the fact that $\omega = 2\pi f$, where f is the frequency, we obtain:

$$Q \equiv 2\pi \frac{\left(\frac{LI_{\max}^2}{2} \right)}{\left(\frac{\pi R I_{\max}^2}{\omega} \right)} = \frac{2\pi fL}{R} = \frac{X_L}{R} \quad (\text{Eq 7})$$

That is the classical definition: The Q of a pure inductor is the ratio of the inductive reactance to the resistance at a certain frequency.

It is only a theoretical definition, however. According to that last result, such a coil would have an unbounded Q; it would follow the rise in frequency almost linearly. In a real situation, however, the skin effect raises the resistance with the frequency. Stray capa-

citance also appears between the windings of the coil, giving significant values of capacitive reactance. Since a pure inductor is an abstraction, it is much more realistic to consider and analyze a coil in the context of an RLC series circuit.

Such a circuit has an impedance, Z_{in} , of:

$$Z_{in} = R + j \left(\omega L - \frac{1}{\omega C} \right) \quad (\text{Eq 8})$$

The used power, P, is:

$$P = I_{\text{eff}}^2 R = \frac{V_{\text{eff}}^2 R}{|Z_{in}|^2} \quad (\text{Eq 9})$$

At resonance, the maximum value becomes P_{\max} :

$$P_{\max} = \frac{V_{\text{eff}}^2 R}{R^2} = \frac{V_{\text{eff}}^2}{R} \quad (\text{Eq 10})$$

We also have:

$$P = \frac{P_{\max}}{2} \quad (\text{Eq 11})$$

$$\text{if } \frac{V_{\text{eff}}^2 R}{|Z_{in}|^2} = \frac{V_{\text{eff}}^2}{2R} \quad (\text{Eq 12})$$

and then

$$|Z_{in}|^2 = 2R^2 \quad (\text{Eq 13})$$

After simplifications:

$$\omega L - \frac{1}{\omega C} = \pm R \quad (\text{Eq 14})$$

or

$$\omega^2 \mp \frac{R\omega}{L} - \frac{1}{LC} = 0 \quad (\text{Eq 15})$$

These quadratic equations have the solutions:

$$\omega_{\text{sup}} = \frac{R}{2L} + \sqrt{\left(\frac{R}{2L}\right)^2 + \frac{1}{LC}} \quad (\text{Eq 16A})$$

and

$$\omega_{\text{inf}} = -\frac{R}{2L} + \sqrt{\left(\frac{R}{2L}\right)^2 + \frac{1}{LC}} \quad (\text{Eq 16B})$$

Subtracting those values, we obtain:

$$\omega_{\text{sup}} - \omega_{\text{inf}} = \frac{R}{L} = \frac{2\pi f}{Q} \quad (\text{Eq 17})$$

If the value of f is the resonant frequency, f_0 :

$$Q = \frac{2\pi f_0}{\omega_{\text{sup}} - \omega_{\text{inf}}} = \frac{2\pi f_0}{2\pi f_{\text{sup}} - 2\pi f_{\text{inf}}} = \frac{f_0}{f_{\text{sup}} - f_{\text{inf}}} \quad (\text{Eq 18})$$

That last result gives a practical way to obtain Q . We determine the resonant and the half-power frequencies, f_{inf} and f_{sup} , giving a power drop of 3 dB, and all we have to do is the corresponding division. That is the first method.

The second method is to calculate the ratio of the maximum voltage, V_m , across the inductance at resonance to the excitation voltage, V_s . In fact, at resonance, the only remaining resistance is R and:

$$I = \frac{V_s}{R} \quad (\text{Eq 19})$$

yielding

$$\frac{V_m}{V_s} = \frac{IX_L}{V_s} = \frac{V_s}{R} \frac{2\pi f_0 L}{V_s} = \frac{2\pi f_0 L}{R} = Q \quad (\text{Eq 20})$$

Since both methods are using the same fundamental ideas, they give the same results.

Pierre Desjardins, VE2PID, was a calculus and linear algebra teacher for 34 years at Séminaire de Sherbrooke College, and at other posts in Morocco and Togo. He retired in 2002. He holds a BSc in Pure Mathematics and a degree in Pedagogy from University de Sherbrooke. Pierre chose Amateur Radio as a hobby for his retirement, and earned his full Canadian license in 2003. His principal Amateur Radio interest is antenna theory, and he operates mainly CW. QEX



Join the effort in developing Spread Spectrum Communications for the amateur radio service. Join TAPR and become part of the largest packet radio group in the world. TAPR is a non-profit amateur radio organization that develops new communications technology, provides useful/affordable kits, and promotes the advancement of the amateur art through publications, meetings, and standards. Membership includes a subscription to the *TAPR Packet Status Register* quarterly newsletter, which provides up-to-date news and user/technical information. Annual membership \$20 worldwide.



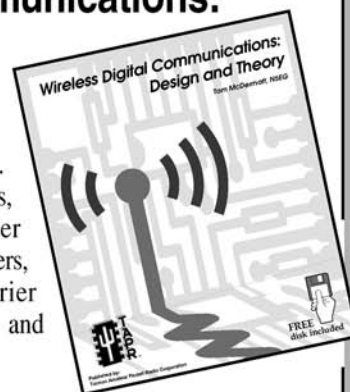
TAPR CD-ROM

Over 600 Megs of Data in ISO 9660 format. TAPR Software Library: 40 megs of software on BBSs, Satellites, Switches, TNCs, Terminals, TCP/IP, and more! 150Megs of APRS Software and Maps. RealAudio Files.

Quicktime Movies. Mail Archives from TAPR's SIGs, and much, much more!

Wireless Digital Communications: Design and Theory

Finally a book covering a broad spectrum of wireless digital subjects in one place, written by Tom McDermott, N5EG. Topics include: DSP-based modem filters, forward-error-correcting codes, carrier transmission types, data codes, data slicers, clock recovery, matched filters, carrier recovery, propagation channel models, and much more! Includes a disk!



Tucson Amateur Packet Radio

8987-309 E Tanque Verde Rd #337 • Tucson, Arizona • 85749-9399
Office: (972) 671-8277 • Fax (972) 671-8716 • Internet: tapr@tapr.org www.tapr.org
Non-Profit Research and Development Corporation

What's Your CQ?

(Curiosity Quotient)

Eric P. Nichols, KL7AJ

What is the source of innovation? If you were to ask that question of the average American adult, you'd probably get some repackaged version of the famous quote, "Necessity is the mother of invention." Surveying our technological environment, one sees numerous evidence that seems to back up that quote. We "need" cell phones, microwave ovens, cable TV and the Internet.

And yet, upon further investigation, we find that most of what we consider the necessities of modern life really came about as a result of some experiment having gone awry at some time. Did anyone in the late 1800s "need" radio? Not too likely! Radio came about as the result of scientific investigation: sheer curiosity. If we are brutally honest, we will see the fallacy of that aforementioned quote. The reality is that, quite to the contrary, invention is the mother of necessity.

I have a sneaking suspicion that the best in Amateur Radio is yet to come, and it won't come about by trying to solve some perceived problem or need. No, it will come about because we have a collective insatiable curiosity about this universe that we inhabit. If a practical application of this lust for knowledge happens to result, so

much the better, but consumerism should not be the driving force behind what we do.

The word "amateur" has a certain stigma attached to it, but it also has a great liberating quality. We make no apologies for being amateurs...remember, professionals built the *Titanic*, while amateurs built the Ark! But beyond that, we need to remember that the word amateur comes from the same Latin root as *amare*: to love.

If we don't do what we do as amateurs because we love it, we have lost something crucial. There are very few endeavors in modern life that allow us the latitude of experimentation that Amateur Radio does. Most governments take a dim view of amateur medical experimentation or personal possession of large quantities of radioactive materials. Even your friendly local "greaser" is hamstrung by EPA regulations when attempting to modify his hot rod engine.

On the other hand, we radio amateurs (within some rather reasonable parameters, of course), are given essentially *carte blanche* to "tickle the ether" as we see fit.

There is a hazard to the ready availability of high tech gadgetry. We can easily lose our curiosity about how these things work and, even more tragically, lose any appreciation for what it took to give us these wonders in the first place. Things exist because somebody thought about them first, and applied large quantities of blood, sweat and *amare* to bring them to life.

We all know about the 20/80 rule of any organization. Twenty percent of the people do 80 percent of the work. Unfortunately, in Amateur Radio ranks, it's probably more like a 1/99 rule — 1 percent of the hams doing 99 percent of the innovation. It doesn't have to be this way. Fortunately, there is a magazine like *QEX* that effectively leverages the innovative energy of that minority of radio amateurs.

Being a true innovator doesn't require a college degree, a government grant or even an exceptionally high IQ. It does, on the other hand, require an extraordinary CQ — Curiosity Quotient.

What's yours?

Eric Nichols, KL7AJ, has held an Amateur Extra Class license since 1977. He has been continuously marinated in high-power RF for most of his career, having worked as Chief Engineer of KJNP AM-FM-TV, followed by several years in ionospheric research at Hipas Observatory. He has written numerous articles in QST and QEX since 1983, and had his first science fiction novel, Plasma Dreams, published in 2005.

Eric is a member of QCWA, SOWP, SKCC and Ten-Ten International. His favorite ham radio activities are low-band DXing, abusing his carpal tunnels with ancient telegraph keys, collecting vacuum tubes, restoring boat anchors and modeling antennas. His deepest radio-related regret is having sold his Central Electronics 100V.



PO Box 56235
North Pole, AK 99705-1235
kl7aj@arrl.net

Upcoming Conferences

ARRL/TAPR Digital Communications Conference

The 25th Annual ARRL and TAPR Digital Communications Conference will be held in Tucson, AZ on September 15-17, 2006 at the Clarion Hotel Tucson Airport, Tucson, AZ.

Topics include, but are not limited to:

Software defined radio (SDR), digital voice, digital satellite communications, global position system (GPS), precision timing, automatic position reporting system (APRS), digital signal processing (DSP), HF digital modes, Internet interoperability with Amateur Radio networks, spread spectrum, IEEE 802.11 and other Part 15 license exempt systems adaptable for Amateur Radio, using

TCP/IP networking over Amateur Radio, mesh and peer to peer wireless networking, emergency and homeland defense backup digital communications, using LINUX in Amateur Radio, updates on AX.25 and other wireless networking protocols.

For more information and registration, see www.tapr.org.

AMSAT 2006 Space Symposium

The AMSAT 2006 Space Symposium and Annual meeting will be held October 5-10, 2006 at the Crowne Plaza Hotel San Francisco Mid-Peninsula hotel located at 1221 Chess Dr, Foster City California. The Symposium will again be a joint meeting with the ARISS International Delegates and will also include the IARU Satellite Advisory Panel annual meeting, and a meeting of AMSAT International Delegates.

For more details and registration information go to www.amsat.org/amsat-new/symposium/.

Microwave Update 2006

The Midwest VHF/UHF Society will host the Microwave Update (MUD) 2006 conference in Dayton, OH on October 19-22, 2006. The event will be held at the Holiday Inn North, Wagoner Ford Road, Exit 57B off I-75, Dayton, OH.

Test equipment will be available for checking noise figure, amplifier gain, output power, phase noise and impedance.

To present papers, contact Gerd Schrick, 937-253-3993 or email wb8ifm@amsat.org

Registration is \$40 before 30 September, \$45 starting 1 October and \$50 at the door. The banquet is \$35 per person. For more information see www.microwaveupdate.org/



Horizontal Bidirectional Wires

In the Antenna Options column in the July/August 2006 issue of *QEX*, we discussed some of the options for bidirectional wire broadside arrays based on the vertical dipole. Since we should be fair to horizontal wires, this collection of notes will focus on bidirectional wire arrays that have their roots in the horizontal dipole. Just as the last collection was incomplete, so this one will be even less exhaustive. Once we have some basic arrays available to use, the permutations and combinations form an endless progression. We can look at the various types of arrays, however.

To be effective, a horizontal array should be well above ground. Although we might disagree on the minimum height for horizontal arrays, placing all arrays at 1λ above ground for the top wire (if the array has a vertical dimension) will keep us well above the minimum. In the preceding notes, I set a height of 50 feet as a limit of sorts, since most serious array users can usually arrange 60-foot support posts, trees, or surplus telephone poles. The physical height restriction leads us to 15 meters, more specifically, a uniform test frequency of 21.225 MHz for all comparative horizontal array data. A wavelength at this frequency is 46.34 feet. To unify further the modeling conditions, the ground will be average, that is, have a conductivity of 0.005 S/m and a relative permittivity of 13. All antenna elements will use AWG no. 12 (0.0808-inch diameter) copper wire. As a result, we can more directly compare the reported performance characteristics for the antennas included in these notes.

Traditionally, we categorize arrays as collinear, end-fire, or broadside. These categories are not mutually exclusive, but they do give us a convenient way of grouping our subject antennas. We must begin with a baseline, however.

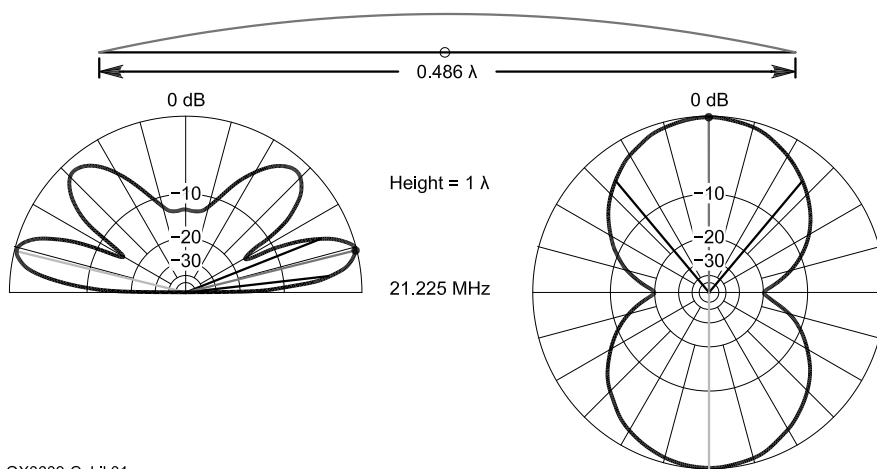
The Standard Antennas

No antenna is more fundamental to amateur (and other) antenna work than the $\frac{1}{2}\lambda$ resonant dipole. Figure 1 shows the outline of the antenna. Superimposed on the antenna is the distribution of the current magnitude along the wire's length. (Adding the current phase would create difficult viewing problems with some of our antennas.) Note that the dipole is electrically resonant, which requires a physical length that is 0.486λ for no. 12 copper wire at the

specified height above average ground. The resonant length of a dipole will vary with the height above ground, especially below about 1.25λ .

Horizontal wire antennas tend to have an elevation angle of maximum radiation (or take off — TO — angle) that depends on

the antenna's height more than any other factor. Hence, all of the basic antennas whose performance reports appear in Table 1 have a TO angle of 14° . The dipole data in the table give numerical meaning to the plots in Figure 1. Note the wide (79°) beamwidth for a standard dipole. A triangle



QX0609-Cebik01

Figure 1 — General outline and elevation and azimuth patterns for a resonant, half-wavelength dipole.

**Table 1
Modeled 15-Meter Standard Wire Antenna Performance Characteristics**

Gain dBi	TO Angle	Beamwidth	Feed Point Impedance
<i>1/2-lambda dipole (See Figure 1.)</i>			
7.62	14°	79°	72.0 + j0.3 Ω
<i>1-lambda doublet (See Figure 2.)</i>			
9.23	14°	51°	4464 - j1.8 Ω
<i>Extended double Zepp (See Figure 3.)</i>			
10.67	14°	36°	230.6 - j1023 Ω (L = 1.20 λ)
10.78	14°	33°	153.5 - j781.6 Ω (L = 1.25 λ)

Notes

- ¹All antennas are bidirectional.
- ²Gain is maximum at the TO angle (or elevation angle of maximum radiation).
- ³Beamwidth is the half-power value for each of the 2 lobes.
- ⁴Impedance values are the resistive and reactive series values.
- ⁵See the indicated figures and the text for the physical description of the individual arrays and their elements.
- ⁶Test frequency is 21.225 MHz. Ground is average (conductivity = 0.005 S/m; relative permittivity = 13).
- ⁶These notes apply to all subsequent tables of modeled performance figures.

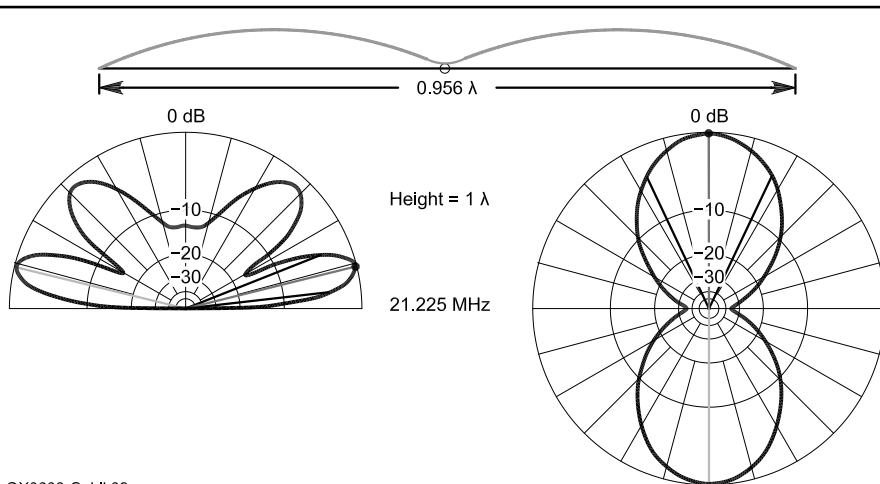
of dipoles would suffice to cover the entire horizon. The dipole gain of 7.6 dBi becomes the baseline against which we may measure the gain of all subsequent arrays.

The second standard antenna can go by several names. The table and Figure 2 both refer to a 1- λ center-fed doublet. An equally apt way to refer to the antenna is as a collinear array of two half-wavelength wires. The current magnitude curve on the antenna outline shows why this name makes good sense, since we observe two complete cycles of current rise and fall. Like the dipole, the physical length will be shorter than the electrical length. For the test conditions, we obtain resonance with a length of 0.956λ of wire. Finding the resonant length of a center-fed 1- λ wire is tedious in modeling and virtually impossible with real wire. The resonant point occurs at a very high value of resistive impedance, where the reactance changes in a very short space from very inductive to very capacitive. Hence, there is an air of artificiality about the reactance number in the table, although the resistive part is a good indicator of what to expect at the feed point. One way to bring the impedance down to a value that is more amenable to our coaxial ways is to use a $\frac{1}{4}$ - λ section of 450- Ω line.

The pattern and the gain value are both very real and usable. The 1- λ wire provides about 1.6 dB additional gain relative to a dipole under equal conditions, but at a cost in the beamwidth. The longer wire has a beamwidth of about 51° . A triangle of 1- λ wires will not cover the horizon.

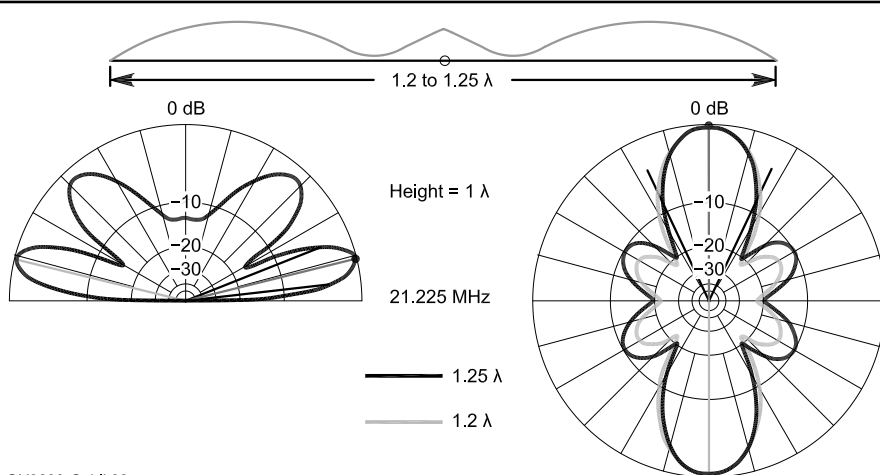
The third standard wire antenna is the extended double Zepp (EDZ). We operate this antenna off resonance. We sometimes say that the antenna is non-resonant, but there is another use for this term. Many traveling wave and frequency-independent antennas show no cyclical appearance of resonant frequencies as we operate the antenna over a large frequency range. Many texts call these antennas non-resonant in contrast to antennas like a center-fed wire of fixed physical length. This antenna is resonant in the sense of showing cyclical reappearances of zero reactance at the feed point as we sweep through a wide frequency range. So, we may be content in calling the EDZ an off-resonance antenna. Figure 3 shows the current magnitude distribution for a physical length of 1.25λ . The antenna qualifies as a collinear array.

As we increase the length of a center-fed wire beyond 1λ , we find that the gain increases until the length passes the $1.25\text{-}\lambda$ mark. The azimuth patterns and the tabular data, however, show us other dimensions of what is occurring. As we move from about 1.2λ to 1.25λ , the resistive and capacitive reactance components of the feed point



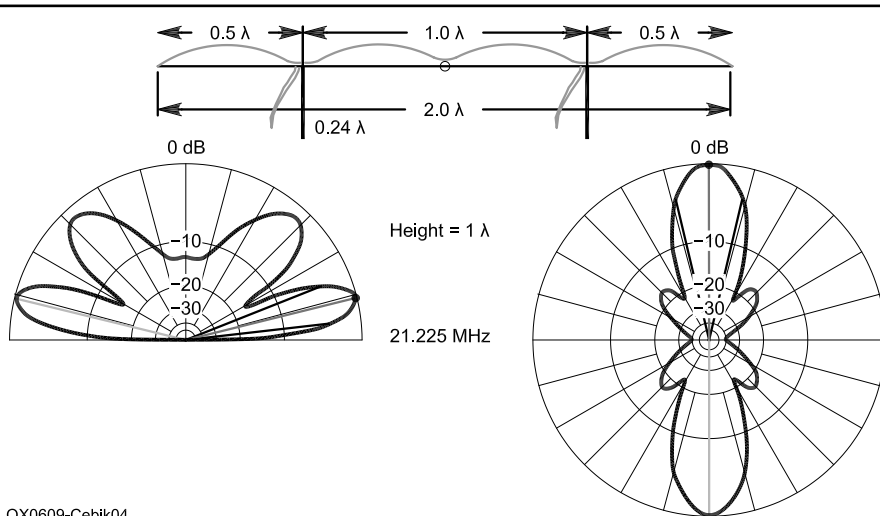
QX0609-Cebik02

Figure 2 — General outline and elevation and azimuth patterns for a resonant, one-wavelength doublet.



QX0609-Cebik03

Figure 3 — General outline and elevation and azimuth patterns for an extended double Zepp (EDZ) antenna/array.



QX0609-Cebik04

Figure 4 — General outline and elevation and azimuth patterns for a collinear array using $\frac{1}{2}$ - λ sections.

impedance decrease. (The gain changes only by about 0.1 dB.) Offsetting the reduction in the feed point impedance is the growth of the side lobes that give an EDZ azimuth pattern its distinctive look. With a length of 1.2λ , the side lobes are about 13 dB lower in gain than the main lobe. By a length of 1.25λ , the side lobes have grown by 3 dB. At a total length of about 1.5λ , the side lobes would be as strong as or stronger than the main or broadside lobe. As well, the beamwidth continues to shrink as we lengthen the wire and increase the peak gain. Hence, the EDZ represents a sort of limit to the length of collinear arrays unless they employ techniques to correct phasing along the wire.

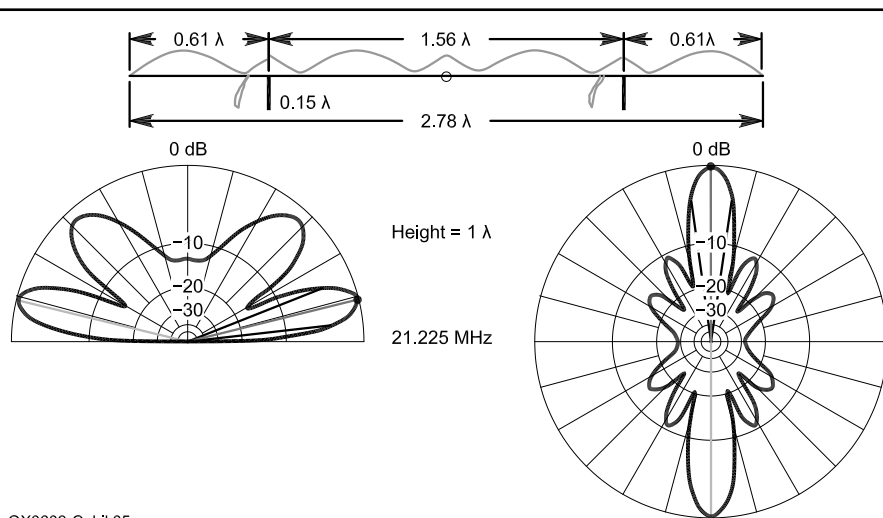
Collinear Arrays

One technique that allows us to obtain increased gain with straight wires is to introduce at critical points along the wire a phase-changing stub. Consider a 2λ center-fed wire, such as the one shown in Figure 4. We see four complete half-wavelength current cycles. If we had just used a continuous length of wire, however, the phasing of the current at the outer half-wavelength sections would have been 180° out of phase for producing a simple broadside pattern. Indeed, we would see for such a wire a four-lobe pattern that forms a cloverleaf. By introducing $\frac{1}{4}\lambda$ -shorted transmission-line sections, we change the phase of the current at the beginning or inner end of the outer sections so that the radiation adds to the radiation of the center section. The result is a narrow main beam (the width is 26°) with more than 1 dB gain over the EDZ. The tabular data for the collinear arrays appears in Table 2, for comparison with the patterns in the relevant figures.

Like a 1λ wire, which is what we find at the center of our collinear array that uses $\frac{1}{2}\lambda$ sections, the feed point impedance is very high. As well, the azimuth pattern shows small EDZ-like side lobes that are normal to very closely spaced $\frac{1}{2}\lambda$ sections — in this case, the end sections relative to the longer inner section of the array.

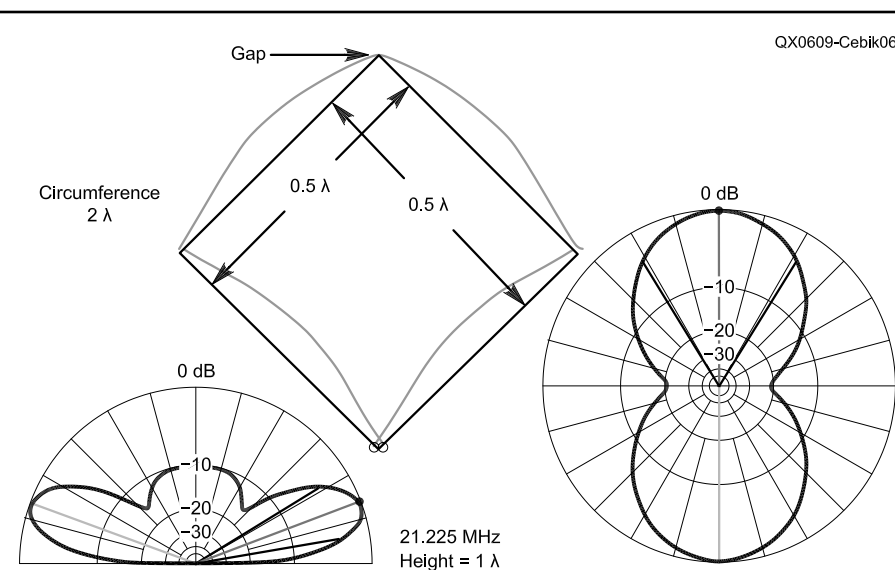
We need not limit ourselves to using $\frac{1}{2}\lambda$ sections as the basis for a collinear array. As shown in Figure 5, a $\frac{5}{8}\lambda$ section will work as well, and provide additional gain. The collinear array shown uses such sections and has a total length of 2.78λ to achieve a peak gain of 13.5 dBi, about 1.5-dB higher than the comparable array using $\frac{1}{2}\lambda$ sections. The beamwidth has shrunk to 16° , however. This array is for point-to-point communications.

The array shows twice as many side lobes because we have — in effect — a doubled EDZ structure. The inner section is slightly over 1.5λ , which seems long for an EDZ. If



QX0609-Cebik05

Figure 5 — General outline and elevation and azimuth patterns for a collinear array using $\frac{5}{8}\lambda$ sections.



QX0609-Cebik06

Figure 6 — General outline and elevation and azimuth patterns for a bi-square array.

Table 2
Modeled 15-Meter Collinear Array Performance Characteristics

Gain dBi	TO Angle	Beamwidth	Feed Point Impedance
<i>Collinear array based on $\frac{1}{2}\lambda$ sections (see Figure 4)</i>			
11.97	14°	26°	$2189 + j28.9 \Omega$
<i>Collinear array based on $\frac{5}{8}\lambda$ sections (see Figure 5)</i>			
13.50	14°	16°	$250 - j733.3 \Omega$
<i>Bi-square array (see Figure 6)</i>			
10.29	20°	63°	$3344 - j100.4 \Omega$

See Notes for Table 1.

you examine the current magnitude curve on the outline sketch, however, you will see that it requires the added current rise not only at the feed point, but also at the location of the phasing lines. Because these regions are already reactive, the phasing lines can be shorter to effect the required phase reversal — in this instance, about 0.15λ . The feed point impedance is normal for an EDZ-type antenna. Moreover, despite the high increase in array complexity, it still shows a TO angle of 14° because of the $1\text{-}\lambda$ height above ground.

In the models for both of the collinear arrays, the phase lines are physical wire structures and not NEC TL constructs.¹ The non-radiating TL lines are most accurate at high current regions of an antenna, where the current changes very slowly over appreciable distances along the wire. They become less accurate in regions of the antenna in which the current changes rapidly over short distances. Since both collinear arrays show relatively low currents at the phase-line locations, physical lines are necessary for best accuracy in the models. The modeled line wires should be the same diameter as the antenna element wire, and the spacing should not be excessively close.

The final sample of a collinear array takes an odd turn — upward. The bi-square array is a center-fed $2\text{-}\lambda$ wire with the ends turned upward to form a square that is $\frac{1}{2} \lambda$ on a side. The wire ends do not meet, however, but leave a gap. Figure 6 shows the general outline and the current magnitude curves for each of the four wires. Because we have set a $1\text{-}\lambda$ limit for the top structure, the low point for the array is about 0.3λ above ground. The net effect is to raise the TO angle of the

array as a whole. A useful rule of thumb for any array consisting of multiple wires in the vertical plane is that the effective height of the array is about $\frac{2}{3}$ of the way up the array from the low point to the high point. Hence, the effective height of the bi-square in the illustration is about 0.75λ .

The bi-square has a beamwidth of about 63° , although its gain is about halfway between the values for the $1\text{-}\lambda$ and the EDZ arrays. Both antennas exhibit narrower beamwidths. If you compare the elevation pattern for the bi-square with those for the other two relevant wires, you will discover that the bi-square lacks most of the upper structure or second elevation lobes that characterize the elevation patterns of the single wire antennas. The bi-square lends itself to single-support mounting, and you

may place two such antennas at right angles on the support, switching to the one that yields best signal strength.

End-Fire Arrays

If a set of elements radiates in the plane of the elements, with the lobes broadside to the element wires, then we have an end-fire array. Among basic arrays, we need only one sample: the W8JK “flat-top” array, developed by John Kraus, W8JK. The antenna has many incarnations using various element lengths and forms, and using many spacing distances. In general, the longer the elements for a given spacing, the higher will be the gain. Equally generally, the closer the spacing, the higher the gain will be. Hence, every W8JK is a compromise based on best achieving a particular set of goals for the antenna.

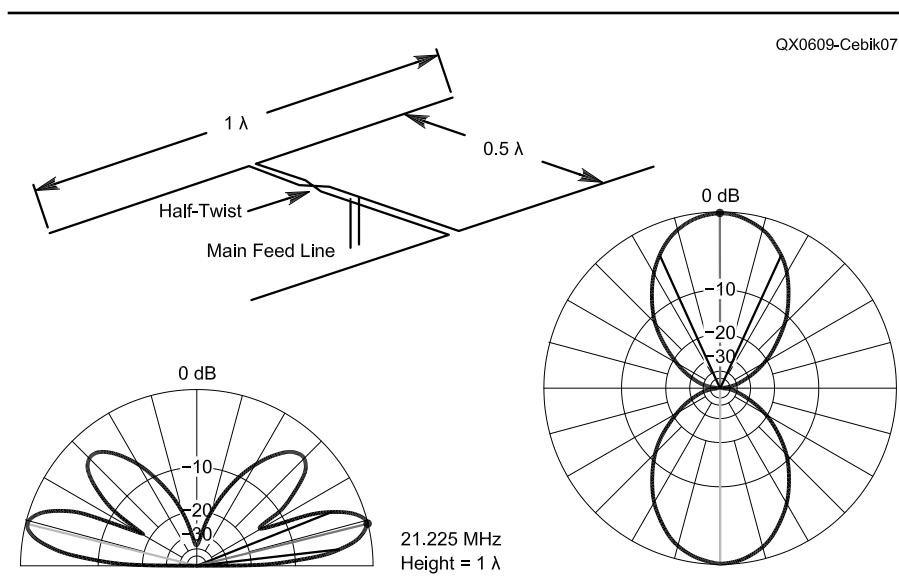


Figure 7 — General outline and elevation and azimuth patterns for a 15-meter W8JK “flat-top” end-fire array.

¹Models for the antennas discussed in this “Antenna Options” column are available in EZNEC format on the ARRL Web site at www.arrl.org/qexfiles. Look for 9x06_AO.zip.

Table 3
Modeled 15-Meter End-Fire Array Performance Characteristics

Frequency	Gain dBi	TO Angle	Beamwidth	Feed Point Impedance*
<i>W8JK phased horizontal element (“flat-top”) array (see Figure 7 and Figure 8)</i>				
21.225 MHz	11.21	14°	49°	$23.8 + j29.1 \Omega$
10.25	9.41	26°	65°	$17.7 + j157.9 \Omega$
14.175	10.65	20°	61°	$104.6 - j405.1 \Omega$
28.5	11.56	11°	32°	$291.1 + j639.8 \Omega$

See Notes for Table 1.

*Impedance values are for 450Ω , $VF = 0.9$ phase lines.

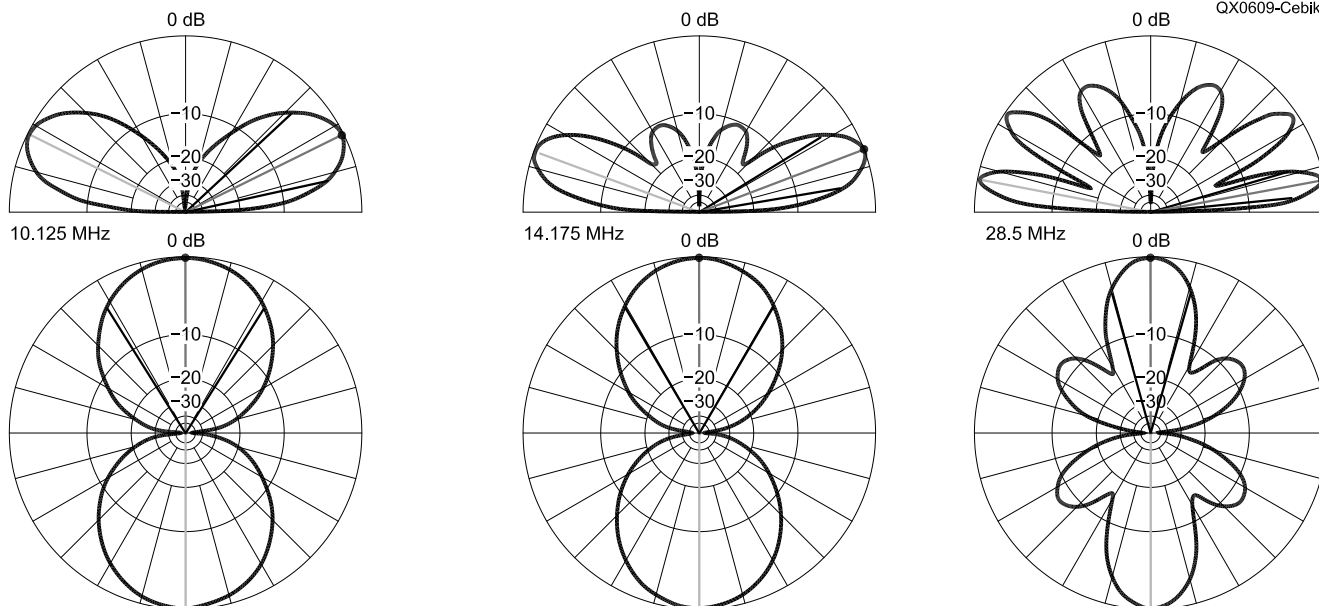


Figure 8 — Elevation and azimuth patterns of a 15-meter W8JK bidirectional array on 30, 20, and 10 meters.

Figure 7 shows the outline of the 15-meter version that we shall examine. It uses a pair of $1-\lambda$ elements (or collinear $\frac{1}{2}-\lambda$ elements) spaced $\frac{1}{2} \lambda$ apart. Between the elements, we find two phase lines of equal length, meeting at a central point where we attach the main feed line. Note that the elements require a 180° phase difference, so one and only one of the phase lines receives a single half-twist. The modeled impedance data in Table 3 rests on the use of $450-\Omega$ phase lines with a velocity factor of 0.9. Other line values will produce other impedances. The 15-meter patterns in Figure 7 are very clean with a bidirectional gain similar to that of a two-element reflector-driver Yagi.

The selection of the element length and spacing for this sample becomes apparent from the patterns in Figure 8. As we raise the operating frequency, the spacing increases to reduce the gain, but the element lengths increase to raise it. Lowering the

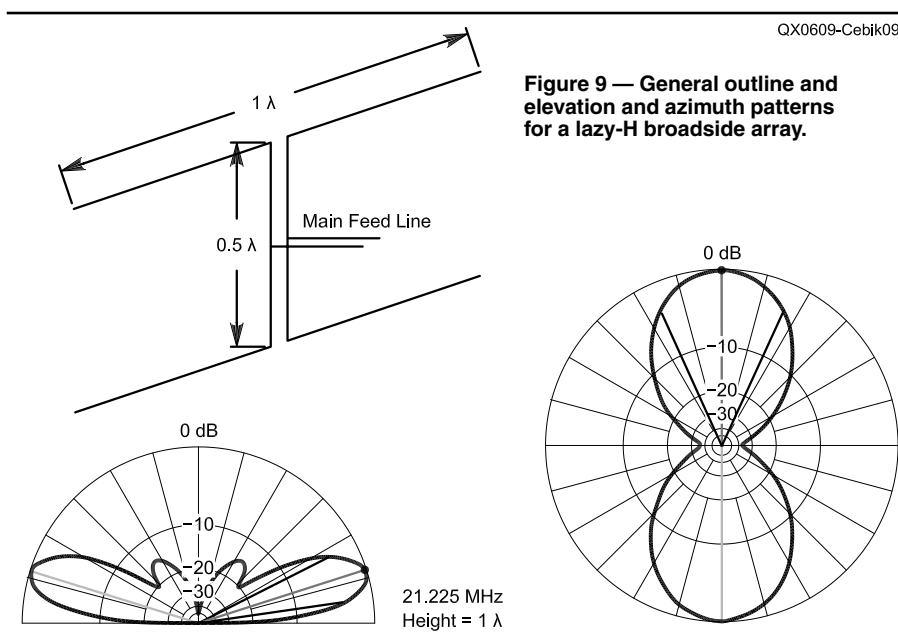


Figure 9 — General outline and elevation and azimuth patterns for a lazy-H broadside array.

Table 4
Modeled 15-Meter Broadside Array Performance Characteristics

Frequency	Gain dBi	TO Angle	Beamwidth	Feed Point Impedance*
<i>Lazy H phased horizontal element ("flat-top") array (see Figure 9 and Figure 10)</i>				
21.225 MHz	12.32	17°	49°	$33.8 + j5.1 \Omega$
14.175	8.47	25°	74°	$662.6 - j527.7 \Omega$
28.5	13.45	12°	27°	$1540 + j1851 \Omega$

See Notes for Table 1.

*Impedance values are for 600Ω , $VF = 1.0$ phase lines.

operating frequency produces opposite effects. The result is an array that one might use over several bands with remarkably similar performance. The remaining gain changes are largely a function of the antenna's changing height when measured in wavelengths.

The W8JK first emerged in 1937. For other configurations, see Kraus' *Antennas*, 2nd Ed, p 458, as well as innumerable articles in *QST* over the years since the antenna first appeared. The array also lends itself to becoming part of more complex array systems.

Broadside Arrays

If the main radiation lobes of an antenna are at right angles to the plane of the elements, then we have a broadside array. Standard HF horizontally polarized arrays tend to require a vertical plane for the elements for broadside use, although NVIS operations might set the element in a horizontal plane for straight-up radiation. The most common simple two-element broadside array for the 15-meter and other upper HF bands is the Lazy-H, shown in Figure 9. Like the W8JK, the elements are $1-\lambda$ long and spaced vertically $\frac{1}{2}\lambda$ apart. We feed the elements in phase, however, so we do not twist either of the two phase-lines. (An alternative feeding system brings the main feed line to the bot-

tom element. The line connecting the elements receives a half twist to produce a 360° phase change in the 180° phase line. The

resulting feed point impedance is very high and requires a matching section.) Table 4 provides the modeled data for the center-fed

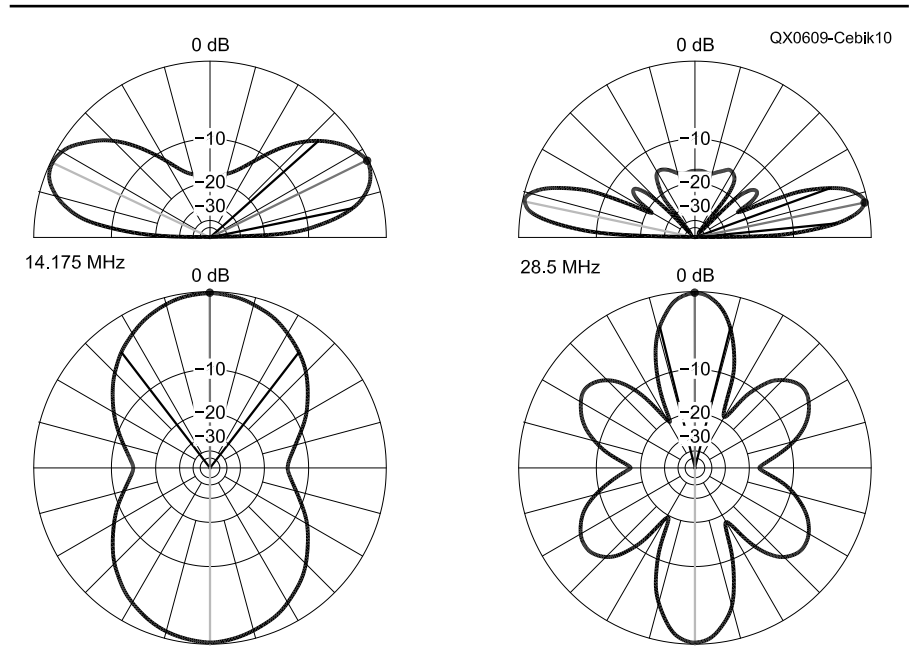


Figure 10 — Elevation and azimuth patterns of a 15-meter lazy-H bidirectional array on 20 and 10 meters.

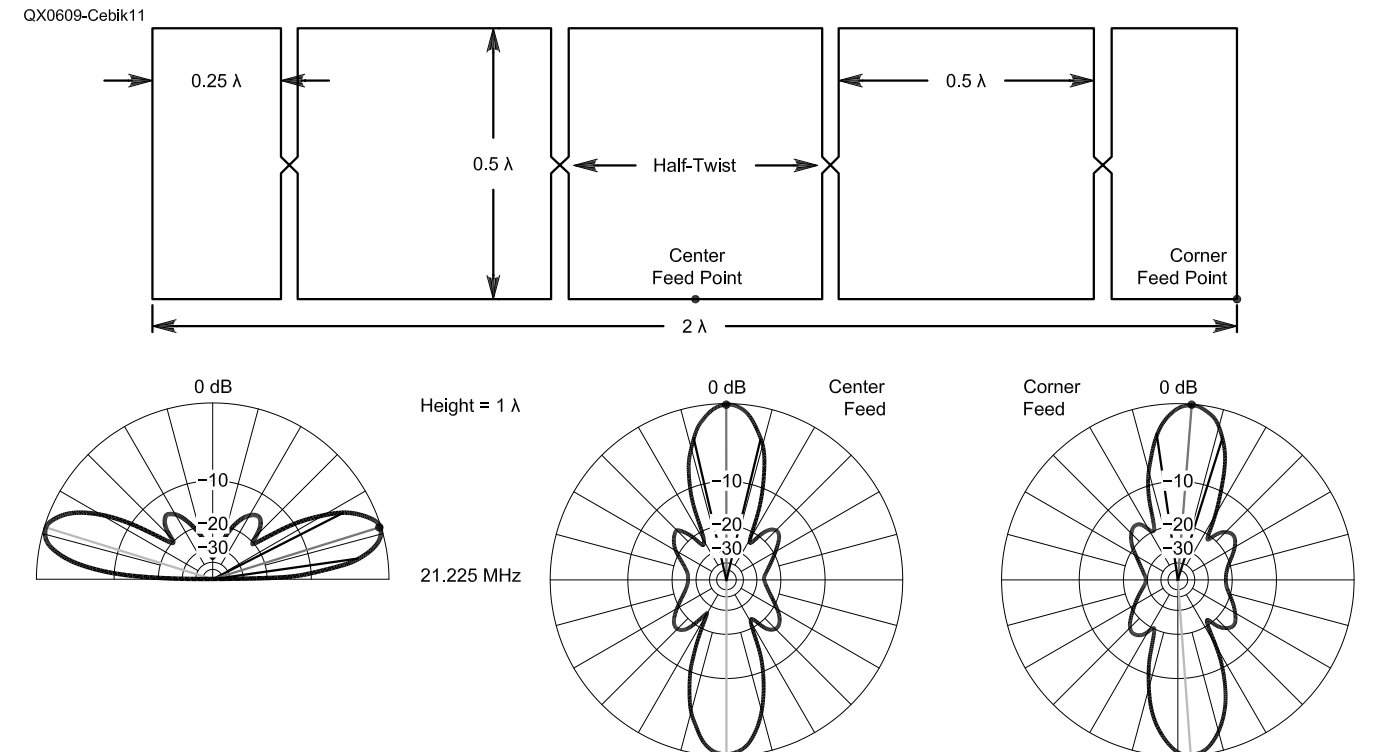


Figure 11 — General outline and elevation and azimuth patterns for a 3-section Sterba curtain.

version of the array. The impedance reports rest on the use of 600-Ω phase lines having a velocity factor of 1.0.

With elements at $\frac{1}{2}\lambda$ and 1λ above ground, the lazy-H outperforms the W8JK on 15 meters, even though the effective height is only a bit over 0.8λ . The increased gain is partly a function of suppressing the upper lobe structure that we see in the W8JK pattern as a result of the lazy-H vertical stack of elements at a $\frac{1}{2}\lambda$ spacing. Like the W8JK, we can use the lazy-H on other bands, as shown both in the tabular data and the patterns of Figure 10. Even though the elements are not spaced for maximum vertical lobe suppression on other bands, the elevation patterns show good reduction in higher angle lobes compared to a flattop array. As we reduce the operating frequency, the height of the lower wire in the lazy-H grows closer to the ground when measured as a fraction of a wavelength. Hence, the bidirectional pattern for 30 meters does not appear, since it would be weaker than a simple dipole at 46 feet above ground and have a higher TO angle. Nevertheless, the antenna is operable on that band. Unlike the W8JK, the lazy-H shows considerable variation in gain as we move from one band to the next.

The pattern for 28.5 MHz calls for a brief note. Using elements that are 1λ long for 15 meters produces a 10-meter pattern with very strong side lobes, since the elements are over 1.3λ long on that band. Instead of beginning with a standard 15-meter design, we might have designed a lazy-H for 10 meters that uses 1.25λ elements with $\frac{5}{8}\lambda$ spacing — about 44 feet and 22 feet, respectively. The result would not change the 10-meter gain significantly, but it would yield an EDZ-type pattern with lower side lobe content. As well, the antenna would operate over the same frequency range as our sample. This is the so-called expanded or extended lazy-H.

The lazy-H is the foundation for many more complex arrays. In principle, we may combine the lazy-H and the W8JK into a four-element array. The lazy-H also finds extensive use in commercial array construction for shortwave broadcasting. Consider a vertical bay of elements fed in phase, with as many elements at $\frac{1}{2}\lambda$ spacing as vertical supports will allow. Now place further columns of such arrays next to each other. Finally, place a large screen between $\frac{1}{4}\lambda$ and $\frac{1}{2}\lambda$ behind the rows and columns of antennas. In the late 1920s, we would have called the antenna a billboard array. If we reduce the element lengths to about $\frac{1}{2}\lambda$ and use special wide-band forms of dipole elements, we end up with the modern dipole directional array. By staggering the feed current phase angle from

Table 5
Modeled 15-Meter Sterba Curtain Performance Characteristics

Three-Section Sterba Curtain (see Figure 11)

<i>Gain dBi</i>	<i>TO Angle</i>	<i>Beamwidth</i>	<i>Feed Point Impedance*</i>
14.47	17°	26°	570.7 + j49.2 Ω

one vertical bay to the next, we can actually slew the direction of the main lobe without ruining the overall characteristics of the antenna pattern. This brief account of modern dipole arrays overlooks a myriad of both electrical and mechanical engineering feats necessary to implement such an array, but it does show the fundamental place of the lazy-H among broadside arrays.

Our final sample broadside array is a curtain, one that passed out of common use long ago. Nevertheless, it serves well as a sample of an antenna that continues to attract amateur attention for its pattern properties. In Figure 11 we have the outline of a three-section Sterba curtain, first reported in antenna literature in 1931. Basic to the design are the $\frac{1}{2}\lambda$ by $\frac{1}{2}\lambda$ inner sections, with end sections that are $\frac{1}{4}\lambda$ wide by $\frac{1}{2}\lambda$ high. We may use as many inner sections as we desire, but a centered feed point requires an odd number. The lines between sections are critical: they must be $\frac{1}{2}\lambda$ long parallel transmission lines with a half-twist in each line to keep the top and bottom wires in phase with each other. The sample places the bottom wire $\frac{1}{2}\lambda$ above ground to keep the array within our maximum height limits.

Table 5 provides the modeled data to accompany the patterns in Figure 11. Like the lazy-H, the elevation pattern shows good suppression of higher-angle lobes. The figure shows two azimuth patterns to accommodate the two most common feed points for Sterba curtains: the center of the lower element structure and the corner. The table includes only one data set, since there is no significant difference in the gain, the beamwidth, or the feed point impedance. A 600-Ω feed line would handle either central or corner feeding very effectively. With central feeding, we have a bidirectional pattern that is exactly broadside to the array itself. If we feed that antenna at a corner, however, we bend the pattern by nearly 5° in the direction of the feed point. For such a large array (even though only 2λ or about 92 feet long), copper losses are sufficient to distort the pattern direction, although one might compensate through a tedious task of making slight dimension alterations.

Like a lazy-H that uses a bottom feed

point and a $\frac{1}{2}\lambda$ half-twist phase-line, the Sterba curtain is a monoband antenna. On other frequencies, it becomes simply a semi-random collection of wire. As well, the Sterba requires a great quantity of wire. Consider once more the collinear array that used half-wavelength sections. If we stack a pair of these antennas vertically, the total array length and height will be the same as for a Sterba curtain. We require only a single phase-line between the two, however, to connect the feed points to the main feed line. The resulting array (with wires at $\frac{1}{2}\lambda$ and 1λ heights) will have a gain of nearly 15 dBi, but with a very great saving in wire.

Another Interim Conclusion

For the wire fans, horizontal bidirectional arrays offer considerable potential in the form of relatively simple, reliable, and inexpensive arrays. In the upper HF region, such antennas have a long-term home if we use care in the ones we select. The lazy-H and the W8JK may be the most flexible arrays in terms of potential multi-band use. We must consider the impedances at the tuner end of the main feed line, however. In some cases, a low antenna feed point impedance may create significant line losses, even in parallel lines. We may need to change dual phase-line lengths and impedances to arrive at the best compromise efficiency level on all bands. Monoband arrays with very high impedances will likely require matching sections to arrive at the lower impedances of common coaxial or parallel transmission lines. Simple antennas can present not-so-simple feeding challenges.

Likewise, we must use care in our selection of an array in terms of the gain-versus-beamwidth question. If we had just one friend with whom we wish to communicate (or two friends at 180° separation), then we might use gain alone as our desideratum. In most cases, however, we shall want to balance gain against coverage. Hence, it is likely that we shall have to trade some gain to obtain adequate beamwidth.

Just when we might think we have reached an ending, someone has whispered to me, "How do we convert a bidirectional array into a directional array?" It turns out that, even here, we have options. QEX

Letters to the Editor

An Effective 80 and 40 Meter SSB/CW Receiver (Jan/Feb 2005)

Gentlemen,

Careful examination of the article by Dave Lyndon, AK4AA, seems to indicate to me that if you reference the oscillator board schematic, Figure 4, there is a missing coupling capacitor that should be in the circuit between T202 and T203 to dc isolate the collector of Q206 from the rest of the circuit.

Can you please confirm this? I do not know if this has been seen by other readers. — Thank you, Paul Parker, WB6DHH, pjldparker@juno.com

Hi,

Yes, there should be a coupling capacitor as Paul's sharp eye reveals. I checked the actual physical circuit, and there is a 0.1 μF disc ceramic capacitor from the junction of the T202 primary and secondary connection to the junction of C220 and the "Q" side of T203. It's important that this be a value much larger than C220.

Sorry for the omission in the schematic, and thanks to WB6DHH for spotting it. [The corrected portion of the schematic is printed here as Figure 1. — Ed.]

— 73, Dave Lyndon, AK4AA, dlyndon@hughes.net

In Search of New Receiver Performance Paradigms (Empirical Outlook, May/June 2006)

Hi Doug,

I think it's fair to say that third-order intercept point (TOIP) has never been an exact scientific parameter of receiver performance comparison. It's a useful (sometimes!) performance parameter for components, but for the receiver as a whole, it has enormous "ifs and buts."

Let's go back a few (40!) years. HF marine receivers here in the UK had an intermodulation performance requirement that a signal at +80 dB μV would produce an IMD product at no more than +30 dB μV . From memory, the spacings were 50 and 100 kHz. Those receivers were adequate, if not particularly good — the intercept point works out at about -2 dBm, and most were about +5 dBm. At that time, they had tuned front ends.

In the early 1980s, an "advanced design" receiver appeared. (I won't say which company, but they were international and no longer exist.) It used 1-bit

sampling at 500 MHz, and then resampled at progressively higher bit resolutions and lower frequencies, and it passed all the type-approval tests. Installed on a ship, it proved such a disaster that according to reports, having set sail from Holland on the first fitting, they stopped in the UK for a conventional receiver to be fitted! But it met the specification.

TOIP is not a very good indicator of overall IMD performance because it doesn't take into account the front-end bandwidth that is handling all the unwanted signals. It has some use when designing for comparing parts; but even then, quoting intercept points in dBm is capable of leading to great problems because of what I call "The Great 50-ohm Scam." Everybody happily talks of levels in dBm; but once you're away from 50 Ω , it gets more than a bit meaningless. I see this in my work (advanced systems design of RF CMOS integrated circuits for low power applications such as transceivers in pacemakers, endoscopes and the like) where you have to work in μV of intercept. Impedances are such that dBm requires multiple calculations as you go from one impedance to another.

Incidentally, RF sub-micron CMOS devices are pretty good at following the cube law, right up to where they hit gain compression. The usual rule of thumb that "TOIP is 10 to 15 dB above 1-dB gain compression" doesn't apply very well with RF CMOS.

So we can confidently say that a receiver with a narrowband tuned front end on 7 MHz (such as the old National HRO) and

a receiver with a wide band (sub-octave filter, up-conversion) can have TOIPs that favor the up-conversion receiver and still not work as well as the HRO.

I've seen it written somewhere (I can't remember where) that classical two-signal IMD tests do not give representative results when used on a receiver with early digitization and DSP filters. I didn't see an explanation (Cynicism suggests it's because the results come out badly!) but in reality, the measurements require multiple signals. The best measurement would be done at varying input levels of very wideband noise, with a notch at the receive frequency, measuring the SNR degradation of a signal at the 10-dB SNR level. Such a measurement is, regrettably, impracticable.

More to the point would be to have a standard level at which the intermodulation ratio is measured, probably somewhere around 60 mV (-10 dBm). A +20 dBm IP receiver would then show IMD signals at -70 dBm. A better approach would be to use mV EMF, which takes out the anomaly of dBm in that they represent the power that would be delivered if the load were 50 Ω . Historically, the US used μV PD (potential difference) at the antenna terminals, while Europe used the EMF. That gave a 6 dB advantage in the US for the marketing department to exploit, while EMF is a better parameter to represent practice. The dBm comparison crawled in from the radar/ECM field, but is so misleading in receiver design that far too often, it is, in reality, as much use as teats on a bull!

TOIP and IMD measurements are only

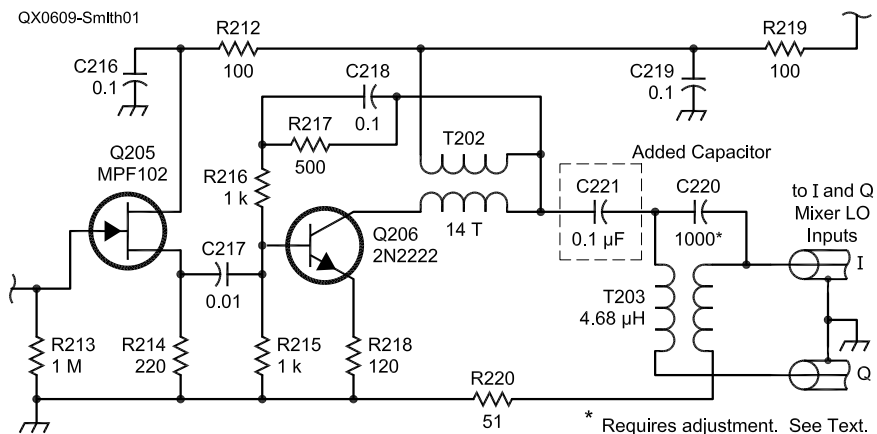


Figure 1 — This schematic diagram shows a corrected portion of the Oscillator Board, Figure 4 from "An Effective 80 and 40 Meter SSB/CW Receiver" by Dave Lyndon, AK4AA in the January/February 2005 issue of QEX. A 0.1 μF capacitor is added between T202 and T203.

a little part of the receiver performance story, though, and as I showed in my *QEX* article some four years ago, phase noise can be far more limiting.¹

— 73, Peter E. Chadwick, G3RZP, g3rzp@g3rzp.wanadoo.co.uk

Hi Peter,

Good to hear from you again. To get right to the point: You and the others I'm talking to seem to agree that a fixed input level is the right way to go for IMD3 measurement in receivers. The only thing is that those who operate near the noise floor have one criterion and those who contest may have another. It's unclear to me how we can avoid measuring IMD3 performance at several levels when units don't obey a cube law.

What's bound to be puzzling to readers is that many published IP3 measurements don't comply with the traditional definition of IP3. That is while heavy emphasis is being placed on receiver IP3 performance by those marketing departments you mentioned. You're right that complex systems don't necessarily play by rules applicable to component parts but equipment reviewers also emphasize IP3, even regardless of their own admissions of its invalidity. Something has to give. Readers deserve a fair shot at comparing old data with new.

It's also true that units with early digitization — and even some with late digitization — do not behave at all like cube law. We do have some studies of how they do behave coming here in *QEX*. At least one of our friends there in Europe is intensely examining the situation.

— 73, Doug Smith, KF6DX, *QEX* Editor, kf6dx@arrl.org

I-V Curve Tracing With a PC (Jul/Aug 2006)

Doug,

What is with the reprinting of *QEX* articles in lightly edited form with slightly different titles in *QST* (or is it the other way around)? Most recently, WB9LVI's curve tracer write-up was published in both magazines in the same month. I seem to recall one other similar situation.

I subscribe to both magazines and expect to get unique content in return for the unique checks that I send in for each publication. I seem to remember from my limited experience as an author, that one of the first questions that I was asked was, "Has this been submitted anywhere else?" It was considered a cardinal sin to do so

¹P. Chadwick, G3RZP, "HF Receiver Dynamic Range: How Much Do We Need?" *QEX*, May/June 2002, pp 36 – 41.

without notifying the publishers of each magazine. As *QEX* and *QST* are both ARRL products and the other publication was referenced in the footnotes in both articles, the cross-publication must have been an overt act by ARRL management, rather than by the author.

You have done a stunningly good job of improving *QEX*, and I salute you for doing that. There really is no need to pad the publication with reprints from the sister magazine.

— 73, Ted Gisske, K9IMM, gisske@offex.com

Dear Ted,

Thanks for writing and giving me the chance to explain. The situation is this: Sometimes we feel a project deserves exposure in both publications and we leave the heavy technical content out of the *QST* companion piece. WB9LVI's article was accepted in basically the form you see it for *QEX*, then *QST* decided to run a slightly less technical version of it. We don't do that often but we have a selfish motive: to steer ARRL members to *QEX* and to steer non-members to *QST*.

As I think you know, *QST* has a circulation of over 140,000 and *QEX* is under 10,000. We'd like to see *QEX* grow, and we're of the impression that many ARRL members don't read *QEX* because they don't realize what they are missing. We'd like to improve that situation.

Thanks for your kind words. As our silver anniversary approaches, I'm particularly proud to be part of *QEX*. It would be

easy for me to take the credit but you writers are the real heroes of this forum.
— 73, Doug Smith, KF6DX, *QEX* Editor, kf6dx@arrl.org

Hello Larry and Doug,

I just opened my issue of *QEX*, went to read my article and saw that Equation 1 on page 4 was incomplete. This is very strange as it was okay in the PDF proof that you sent me. I'm wondering if it is a printer's error, or do I have a bad copy of *QEX*?


If the printer goofed then I think the correct equation should be printed in the next issue as it will help readers in following the derivation. By the way Larry, Equations 2 and 3 that you fixed came out just right!

— Best wishes, George Steber, WB9LVI, steber@execpc.com

Hi George,

That error was apparently caused by a bug in our layout software. It's happened before — in one of my articles! It happens sometimes when the final file is created to send to the printer, but no one is sure why. Unfortunately, it's tough to catch after everybody has signed off on the proofs. The complete equation appears here.

$$\frac{V_2}{V_1} = G_1(s) = \frac{R_1 C_1 s}{R_1 C_1 s + 1} \quad (\text{Eq 1})$$

— 73, Doug Smith, KF6DX, *QEX* Editor, kf6dx@arrl.org 



QEX Subscription Order Card

QEX, the Forum for Communications Experimenters is available at the rates shown at left. Maximum term is 6 issues, and because of the uncertainty of postal rates, prices are subject to change without notice.

Subscribe toll-free with your credit card **1-888-277-5289**

ARRL
225 Main Street
Newington, CT 06111-1494 USA

For one year (6 bi-monthly issues) of QEX:

In the US

ARRL Member \$24.00
 Non-Member \$36.00

In the US by First Class mail

ARRL Member \$37.00
 Non-Member \$49.00

Elsewhere by Surface Mail
(4-8 week delivery)

ARRL Member \$31.00
 Non-Member \$43.00

Canada by Airmail

ARRL Member \$40.00
 Non-Member \$52.00

Elsewhere by Airmail

ARRL Member \$59.00
 Non-Member \$71.00

Renewal New Subscription




Name _____ Call _____

Address _____

City _____ State or Province _____ Postal Code _____

Payment Enclosed to ARRL

Charge:

Account # _____ Good thru _____

Signature _____ Date _____

Remittance must be in US funds and checks must be drawn on a bank in the US.
Prices subject to change without notice.

06/01

In the next issue of

QEX

Paul Wade, W1GHZ, returns (yes!) with a discussion of waveguide to coaxial cable transitions. Paul takes a largely em-

pirical approach to determining optimal dimensions and placements of probes at the interface. Ample measured data are included. Practical construction considerations are also covered in this article that fills in some significant gaps in the ham radio literature.

Microwave fans: Check it out! You may save yourself a lot of time and effort.

QEX

ELECTRONICS OFFICER TRAINING ACADEMY

The Complete Package To Become A Marine Radio Officer/Electronics Officer

ELKINS, with its 54-year history in the radio and communications field, is the only school in the country providing all the training and licensing certification needed to prepare for the exciting vocation of Radio Officer/Electronics Officer in the Merchant Marines.

Great Training | Great Jobs | Great Pay



Call, Fax or Email for More Information:

ELKINS Marine Training International
P.O. Box 2677; Santa Rosa, CA 95405
Phone: 800-821-0906, 707-792-5678
Fax: 707-792-5677
Email: info@elkinsmarine.com
Website: www.elkinsmarine.com

Electronics Officers Needed for U.S. Flag Commercial Ships Worldwide

Skills required: Computer, networking, instrumentation and analog electronics systems maintenance and operation.

Will assist in obtaining all licenses.

Outstanding pay and benefits.

Call, Fax or e-mail for more information.



American Radio Association, AFL-CIO

Phone: 504-831-9612

Fax: 775-828-6994

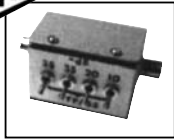
arawest@earthlink.net

NATIONAL RF, INC.



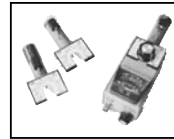
VECTOR-FINDER

Handheld VHF direction finder. Uses any FM xcvr. Audible & LED display.
VF-142Q, 130-300 MHz \$239.95
VF-142QM, 130-500 MHz \$289.95



ATTENUATOR

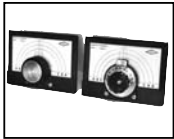
Switchable, T-Pad Attenuator, 100 dB max - 10 dB min BNC connectors
AT-100, \$89.95



DIP METER

Find the resonant frequency of tuned circuits or resonant networks—ie antennas.

NRM-2, with 1 coil set, \$219.95
NRM-2D, with 3 coil sets (1.5-40 MHz), and Pelican case, \$299.95
Additional coils (ranges between 400 kHz and 70 MHz avail.), \$39.95 each



DIAL SCALES

The perfect finishing touch for your homebrew projects. 1/4-inch shaft couplings.

NPD-1, 3 1/4 x 2 1/4 inches 7:1 drive, \$34.95
NPD-2, 5 1/8 x 3 7/8 inches 8:1 drive, \$44.95
NPD-3, 5 1/8 x 3 7/8 inches 6:1 drive, \$49.95

S/H Extra, CA add tax

NATIONAL RF, INC
7969 ENGINEER ROAD, #102
SAN DIEGO, CA 92111

858.565.1319 FAX 858.571.5909
www.NationalRF.com

Down East Microwave Inc.

We are your #1 source for 50MHz to 10GHz components, kits and assemblies for all your amateur radio and Satellite projects.

Transverters & Down Converters, Linear power amplifiers, Low Noise preamps, coaxial components, hybrid power modules, relays, GaAsFET, PHEMT's, & FET's, MMIC's, mixers, chip components, and other hard to find items for small signal and low noise applications.

We can interface our transverters with most radios.

Please call, write or see our web site
www.downeastmicrowave.com
for our Catalog, detailed Product descriptions and interfacing details.

Down East Microwave Inc.
954 Rt. 519
Frenchtown, NJ 08825 USA
Tel. (908) 996-3584
Fax. (908) 996-3702

Try
These

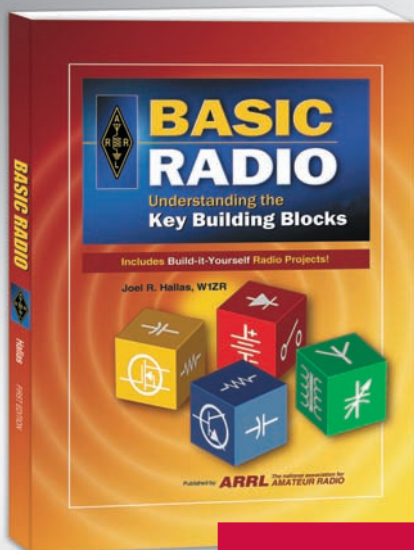
Publications from **ARRL**



SHOP DIRECT or call for a dealer near you. ORDER TOLL-FREE 888/277-5289 (US) ONLINE WWW.ARRL.ORG/SHOP



**Basic Radio
brings the
magic of radio
to life!**



**Includes
Build-it-Yourself
Radio
Projects!**

Basic Radio— Understanding the Key Building Blocks

by Joel Hallas, W1ZR

ARRL Order No. 9558 \$29.95*

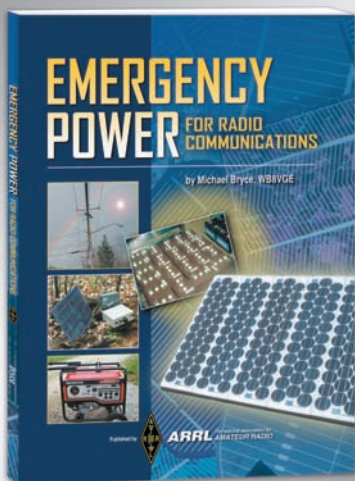
*shipping: \$8 US (ground)/\$13 International

**FINALLY—an introduction to radio FOR EVERYONE!
—what it does and how it does it.**

Basic Radio reveals the key building blocks of radio: **receivers; transmitters; antennas; propagation; radionavigation; and radiolocation.** This book includes simple, build-it-yourself projects to turn theory into practice—helping reinforce key subject matter.

WHO NEEDS THIS BOOK?

Basic Radio builds upon knowledge of elementary electronic concepts as presented in ARRL's *Understanding Basic Electronics* or a similar course. This book will provide the foundation in radio theory and practice necessary for anyone undertaking more advanced topics such as those presented in *The ARRL Handbook for Radio Communications*.



**Tools for...
Emergency or
Backup Power!
Energy Independence!
Portable Energy!**

Emergency Power for Radio Communications

by Michael Bryce, WB8VGE

ARRL Order No. 9531.....\$19.95

*shipping: \$7 US (ground)/\$12 International

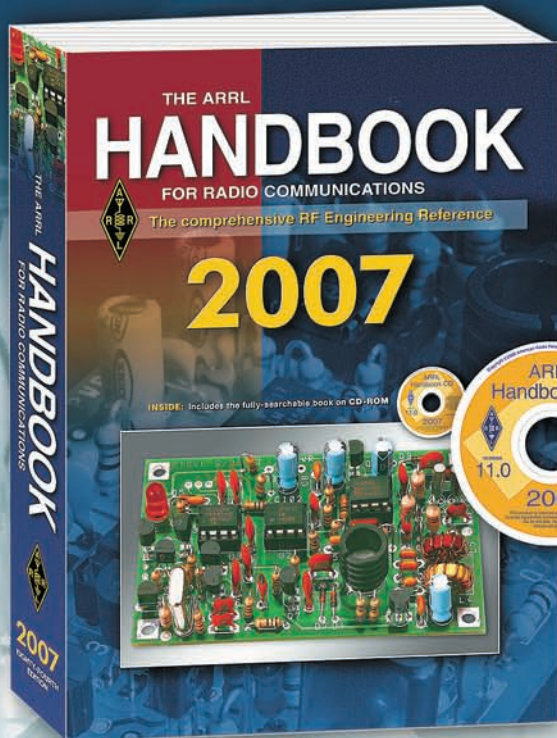
With this comprehensive guide you can explore the various means of electric power generation—from charging batteries, to keeping the lights on. This book covers the foundation of any communications installation—the power source. Use this book to plan ways to stay on the air when weather or other reasons cause a short-term or long-term power outage. **When all else fails...how will you communicate?**

Find ways to reach beyond the commercial power grid. Identify methods for alternative power generation that will work best in your particular situation, perhaps taking advantage of possibilities already on hand.

Contents

- Keeping the Signals on the Air
- Hey, I Am In The Dark: Keeping The Lights On In The Ham Shack With Emergency Power
- Solar Power
- Charge Controllers for PV Systems
- Generators: Gas, Wind and Water
- Load Sizing
- Holding Your Volts: Battery Systems and Storage
- Systems for Emergency Power
- Inverters
- Station Instrumentation
- Safety
- Emergency Practices

Pre-order the ARRL Handbook — 2007 Edition with Bonus "January 1942 QST" Reissue



World War II Commemorative QST Offer!
Available from ARRL and Select ARRL Publication Dealers



You get all this when you pre-order:

- **The ARRL Handbook**—2007 edition. Up-to-date and always revised!
- **The ARRL Handbook on CD-ROM**—version 11.0, included with every book.
- **BONUS "January 1942 issue of QST" reissue**—Limited edition.

The ARRL Handbook—2007
Eighty-Fourth Edition

The greatest applied electronics and communications reference of all time! Information on fundamental electronics concepts, components and building blocks, analog and digital radio design, troubleshooting techniques, antennas and much more. Make **The Handbook** your one-stop source for practical construction projects and weekend builds: radios, antennas, amplifiers, test equipment, DSP, accessories and more. Includes many new and updated projects:

- **High Power 50 MHz Low Pass Filter**
- **HiMite Low Power Transceiver**—build it for 20, 17, 15, 12 or 10 meters.
- **12-V dc Boost Regulator for Mobile Operation**—maintains 13.8 V when battery voltage decreases.
- **The TiCK-4**—a tiny CMOS keyer.

Plus, an improved digital communication interface for HF digital modes, low-cost remote antenna switch, a PIC-based HF/VHF power meter, top-loaded low-band antenna, and more.

65 Year Commemorative Reissue

Facts about the January 1942 issue of QST!

- First issue following Pearl Harbor attack, Volume XXVI, Number 1
- Contains last-minute press pages: "WAR COMES!"
- Includes the FCC Order suspending Amateur Radio operation in the US, issued December 8, 1941
- 100 pages of nostalgic editorial, feature articles, advertisements, and cartoons

Sixty-five years later, this commemorative reproduction of *QST* is a time capsule—a tribute to the perseverance and patriotism of radio amateurs!

CD-ROM INCLUDED! This edition is bundled with **The ARRL Handbook CD (version 11.0)**—the complete and fully searchable book on CD-ROM, including many color images, PC board templates, additional software and reference material.

Pre-order Today www.arrl.org/shop or Toll-Free 1-888-277-5289 (US)

Softcover. Includes book, CD-ROM and Bonus "January 1942 QST" reissue. ARRL Order No. 9760 **\$44.95** plus s&h

Hardcover. Includes book, CD-ROM and Bonus "January 1942 QST" reissue. ARRL Order No. 9779 **\$59.95** plus s&h

Pre-order now and get the special Bonus "January 1942 QST" reissue! Offer expires September 30, 2006, or while supplies last. Pre-orders will ship after October 1.

Bonus "January 1942 QST" reproduction offer expires 11:59 UTC, September 30, 2006 or while supplies last. A limited supply will be printed before it is returned to the "ARRL vault" for at least 10 years. Bonus "January 1942 QST" premium cannot be redeemed for cash. No returns. Exchanges must be accompanied by premium. Valid only on pre-orders direct from ARRL or from Select ARRL Publications Dealers. This offer may be canceled or modified at any time due to system error, fraud or other unforeseen problem. Void where prohibited.

Shipping and Handling charges apply. Sales Tax is required for orders shipped to CA, CT, VA, and Canada. Prices and product availability are subject to change without notice.

ARRL The national association for
AMATEUR RADIO

225 Main Street, Newington, CT 06111-1494 USA

SHOP DIRECT or call for a dealer near you.

ONLINE WWW.ARRL.ORG/SHOP

ORDER TOLL-FREE 888/277-5289 (US)

QEX 9/2006